MICROWAVE ABSORPTION BY ORTHO PAIRS
IN SOLID HYDROGEN

by

BRYAN WAYNE STATT

B.Sc. University of British Columbia, 1976

A THESIS SUBMITTED IN PARTIAL FULFILLMENT
OF THE REQUIREMENTS FOR THE DEGREE OF
MASTER OF SCIENCE

in

THE FACULTY OF GRADUATE STUDIES
DEPARTMENT OF PHYSICS

We accept this thesis as conforming
to the required standard

THE UNIVERSITY OF BRITISH COLUMBIA

February, 1979

Department of Physics

The University of British Columbia
2075 Wesbrook Place
Vancouver, Canada
V6T 1W5

Date Feb. 1, 1979

ABSTRACT

The microwave absorption spectra of ortho pairs in low ortho concentration samples of solid hydrogen is studied theoretically and experimentally. A theory is developed for several line broadening mechanisms and a comparison made with experiment. Phonon induced lifetime effects are calculated to be less than 2 MHz in the temperature range T=1.2-4.2 K but have not yet been observed experimentally. Inhomogeneous broadening due to isolated ortho molecules and to isotopic mass defect impurities is observed and found to be consistent with theory. Several new lines in the out-of-plane pair configuration are reported which confirm the assignments made previously, whereas two new lines in the next nearest neighbor configuration support a reassignment of these transitions. Also, three excited state transitions which fix the position of the 10Γ level are reported and compared with the theoretical predictions of Harris et.al. (1977) and Luryi and Van Kranendonk (1979).

TABLE OF CONTENTS

LIST OF TABLES

LIST OF FIGURES

ACKNOWLEDGEMENTS

I would like to acknowledge the support of Dr. W.N. Hardy in the supervision of this project. I have also benefited greatly from numerous discussions with Dr. A.J. Berlinsky. Finally I wish to thank the National Sciences and Engineering Research Council of Canada for a Postgraduate Scholarship.

CHAPTER I Introduction

In this thesis a study of the ortho pair spectrum in samples of solid hydrogen of low ortho concentrations is presented. Hydrogen is a molecular solid whose molecules are essentially free rotors. The rotational energies given by

$$E=BJ(J+1) \tag{1}$$

where $B=60cm^{-1}$ (86.4 Kelvin) for H_2, are large compared to the anisotropic interactions in the solid which are of order $7cm^{-1}$ (10 K). This implies that J is a good quantum number in the solid. Since a hydrogen molecule is composed of two nuclei of spin $\frac{1}{2}$, the total wavefunction must be antisymmetric under particle permutation. This requires the symmetric rotational wavefunctions of even J to be associated with the antisymmetric nuclear spin state I=0 (para species) and similarly odd values of J must have I=1 (ortho species). Conversion between these species is generally very slow and hence only the J=0 and J=1 levels are populated at the temperatures of the solid (triple point 13.8 K). At the low ortho concentrations of interest here the solid is known to be hexagonal close packed (hcp) at all temperatures.

The ortho pairs, in this case nearest or next nearest neighbours in the lattice, have nine states whose levels are determined by interactions between the two molecules of the pair and other two- and three-body interactions between the pair and surrounding para molecules. The dominant interaction between ortho molecules is the electric quadrupole-quadrupole (EQQ) interaction. This splits the F=2 levels (F is the total angular momentum of the pair) but leaves the F=0 and F=1 levels degenerate. This degeneracy is then removed by other interactions such as the crystal field or electronic polarizability. These interactions are discussed in detail in Harris et.al (1977) (HBHII) . Electromagnetic radiation can be absorbed by ortho pairs via the quadrupole induced dipole mechanism even though the hydrogen molecules themselves have no permanent dipole moment. This effect derives from the dipole moment induced in the surrounding para molecules by the quadrupole moment of an ortho molecule. In this case microwave energy can then be absorbed through pair transitions. These transitions have been observed by Hardy et.al. (1977) (HBHI) and have been described in some detail. Some of these transitions are studied more extensively here and other previously unobserved transitions are reported.

A major part of this thesis is concerned with the line-shapes of these transitions. The energy levels of an ortho pair in an otherwise pure para hydrogen lattice will be homogeneously broadened by phonon processes. However, in a sample of finite ortho concentration the relatively more abundant isolated ortho molecules give rise to an inhomogeneous broadening of the pair levels via the EQQ interaction. Theories are developed for both phonon and ortho broadening and experimental verification is attempted.

A less interesting, but unfortunately often dominant form of broadening is caused by strains in the sample. The EQQ interaction determining the pair levels is proportional to r^{-5} where r is the separation between the pair molecules. Therefore a distribution of pair spacings will cause an inhomogenous broadening of the pair spectrum. The major source of this inhomogeneity is mechanical strain on the sample. This unavoidable effect is a result of the procedure used to grow the H_2 samples. The temperature of the niobium cell containing liquid H_2 is slowly lowered until solidification takes place. Upon further cooling to 4 K a free standing sample would contract by about 3%. However the hydrogen sticks to the walls of the cell resulting in an inhomogeneous strain field. It is not surprising that the hydrogen sticks well to the metallic walls. A molecular solid is held together by Van der Waal's forces which are weaker for two hydrogen molecules than for an H_2 molecule and a metal surface. Thus the solid would rather stick to the metal walls than pull away when contraction occurs.

This strain broadening makes observance of the previously mentioned broadening mechanisms very difficult because of its unpredictable nature and potentially large size. A substantial effort has been made in the present work to make these effects as small as possible. However it seems clear that one must develop techniques for growing free standing single crystals before strain effects can be further reduced.

CHAPTER II Computer Controlled Microwave Spectrometer

The system to be described is a computer controlled phase-locked microwave source with data collection, real time processing, and display facilities. The Nova 2 minicomputer is interfaced to the microwave equipment through digital to analog (D/A) converters which allow the computer to sweep the microwave source as desired. The microwave sources are backward wave oscillators (BWO's) which are phase-locked to a 0.01-500 MHz frequency synthesizer. The frequency ranges covered by this system at present are 8-12.4 GHz, 12.4-18 GHz, 18-26.5 GHz, 26.5-40 GHz, 60-90 GHz, and 75-120 GHz. In addition to sweeping the microwave frequency the computer collects data through analog to digital (A/D) converters and can process it in real time to display a spectrum as it is collected. A moving head disk unit is used for storing data as well as the operating system software. The high level languages available in the system also allow one to carry out sophisticated data processing if desired.

2.1 Computer System:

This section will describe the hardware available in the present system and the software used to control these devices. The Nova 2 minicomputer is interfaced to several standard peripherals as well as a custom designed interface. Software supplied by Data General is used to control the standard devices whereas user defined support routines control the interface. The standard commercial equipment in this system is as follows:

- -Nova 2 minicomputer
- -Diablo 44 Disk Drive and controller
- -LA36 Decwriter II
- -High speed paper tape punch, reader and controller

The Real Time Disk Operating System (RDOS) is used to provide basic communication between the user and the system. This is a file orientated system and standard commands exist for controlling the commercial peripherals. An assembler is available for writing machine langauge programs as well as an editor and several debugging programs. These programs are useful in the development of the interface controlling software. Several high level languages are available as well. These are Basic, Fortran and Algol, which along with all the other software is stored on disk and readily accessible.

The interface was built by the UBC Physics department's electronics shop and is designed to allow the computer to have control of the experimental apparatus. The devices presently in the system are:

- -16 bit D/A converter
- -Two 12 bit D/A converters
- -8 input multiplexed A/D converter
- -Programmable interval timer
- -Timer clock
- -Synthesizer control latches
- -Auxilary I/O latches
- -4 input and 6 output digital ports
- -6 reed relays
- -9 digit LED display

The device codes and instructions for the use of these devices are presented in Appendix A. The following paragraphs describe how each device is used in the present system.

The 16 bit D/A converter is used to supply a presetting voltage to the external frequency control input of the BWO supply. This ensures that the BWO frequency will be within the capture range of the phase-lock system. Sweeping this voltage in step with the synthesizer maintains the phase-lock throughout the sweep. The synthesizer frequency can be set by applying the desired binary coded decimal (BCD) signals to its external inputs. This is done through the aid of a group of latches which allows the computer to set and hold the desired frequency.

Event synchronization is maintained with the programmable interval timer. This device generates a pulse of specified length which is used to control timing for the sweeper, CRT display, plotting etc.

The two 12 bit D/A converters are used to provide a visual display of data either to a monitor scope, strip chart recorder or X-Y recorder. The two outputs are routed through the reed relays to the three devices in such a way that only one device is operative at any given time. One of the digital outputs is used to provide blanking for the CRT during retrace and when the CRT is not in use.

Data is collected with the 14 bit A/D converter. This device is preceded by an eight input multiplexer which allows the A/D to measure one of the eight available inputs. The user selects which input is to be measured and then starts the conversion. About 50 microseconds later the conversion is completed and the digital representation of the input voltage is ready to be read in.

The subroutines used to access the interface are called through Extended Basic. This langauge is chosen because it is interactive and has facilities for calling user assembler language subroutines. Although Basic is slow to execute and a cumbersome language to work with compared to Fortran, the former properties outweigh these disadvantages. Each assembler language subroutine used is described in Appendix B. The two main Basic programs used to run the spectrometer are listed in Appendix C and their use will now be described.

The first program creates a voltage to frequency conversion table for presetting the microwave frequency of each BWO . This is done with the program CALIBRATION which sweeps the 16 bit D/A starting at a preselected voltage and speed. As an example one could calibrate the D/A every 250 MHz throughout the band. This is done with a "pushbutton box" which collects the voltages desired as well as changing the speed and direction of the sweep. Once this has been done the voltages collected are stored on disk for later use.

The second program is stored in SWCONTROL and consists of two parts. The first part runs the spectrometer and has facilities for outputing data to the disk, CRT and plotters. The other part is used for data analysis. When the program is first run it will ask for the default data directory and then the calibration points filename. Once these are entered the spectrometer is limited to the band specified. The program must be run again in order to change the operating band. The program then enters the command mode and signifies this by typing the prompt >. In the analysis mode the prompt is #. Commands to be entered are either one or two letters followed by a carriage return (CR). The first letter indicates the type of command and the second letter indicates a change in mode(M) or parameters(P). The mode is associated with the sweeper and plotting routines and signifies either the slow, fast or synthesized sweep or is used to indicate the X-Y or strip chart recorder when plotting. The parameters of a command are entered upon request after the command is issued and can be used again by the same command if only the command letter is typed. If a change in parameters is desired a P is entered as the second letter. For convenience the input requests are not typed out in the analysis mode unless an S is entered as the second letter in the command. Table I lists all of the available commands. The program segregates the data array DATA into four sections as follows:

Array	Start
CAL.TBL.	1
T0	2002
T1	4004
TPLOT	6006

where the voltage-frequency conversion table is stored in CAL.TBL. and the other three sections are used for data collection . In the analysis mode one has access to any portion of DATA and is not restricted by these boundaries. When the program is first run the calibration points read from the disk are temporarily stored in DATA starting at location 7500. These points are then transfered to a Basic array and hence may be overwritten at any time.

The following command and response sequence illustrates the use of the program. The underlined portions are those typed in by the operator. These commands will take two spectra, store them on disk, enter the analysis mode, divide the two spectra, plot the result on the scope and the strip chart recorder, store the result on disk and then return to the command mode.

TABLE I Sweeper Commands

Command Mode (>)		Mode/Parameter Switch
R	run the spectrometer	(M,P)
S	strip chart or X-Y recorder	(M,P)
P	monitor scope plot	(P)
D	disk read or write	
A	go to analysis mode	

Analysis Mode (#)		
M	array multiplication	
A	array addition	
V	array division	
P	monitor scope plot	(P)
B	slope addition to array	
D	disk read or write	
X	find min. and max. values in array	
S	strip chart or X-Y recorder	(M,P)
T	output array to teletype	
I	integration	
R	return to command mode	

```
>RP FSTART,DELTA F,NO.PT,DELTA T,A/DCHAN 12,.001,1001,1000,0
       S=0
       SYNTH.  FREQ.= 381.25 MHZ   DELTA F=31.25 KHZ
       RUN 0
>D WRITE(0) OR READ(1) ?  0 ENTER FILENAME & NO.PT A.1,1001
TO BE WRITTEN OR READ FROM
CAL.PTS.(0),CAL.TBL.(1),T0(2),T1(3),TPLOT(4) 2
>R RUN 0
>D WRITE(0) OR READ(1) ?  0 ENTER FILENAME & NO.PT A.2,1001
TO BE WRITTEN OR READ FROM
CAL.PTS.(0),CAL.TBL.(1),T0(2),T1(3),TPLOT(4) 2
>A
DEFAULT DIR.  DATA:

  #D WRITE(0) OR READ(1) ?  1 ENTER FILENAME & N A.1,1001
    TO BE WR OR READ FROM 0,1,2,3,4 1
  #VS D(I)=C1*D(J)/(D(K)+C2) ENTER I,J,K,N,C1,C2
4004,2002,1,1001,16384,0
  #PP 3,1001
  #S STRIP CHART(19) OR X-Y(18) OR POINT(21) 18
    ? 1,1001,100,6006
  #D WRITE(0) OR READ(1) ?  1 ENTER FILENAME & N A.1,1001
    TO BE WR OR READ FROM 0,1,2,3,4 1
  #R

>
```

The input S allows one to correct for the drift in the 16 bit D/A converter. S is added to the 16 bit code used to set the D/A. A number of the order of 500 can move the setting frequency completely through the capture range of the phase-lock system. This program is also listed in Appendix C.

Once the data has been collected and initially processed with the above program it is then possible to do relatively sophisticated analysis of the data using programs written in Fortran. For example one can put the data through a low pass filter or perhaps fit a spectrum with a desired lineshape. The computer can also carry out calculations used to interpret the results of the data analysis.

2.2 Phase-Locking System:

This system consists of a frequency synthesizer, a frequency multiplier chain, and electronics to phase lock the BWO to a harmonic of the synthesizer. The BWO and synthesizer can be swept synchronously, while maintaining the lock, and the combination constitutes a high resolution microvave spectometer. The output of the synthesizer (frequency f_o) is fed into a frequency doubler chain which provides a signal with a frequency eight times that of the synthesizer at essentially the same power level. This signal is mixed with a sampled portion of the BWO output frequency (f) in a harmonic mixer. The intermodulation frequency ($IF=8Nf_o-f$) is divided by ten with a digital prescalar and then fed into a synchronizer. This device provides a DC error signal proportional to the difference in phase of the IF signal and a reference 20 MHz oscillator signal. The error signal is then fed into the FM input of the BWO, completing the phase lock loop. The power levels present are sufficient to phase lock the BWOs up to 40 GHz but another locking system must be used to lock the millimeter wave sweeper. First the X8 multiplier chain will be discussed and then the phase locked loop.

2.3 Multiplier Chain:

The purpose of this chain is to ensure that the harmonic mixer produces an acceptable IF signal. If the synthesizer frequency were mixed directly with the BWO signal the harmonic of f_o would normally be too high to produce an IF signal of sufficient power. The multiplier chain does some of the harmonic multiplying and provides a signal of about 5 dBm (i.e. 5 dB above 1 milliwatt) in the frequency range 2.8-4.0 GHz. This reduces the harmonic number in the mixer used to lock the BWO.

A block diagram of the multiplier chain is shown in fig.1. The output of the frequency doublers closely approximates a rectified sine wave and consists predominantly of the second harmonic of the input frequency. However the efficiency of the doubling process drops if the other harmonics are not filtered out. The band pass filters present serve this purpose. In addition the broad-band amplifiers are chosen to amplify only signals in the frequency ranges of interest, ie. 0.5-1.0 GHz. for the first stage of multiplication. The finite width of the skirts of real filters requires one to restrict the sweeping range to less than one octave (e.g. f_o=350-500 MHz).

2.4 Phase Locked Loop:

The phase locked loop is the feedback system which keeps the BWO frequency locked to a harmonic of the synthesizer frequency. This removes the instability of the BWO frequency and results in a very narrow spectral width governed by the synthesizer, multiplier chain and synchronizer phase noise and stability.

A block diagram of the phase locked loop in fig.2 shows the rest of the apparatus in the spectrometer. Starting at the BWO output the microwaves are sampled with two 10 dB directional

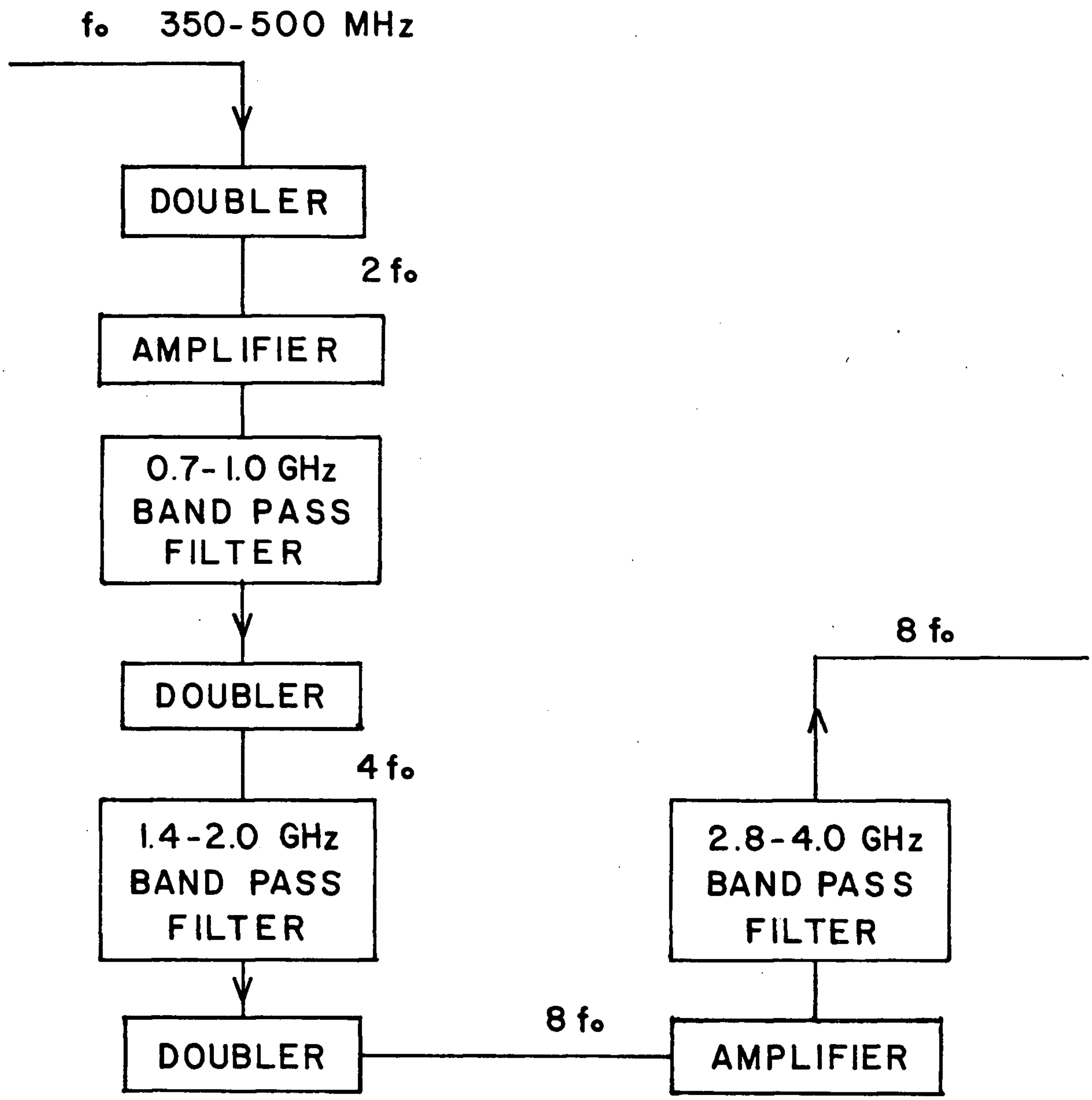

Figure 1 Multiplier Chain

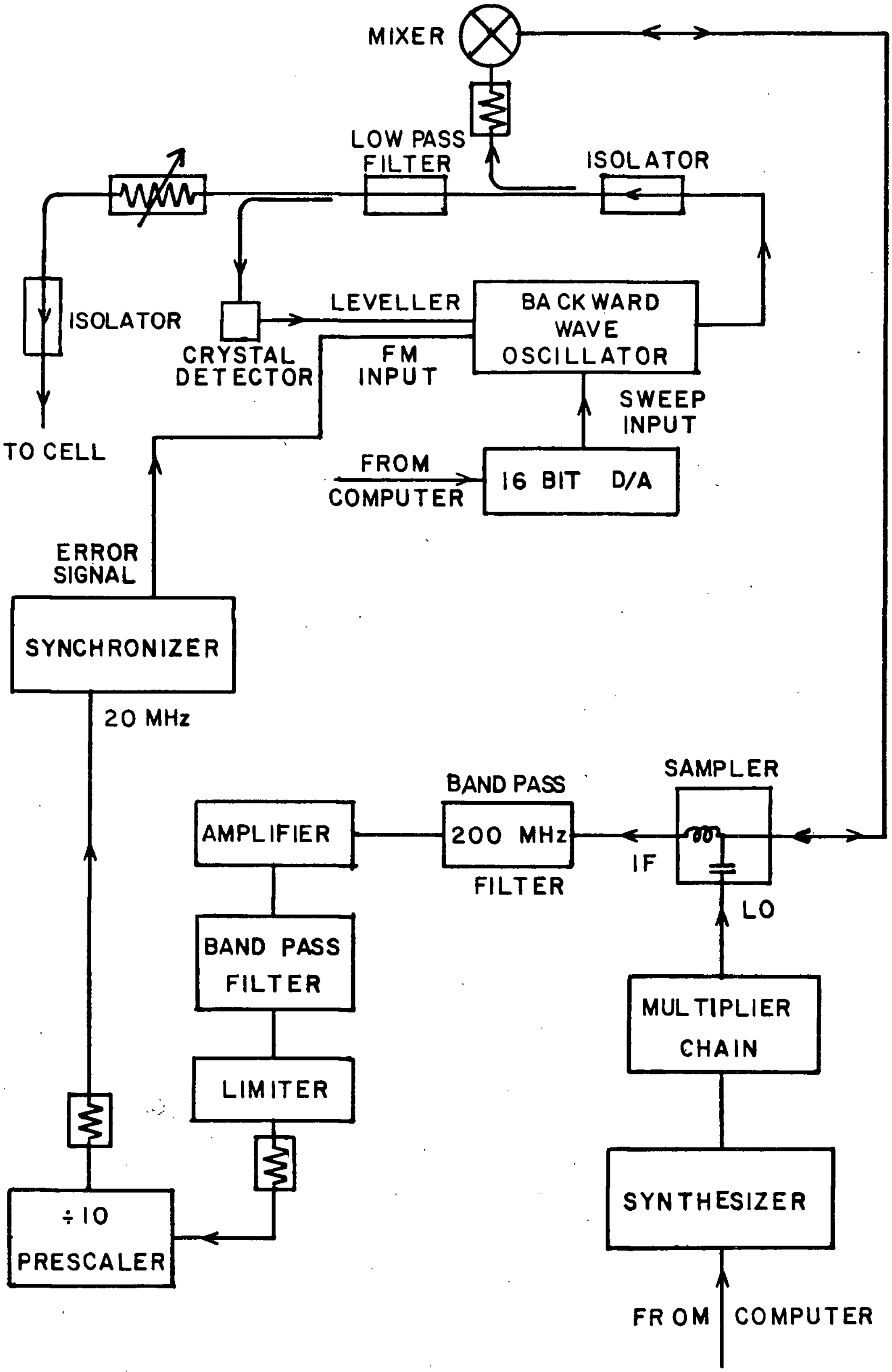

Figure 2 Phase Locked Loop

couplers. The second coupler is connected to a crystal detector whose output is used in the leveller circuit of the BWO to keep the power level constant with frequency. The leveller circiut keeps the detector voltage constant and hence the power spectrum essentially takes on the response function of the detector. The second coupler is connected to the harmonic mixer. The low pass filter prevents harmonics from entering the experiment and the isolators prevent reflected signals from entering the BWO and levelling loop.

The output of the multiplier chain is fed into the harmonic mixer and the output is amplified and put through a 200 MHz bandpass filter. The signal then goes through a limiter and a divide by ten prescalar and then the synchronizer. This device compares the incoming frequency to its reference 20 MHz oscillator with two phase sensitive detectors. A DC error signal is then produced which is proportional to the phase difference measured . The synchronizer will only lock onto one of the IF sidebands, determined by the sign of the voltage-frequency relationship of the FM input of the BWO. The harmonic spacing of $8f_o$ is much greater than the capture range of the phase lock loop ensuring that the BWO frequency is uniquely determined by f_o and the presetting voltage fed to the BWO sweeper unit. The capture range of the synchronizer is increased by a factor of ten with the prescaler which relaxes the initial conditions required to bring the system into lock. Also, the large amount of FM present in the BWO output makes the tighter lock difficult to establish. The larger capture range is also useful in overcoming the drift of the 16 bit D/A converter. However the sensitivity of the loop is decreased by the same amount which increases the phase noise of the output over that for a system not using the divide by ten prescalar. This is quite acceptable in the present situation where the width of the lines measured are greater than one MHz. The 200 MHz narrow band filter is necessary because of the digital nature of the prescaler. Without it the synchronizer could lock onto a harmonic of the prescaler which would mean an IF frequency being a subharmonic of 200 MHz.

A spectrum analyser can be used to monitor the output of the spectrometer when it is phase- locked. In the 12.4-18.0 GHz band the 3 dB point is less than 3 KHz, the smallest bandwidth available on the spectum analyser used. The power spectrum of the spectrometer is shown in fig.3 where f=15 GHz and the total harmonic number is 32. The observed phase noise apparently comes from the synthesizer. To see this we note that after frequency multiplication by n the signal-to-noise ratio of the output decreases by 20log(n) dB (Kroupa, 1973). The signal to noise ratio of the power spectrum 100 KHz away from peak power is 60 dB where the bandwidth is 3 KHz. This implies an incoming S/N of 60 dB + 35 dB + 30 dB = 125 dB with 1 Hz bandwidth. This agrees with the specifications of the synthesizer given by the manufacturer.(Rohde and Schwarz model 103.9968.51)

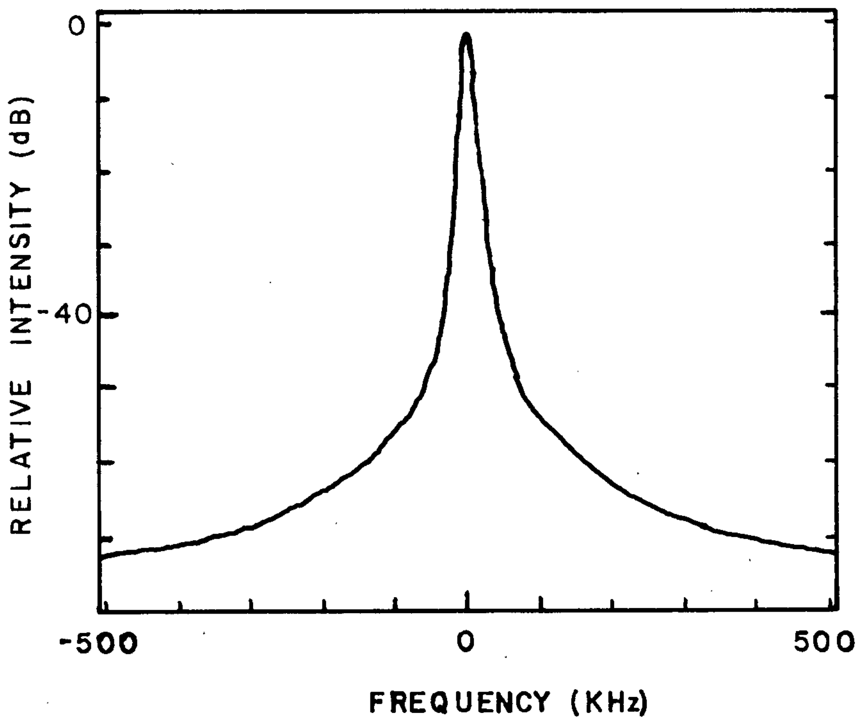

f_0= 14.8 GHz

Bandwidth= 10KHz

Figure 3   15 GHz Locked Signal

2.5 Millimeter Wave Phase Lock System:

The 75-120 GHz BWO cannot be phase locked directly from the multiplier chain since the large harmonic number produces insufficient IF signal. For this reason the millimeter wave BWO is phase locked to the existing 12.4-18.0 GHz synthesizer phase locked source. This unit provides more power than the multiplier chain and also ensures the use of lower harmonics. The locking system is slightly different from the one used before since another synchronizer is not available. Also the phase lock acquired is not as satisfactory as with the previous system because of the increased technical difficulties associated with the higher frequency.

A block diagram of the system in fig.4 shows that the synchronizer has been replaced by a mixer and the frequency presetting voltage is supplied with a wide-band frequency discriminator rather than another D/A converter. The discriminator provides the rough frequency control for the BWO. Initially the millimeter BWO sweeper is manually set so that the system goes into lock. Then as the 12.4-18.0 GHz source is swept the discriminator provides an error signal to the integrator which is then fed into the FM input of the BWO sweeper. The mixer in the discriminator will produce a signal approximately proportional to the difference between the IF frequency and $f = c/\lambda$, where λ is the wavelength for which the time delay corresponds to $\lambda/4$. The $\lambda/4$ delay line is preset to match the 20 MHz reference signal from the phase detector system. This discriminator ensures that the BWO frequency is

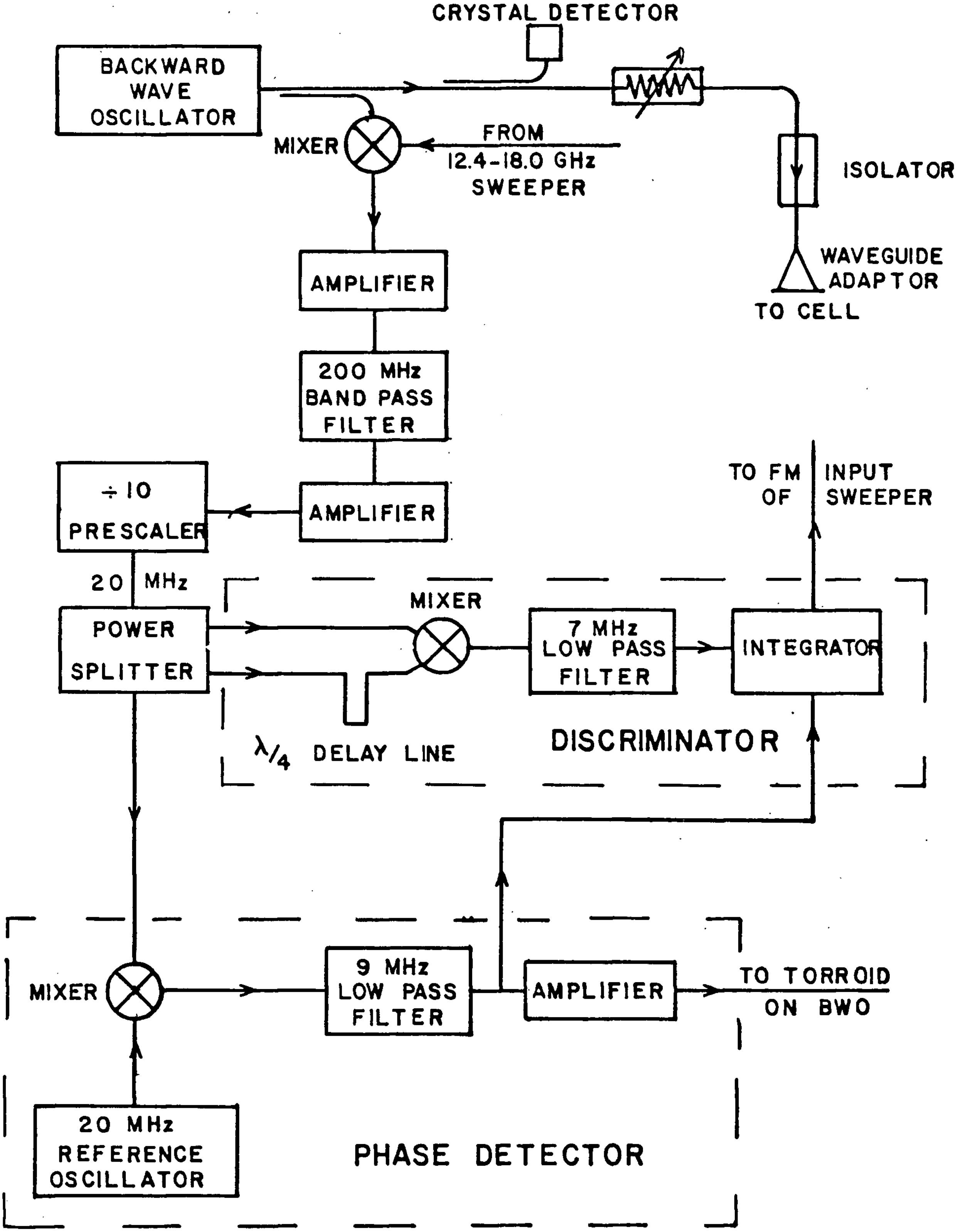

Figure 4 Millimeter Wave Phase Locking System

always close enough to the desired harmonic of the sweeper signal to enable the phase detector system to lock.

The phase detector produces an error signal proportional to the phase difference between the IF signal and the reference oscillator which is then fed into the discriminator's integrator and a coupling toroid on one of the high voltage grids (we have used grid #2) in the BWO tube. The frequency response of the toroid is about 10 KHz to 1 MHz and the FM input response is DC to 10 KHz so that the two systems more or less overlap. The rest of the system is similar to that of the low frequency locking apparatus.

Monitoring the IF spectrum when the system is phase locked reveals that the noise level is much higher than can be attributed to the synthesizer. Apparently the phase detector system does not have a high enough frequency response and cannot compensate for all the phase disturbances occuring in the BWO. When sweeping, the discriminator's integrator gradually supplies a larger DC voltage to the BWO sweeper in order to keep the BWO frequency in line with the sweeper frequency. One disadvantage of this method is that if for some reason the system unlocks momentarily the integrator output may move sufficiently far that lock cannot be reestablished. This means the sweep must be stopped and restarted. A further difficulty is that because of the various interactions between the amplitude and frequency response of the BWO grids, operation of the levelling circuit prevents phase locking. This means that the power level is not constant with frequency. In practise the power level was recorded simultaneously with the spectra and levelling accomplished in the computer analysis.

CHAPTER III Theory

In this chapter some of the contributions to the pair transition linewidths are examined. First a theory is developed for the inhomogeous broadening of the ortho pair lines due to the random distribution of isolated ortho molecules. This is followed by estimates of the temperature dependent phonon induced lifetime broadening of the pair levels. Finally, the effect of isotopic mass defect impurities on the pair linewidths is examined.

3.1 Ortho Broadening of the Pair Spectrum:

A single ortho pair in an otherwise pure para hydrogen crystal will have its energy levels lifetime broadened by phonon processes. However, in a sample with finite ortho concentration there are other possible mechanisms for broadening. In particular there are many more isolated ortho molecules[1] than there are ortho pairs. These ortho molecules interact with the pair molecules via the dominant electric quadrupole-quadrupole (EQQ) interaction causing a small shift in the pair energy levels. Because of the statistical nature of the distribution of orthos, each ortho pair will experience a different configuration of ortho molecules. This results in an inhomogeneous broadening of the pair levels. The lineshape of a pair transition can then be constructed by forming a distribution function of the differences between the final and initial pair level shifts over all possible ortho molecule configurations and states.

A statistical model describing the NMR spectral density functions of a system of random impurity spins with interactions having radial dependence R^{-n} has been formulated by Hama et.al. and applied to solid hydrogen by Fujio et.al. Since they are looking at the interaction between a random spin distribution and a single spin (rather than a pair of spins) their results are not directly applicable here. However one

[1]From now on isolated ortho molecules will be refered to simply as ortho molecules, which are to be distinguished from molecules that are part of an ortho pair.

would expect the general features of the broadening to be the same in both cases and this does seem to be borne out.

This is an N-body problem involving a random distribution of the interacting species, and even though the interaction Hamiltonian is well known the problem cannot be solved in general. The approximations made here essentially reduces the calculation to a two-body problem. For convenience the ortho pair will be placed at the coordinate origin and the rest of the lattice divided into discrete spherical shells of radius r. In the limit of low ortho concentration the set of ortho molecule configurations consisting of only para molecules inside a sphere of radius r (except the ortho pair), one ortho molecule in the shell r and a random distribution of orthos beyond will approximate the actual set of all possible configurations. In addition the effect on the pair levels of the ortho molecules beyond the first one will be replaced by their average, which is zero, as will be shown later. This is probably acceptable since the EQQ interaction is relatively short ranged (R^{-5}).

The model described so far includes the static shifts in the pair levels assuming no interaction between the ortho molecules outside the first ortho shell. This ignores the correlations between the ortho molecules. For example if two ortho molecules have equal crystal field splittings then each molecule can "flip" its state and still conserve energy. This would lead to a type of motional narrowing observed in nuclear spin systems. In their approach Hama et.al. have tried to take this into account by excluding contributions to the spectral density coming from an ortho molecule which has an ortho neighbour closer than some specified distance. Inclusion of this effect does narrow the central portion of the line as expected. In the present work the correlation effect is ignored.

Now the lineshape function $J(\omega)$ can be written in the form

[2] $$J(\omega) = \sum_i \int_{r_o}^{\infty} d^3r \; p(r) \; \delta(\omega - E_i(r,\Omega))$$

where $d^3r\ p(r)$ is the probability of having the first ortho molecule in the shell of radius r and $E_i(r,\Omega)$ is the pair transition frequency shift caused by an ortho molecule at a distance r and orientation $\Omega = (\theta,\phi)$ with respect to the pair axis. The appropriate lattice sum is replaced by an integral starting at some cut-off radius r_o, chosen to be a few lattice spacings. If N_r is the number of lattice sites in shell r then

[3] $$d^3r\ p(r) = (1-X)^{N_1 + N_2 + \cdots + N_{r-1}} \cdot N_r X (1-X)^{N_r - 1}$$

where $(1-X)^{N_1 + N_2 + \cdots + N_{r-1}}$ is the probability of having no ortho molecules in shells 1 through r-1 and $N_r X(1-X)^{N_r - 1}$ is the probability of having one ortho molecule in shell r. Now let $N = \sum_{i=1}^{r} N_i$ whence

[4] $$d^3r\ p(r) \simeq e^{-NX} N_r X$$

If $\frac{4\pi}{3} r_x^3 = \frac{R_o^3}{\sqrt{2}\, X}$ is the average volume per ortho molecule then

[5] $$d^3r\ p(r) = 3\ e^{-r^3/r_x^3} \frac{r^2 dr}{r_x^3}$$

Therefore

[6] $$J(\omega) = \sum_i a \int_{r_0}^{\infty} \frac{r^2 dr\, d\Omega}{r_x^3} \quad e^{-r^3/r_x^3} \quad \delta(\omega - E_i(r,\Omega))$$

and the normalization constant is

[7] $$a^{-1} = \frac{4\pi}{3} \quad e^{-r^3/r_x^3}$$

An ortho molecule in an otherwise pure para H_2 lattice experiences a crystal field with 3-fold symmetry about the c-axis which splits the J=1 state into levels with $m_J=\pm1$ and $m_J=0$. The sign of the crystal field splitting V_c is not known but it will be assumed that the $m_J = 0$ level is lower in energy than the doubly degenerate $m_J= \pm 1$ level. These levels are associated with the states $|1,m_J\rangle = Y_1^{m_J}(\omega_3)$ where ω_3 is the angle between the ortho molecular axis and the quantization axis (which is the crystal c-axis). In the presence of other ortho molecules the EQQ interaction splits the two degenerate levels an amount of the order of a few MHz for $X \simeq 2\times10^{-3}$. This is much less than the crystal field splitting of 300 MHz and hence only the $m_J = \pm1$ states are mixed.

Diagonalizing the matrix elements $\langle 1,m_J| \mathcal{H}_{EQQ} |1,m_J'\rangle$ with respect to $m_J=\pm1$ leads to the non-degenerate states

[8] $$|1,X\rangle = \frac{1}{\sqrt{2}} \left\{ e^{i\varphi}|1,1\rangle - e^{-i\varphi}|1,-1\rangle \right\}$$

[9] $$|1,Y\rangle = \frac{-i}{\sqrt{2}} \left\{ e^{i\varphi}|1,1\rangle + e^{-i\varphi}|1,-1\rangle \right\}$$

and as before $|1,z\rangle = |1,0\rangle$. These "dumbell orbitals " are oriented with the x and y orbitals each rotated by an angle φ

from the x and y quantization axes respectively. The angle Ψ is determined by the configuration and states of orthos which surround the ortho molecule of interest. In general Ψ is time dependent since the ortho molecules can change states as described earlier. However this effect is being ignored here. The configuration of ortho molecules surrounding the one closest to the pair is not completely random since there can be no other ortho molecules inside the first ortho shell. However, it will be assumed that Ψ is a random variable. Hence the final lineshape will consist of an average of the Ψ-dependent lineshapes.

In order to further simplify the calculation it will be assumed that as the pair molecules undergo a transition, the eigenstates of the closest ortho molecule will not change. This is not precisely correct, since the EQQ interaction with the ortho depends on the state of the pair molecules. However, since the degenerate level is split by the presence of many ortho molecules it is not unreasonable to assume that in most cases the two split states will remain essentially the same.

The level diagram in fig.5 illustrates the effect an ortho molecule has on the pair levels, and on the transitions allowed between these levels. The only transitions considered here are those where the pair state changes but the ortho state remains the same. The following arguement will show that intensities for other types of transitions are much less than the kind considered here.

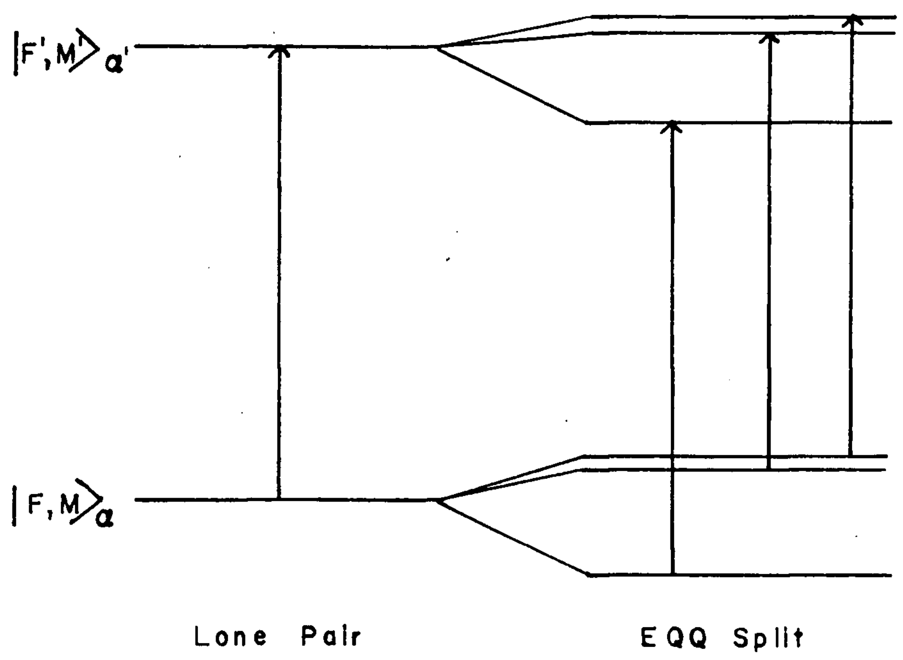

(a) EQQ Split Pair Levels and Transitions

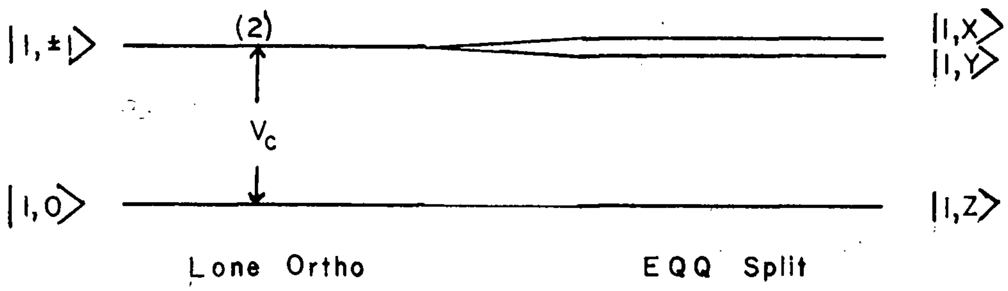

(b) EQQ Split Ortho Molecule Levels

Figure 5 Ortho Shifted Pair Levels

The integrated intensity associated with a pair transition is proportional to a sum of terms containing $\langle f|P^{(n)}|i\rangle\langle i|P^{(m)*}|f\rangle$ (HBHII) where $|i\rangle$ and $|f\rangle$ are the initial and final pair states and $P^{(m)}$ is a component of the dipole moment operator. This operator is split into a scalar and tensor term $P^{(m)} = P_s^{(m)} + P_t^{(m)}$.

Considering first the scalar term

[10] $$P_s^{(m)} \propto \sum_{\nu} C(123;m,\nu)\,(-)^{\nu}\left[\,Y_2^{-\nu}(\omega_1) + \sigma\, Y_2^{-\nu}(\omega_2) + \eta(\Omega)\, Y_2^{-\nu}(\omega_3)\right] d^{(m+\nu)}$$

where ω_1 and ω_2 are the orientation angles of the pair molecules and ω_3 is that of the ortho molecule all with respect to the pair axis. The product states are $|i\rangle = |F,M\rangle^i\,|1,X\rangle^i$ and $|f\rangle = |F,M\rangle^f\,|1,X\rangle^f$. Hence the integrated intensity is proportional to terms

$$^i\langle F,M|\,Y_2^{-\nu}(\omega_1) + \sigma Y_2^{-\nu}(\omega_2)\,|F,M\rangle^f \quad ^i\langle 1,X\,|\,1,X\rangle^f$$

and

$$^i\langle F,M\,|F,M\rangle^f \; ^i\langle 1,X\,|\; Y_2^{-\nu}(\omega_3)\;|1,X\rangle^f$$

For a pair transition the latter term drops out and the former term contributes to the intensity if $|1,X\rangle^i = |1,X\rangle^f$.

The tensor term $P_t^{(m)}$ contains a sum of terms $Y_2^{\nu}(\omega_i)\, Y_2^{m+n}(\omega_j)\, Y_3^{n+\nu}(\Omega_{ij})\, R_{ij}^{-4}$ where i and j label the ortho molecules as before (i,j=1,2; 2,3; 3,1). The intensity therefore contains the i,j=1,2 term multiplied by $^i\langle 1,X|1,X\rangle^f$ and the other two terms contain R_{i3}^{-4} where i=1,2. This latter contribution will be negligible compared to all the others in the low ortho concentration limit where the average ortho-pair distance is many times R_o. It then follows that the strongest pair transitions are those in which the ortho molecule does not change state. The others are too weak to be considered.

The EQQ interaction Hamiltonian is given by (Harris, 1970)

[11] $$\mathcal{H}_{ij} = \frac{20\pi\Gamma_0}{9}\sqrt{70\pi}\sum_{\mu,\nu} C(224;\mu\nu)\left|\frac{R_o}{r_{ij}}\right|^5 Y_2^{\mu}(\omega_i)\,Y_2^{\nu}(\omega_j)\,Y_4^{*\mu+\nu}(\Omega_{ij})$$

where i and j label the interacting ortho molecules. The pair states $|F,M\rangle$ are given by (HBHII)

[12] $$|F,M\rangle = \sum_m C(11F;m,M-m)\;Y_1^m(\omega_1)\,Y_1^{M-m}(\omega_2)$$

where F is the total angular momentum of the pair and M is its projection along the pair axis. These states give rise to a two fold degeneracy for the $|2,\pm2\rangle$, $|1,\pm1\rangle$ and $|2,\pm1\rangle$ states which is lifted by the non-cylindrically symmetric interactions discussed in HBHII. The non-degenerate states are then $|F,|M|\rangle_{\pm} = \frac{1}{\sqrt{2}}\left\{|F,M\rangle \pm |F,-M\rangle\right\}$ where the x-axis is chosen so that the x-z plane is a reflection plane of the crystal.

The states of the ortho molecule are constructed with $|1,m_J\rangle = Y_1^{m_J}(\omega_3)$ where ω_3 is measured with respect to the crystal c-axis. Since it is more convenient to work in the pair frame this quantization axis must be aligned with the pair axis by the rotation

[13] $$R|1,m_J\rangle = \sum_m D^{1*}_{m_J,m}(\alpha,\beta,\gamma)\,|1,m\rangle$$

where α,β,γ are the Euler angles describing the rotation of the crystal c-axis to the pair axis. The y-axis of the crystal field frame can be arbitrarily chosen so that $\alpha=0$ and for the three cases of interest β and γ are given in fig.6.

Evaluation of $E(r,\Omega)$ will require the matrix elements $\langle 1,m_3|\langle F,M|\mathcal{H}_{i3}|F,\pm M\rangle|1,m_3'\rangle$.

[14] $$\langle 1,m_3|\langle F,M|\mathcal{H}_{i3}|F,\pm M\rangle|1,m_3'\rangle = \int d\omega_3 \sum_m d^{\,1}_{m_3,m}(\beta)\, e^{-im\gamma}\, Y_1^{*m}(\omega_3)$$

$$\cdot \int d\omega_i\, d\omega_j \sum_{m_i'} C(11F;m_i',M-m_i')\, Y_1^{*m_i'}(\omega_i)\, Y_1^{*M-m_i'}(\omega_j)$$

$$\cdot \frac{20\pi\Gamma_0}{9}\sqrt{70\pi}\sum_{\mu,\nu} C(224;\mu\nu) \left|\frac{R_0}{r_{i3}}\right|^5 Y_2^{\mu}(\omega_i)\, Y_2^{\nu}(\omega_3)\, Y_4^{*\nu+\mu}(\Omega_{i3})$$

$$\cdot \sum_{m_i} C(11F;m_i,\pm M-m_i)\, Y_1^{m_i}(\omega_i)\, Y^{\pm M-m_i}(\omega_j) \sum_{m'} d^{\,1}_{m_3',m'}(\beta)\, e^{im'\gamma}\, Y_1^{m'}(\omega_3)$$

With the help of Rose (1952)

[15] $$\langle 1,m_3|\langle F,M|\mathcal{H}_{i3}|F,M\rangle|1,m_3'\rangle = R(r_{i3})\, C_{F,M}\, S(m_3,m_3')$$

and

[16] $$\langle 1,m_3|\langle F,M|\mathcal{H}_{i3}|F,-M\rangle|1,m_3'\rangle = R(r_{i3})\, C'_{F,M}\, S'(m_3,m_3')$$

where

$$R(r) = \frac{10}{9}\Gamma_0\sqrt{70\pi}\left|\frac{R_0}{r}\right|^5$$

$$C_{F,M} = \sqrt{\frac{3}{5}}\,[3(2F+1)]^{1/2}\, W(21F1;1F)\, C(2FF;0,M)$$

$$C'_{F,M} = \sqrt{\frac{3}{5}}\,[3(2F+1)]^{1/2} W(21F1;1F)\, C(2FF;2M,-M)$$

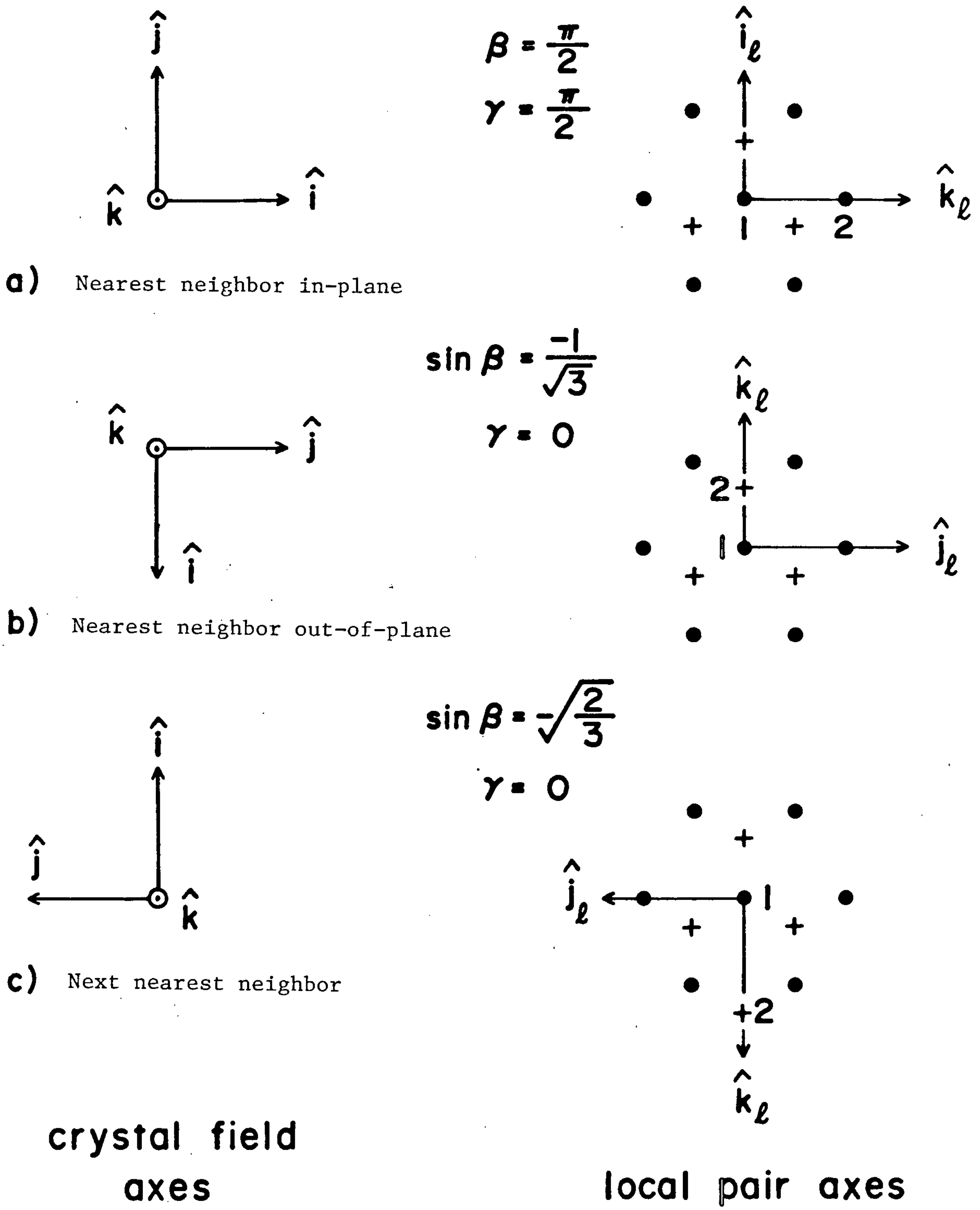

Note that $\hat{i}_\ell \times \hat{j}_\ell = \hat{k}_\ell$ and only the $\hat{i}_\ell$ or $\hat{j}_\ell$ which lies in the basal plane, represented by dots, is shown. The pluses represent the next plane up.

Figure 6 Pair Molecule Orientations in the Solid and

[17] $$S(m_3, m_3') = (-)^{1-m_3} C(112; m_3, -m_3') \sum_{\nu} C(224; 0, \nu) \cdot Y_4^{*\nu}(\Omega_{i3})\, d^{2}_{\nu, m_3-m_3'}(\beta)\, e^{-i\nu(\gamma+\pi)}$$

[18] $$S'(m_3, m_3') = (-)^{1-m_3} C(112; m_3, -m_3') \sum_{\nu} C(224; 2M, \nu) \cdot Y_4^{*2M+\nu}(\Omega_{i3})\, d^{2}_{\nu, m_3-m_3'}(\beta)\, e^{-i\nu(\gamma+\pi)}$$

Note that $C(224;2M,\nu)=0$ if $M=2$ and hence $S'(m_3,m_3')$ does not enter into the matrix elements where $F=M=2$. Using the forms of $|1,X_i\rangle$ in [8] and [9]

[19] $$\langle 1, X_i | {}_{\alpha}\langle F,M | \mathcal{H}_{i3} | F,M \rangle_{\alpha} | 1, X_i \rangle = R(r_{i3})\, C_{F,M} \{ S(m_i, m_i) + \sigma_i \, \mathrm{Re}[e^{-2i\psi} S(m_i, -m_i)] \} + \alpha R(r_{i3}) C'_{F,M}\, \delta_{1,m} \{ \mathrm{Re}[S'(m_i, m_i)] + \tfrac{1}{2} \sigma_i \, \mathrm{Re}[e^{-2i\psi} S'(m_i, -m_i) + e^{2i\psi} S'(-m_i, m_i)] \}$$

where $|F,M\rangle_{\alpha}$ is either $|F,M\rangle\ (\alpha=0)$ or $|F,|M|\rangle_{\pm}\ (\alpha=\pm1)$ and the variables involving i are defined by

i	x_i	σ_i	m_i
1	x	-1	1
2	y	+1	1
3	z	0	0

Now that the matrix elements have been determined one can proceed with the calculation of $J(\omega)$. Assuming that $r_{13} = r_{23} = r$ and $\Omega_{13} = \Omega_{23} = \Omega$ which is acceptable for large r,

[20] $$E_i(r,\Omega) = 2R(r)\,\Delta C\left\{ S(m_i,m_i) + \sigma_i \, Re\left[e^{-2i\psi} S(m_i,-m_i)\right]\right\}$$
$$+ 2R(r)\Delta C'\left\{ Re\left[S'(m_i,m_i)\right] + \tfrac{1}{2}\sigma_i \, Re\left[e^{-2i\psi} S'(m_i,-m_i) + e^{2i\psi} S'(-m_i,m_i)\right]\right\}$$

where

$$\Delta C = C_{F',M'} - C_{F,M}$$

$$\Delta C' = \alpha' C'_{F',M'}\,\delta_{1,M'} - \alpha C'_{F,M}\,\delta_{1,m}$$

and $|F,M\rangle_\alpha$ is the inital pair state and $|F',M'\rangle_{\alpha'}$ the final pair state. Averaging over all ψ and i

[21] $$J(\omega) = \frac{2}{\pi}\int_0^{\pi/2} d\psi \, \frac{1}{3}\sum_i a\int_{r_0}^{\infty} \frac{r^2 dr\, d\Omega}{r_x^3}\; e^{-r^3/r_x^3}\; \delta(\omega - E_i(r,\Omega))$$

Replacing $\delta(\omega - E_i(r,\Omega))$ with $\int d\omega'\, \delta(\omega - (\frac{r_0}{r})^5\omega')\,\delta(\omega' - (\frac{r}{r_0})^5 E_i(r,\Omega))$ gives

[22] $$J(\omega) = 4\pi a\int_{r_0}^{\infty} \frac{r^2 dr}{r_x^3}\, e^{-r^3/r_x^3} \int d\omega'\, \delta(\omega - (\tfrac{r_0}{r})^5\omega')\, \mathcal{J}(\omega')$$

where

[23] $$\mathcal{J}(\omega) = \frac{1}{6\pi^2}\sum_i \int d\psi\, d\Omega\; \delta\left(\omega - (\tfrac{r}{r_0})^5 E_i(r,\Omega)\right)$$

is the spectral distribution function associated with an ortho molecule in a shell of radius r about the pair. This function is independent of r.

$\mathcal{J}'(\omega)$ is now calculated numerically by a computer program which for each point on a grid of Ψ and Ω calculates $\left(\frac{r}{r_0}\right)^5 E_i(r,\Omega)$ and adds one to the appropriate "energy bin" forming a histogram. Two of the checks performed on the results of this program are the comparison of the first and second moments of $\mathcal{J}(\omega)$ which can be calculated analytically.

The first moment is easily calculated and is found to be zero.

[24] $$\int d\omega \;\; \omega \mathcal{J}(\omega) = \frac{1}{6\pi^2} \sum_i \int d\Psi \, d\Omega \left(\frac{r}{r_0}\right)^5 E_i(r,\Omega) = 0$$

since $E_i(r,\Omega)$ is a sum of $Y_4^{*\nu}(\Omega)$ s and $\int d\Omega \, Y_4^{*\nu}(\Omega) = 0$. This also implies that the first moment of $J(\omega)$ is zero leaving the average value of the pair frequencies unchanged.

Calculating the second moment requires a little more algebra resulting in

[25] $$\int d\omega \;\; \omega^2 \mathcal{J}(\omega) = \frac{1}{12\pi} \left[2\left(\frac{r}{r_0}\right)^5 R(r)\right]^2 \Big\{ (\Delta C)^2 \Big[\frac{18}{35}\left(\frac{3}{2}\cos^2\beta - \frac{1}{2}\right)^2$$

$$+ \frac{9}{7}\sin^2\beta\cos^2\beta + \frac{99}{280}\sin^4\beta + \frac{3}{14}\sin^2\beta\left(1+\cos^2\beta\right) + \frac{3}{112}\left(1+6\cos^2\beta+\cos^4\beta\right)\Big]$$

$$+ (\Delta C')^2 \Big[\frac{3}{28}\left(\frac{3}{2}\cos^2\beta - \frac{1}{2}\right)^2 + \frac{261}{1120}\sin^4\beta + \frac{3}{7}\sin^2\beta\cos^2\beta + \frac{1}{4}\sin^2\beta\left(1+\cos^2\beta\right)$$

$$+ \frac{9}{280}\left(1+\cos^4\beta\right) + \frac{53}{280}\cos^2\beta\Big] + 2\left(\Delta C \; \Delta C'\right)\Big[\frac{3\sqrt{6}}{40}\sin^2\beta\left(\frac{3}{2}\cos^2\beta - \frac{1}{2}\right)$$

$$+ \frac{3\sqrt{6}}{160}\sin^2\beta\left(1+\cos^2\beta\right) - \frac{3\sqrt{6}}{28}\sin^2\beta\cos^2\beta + \frac{\sqrt{6}}{56}\sin^4\beta \Big] \Big\}$$

The computer calculated first moment is always less than one half the "bin size" which compares well with the analytical result of zero. A list of calculated second moments and line-widths appear in table II. To the accuracy given in the table, the computer results agreed perfectly with [25].

The lineshape is also calculated by computer but instead of computing the integral from $r=r_o$ to ∞ the change of variable $\omega''=(r_o/r)^5\omega'$ is made which results in the finite integration range of 0 to ω'. Now

[26] $$J(\omega) = \frac{4\pi a}{5}\left(\frac{r_o}{r_x}\right)^3 \frac{1}{\omega}\int_{\omega}^{\omega_m} d\omega'\, \mathcal{J}(\omega')\left(\frac{\omega'}{\omega}\right)^{3/5} \exp\left[-\left(\frac{r_o}{r_x}\right)^3\left(\frac{\omega'}{\omega}\right)^{3/5}\right]$$

where ω_m is the maximum or minimum value of ω depending on whether ω is positive or negative. In the limit of large ω, [26] yields $J(\omega)\sim\omega^{-8/5}$ in agreement with Hama's spectral distribution function. [26] also gives $J(\omega)\sim\mathcal{J}(\omega)$ as $\omega\to 0$.

Before discussing the computer results we note that $E(r,\Omega)$ given in [20] contains two terms with coefficients ΔC and $\Delta C'$. These two coefficients are the only expressions containing F,M and α so that an examination of ΔC and $\Delta C'$ allows one to determine which transitions have identical lineshapes. Also if $\Delta C=\Delta C'=0$ then there is no broadening by this mechanism. Transitions A_2, A_3, G_1, G_5, G_2 and G_3 have zero linewidth and the following pairs of transitions have the same lineshape:

(B_2^-, C_3) (B_2^+, C_1) (G_4, H_3) (A_1, A_5) (G_2, G_3')

Table II Second Moments and Linewidths

Transitions	Second Moment*	Width (FWHM)**
In-plane transitions		
$C_1, B_2^+: (2,1)_+ \rightarrow (1,0)$	0.347	16.1
$C_3, B_2^-: (2,1)_- \rightarrow (1,0)$	0.344	11.9
B_3	0.115	6.7
G_4, H_3	0.115	6.7
$(2,2)_+ \rightarrow (2,0)$	0.230	13.4
Out of plane transitions		
A_1, A_5	0.344	16.1
A_2, A_3	0.000	0.0
B_1', K_2, K_4	0.342	11.9
B_1, K_1, K_3	0.345	16.1
G_1, G_5	0.000	0.0
H_2	0.115	6.7
H_1	0.114	10.3
Next nearest neighbour transitions		
G_2, G_3	0.000	0.0
G_2', G_3'	0.345	16.1
G_6	0.114	10.3
G_7	0.115	6.7
G_8	0.342	11.9
G_9	0.344	16.1

See Table V (pg.73) for transition labelling

*in units of $[\frac{20}{9}\Gamma_0\sqrt{70\pi}(R_0/R)^5]^2 \times 10^{-2}$

**in MHz with X=0.2% and Γ_0 =20.15 GHz

The last three pairs have $J_A(\omega)=J_B(-\omega)$; i.e. they are mirror reflections about the line center, and hence the minus sign.

The computer produced $\mathcal{J}(\omega)$ have been plotted for each transition listed in table II. The apparent noise is due to the Ω grid not having enough points to evenly fill the energy bins of $\mathcal{J}(\omega)$. When the grid size in $\mathcal{J}(\omega)$ is increased the noise is considerably reduced. However, the resulting lineshape $J(\omega)$ is virtually unchanged. Fig.7 shows an example of $\mathcal{J}(\omega)$ and fig.8 the $J(\omega)$'s. In addition to the duplicate lineshapes already mentioned the following transitions, upon inspection of $\mathcal{J}(\omega)$, have essentially the same shapes:

a) $G_4, G_7, H_2, -B_3, -H_3$

b) $B_1, G_2', -G_3', K_1, K_3$

c) $A_1, -A_5, -G_9$

d) $B_1', -G_8, K_2, K_4$

e) H_1, G_6

In the first four groups each line has the same second moment and lineshape but in the last group the $\mathcal{J}(\omega)$'s as well as the second moments are not in exact agreement. Also $\mathcal{J}(\omega)$ in groups b) and c) are quite similar as are their second moments. These results show that their is little difference in $\mathcal{J}(\omega)$ for nn out-of-plane and nnn transitions between like states, whereas there is little similarity between nn in-plane transitions and identical transitions of the other two pair types. This is not transparent upon examination of $E(r,\Omega)$ in [17], [18] and [20].

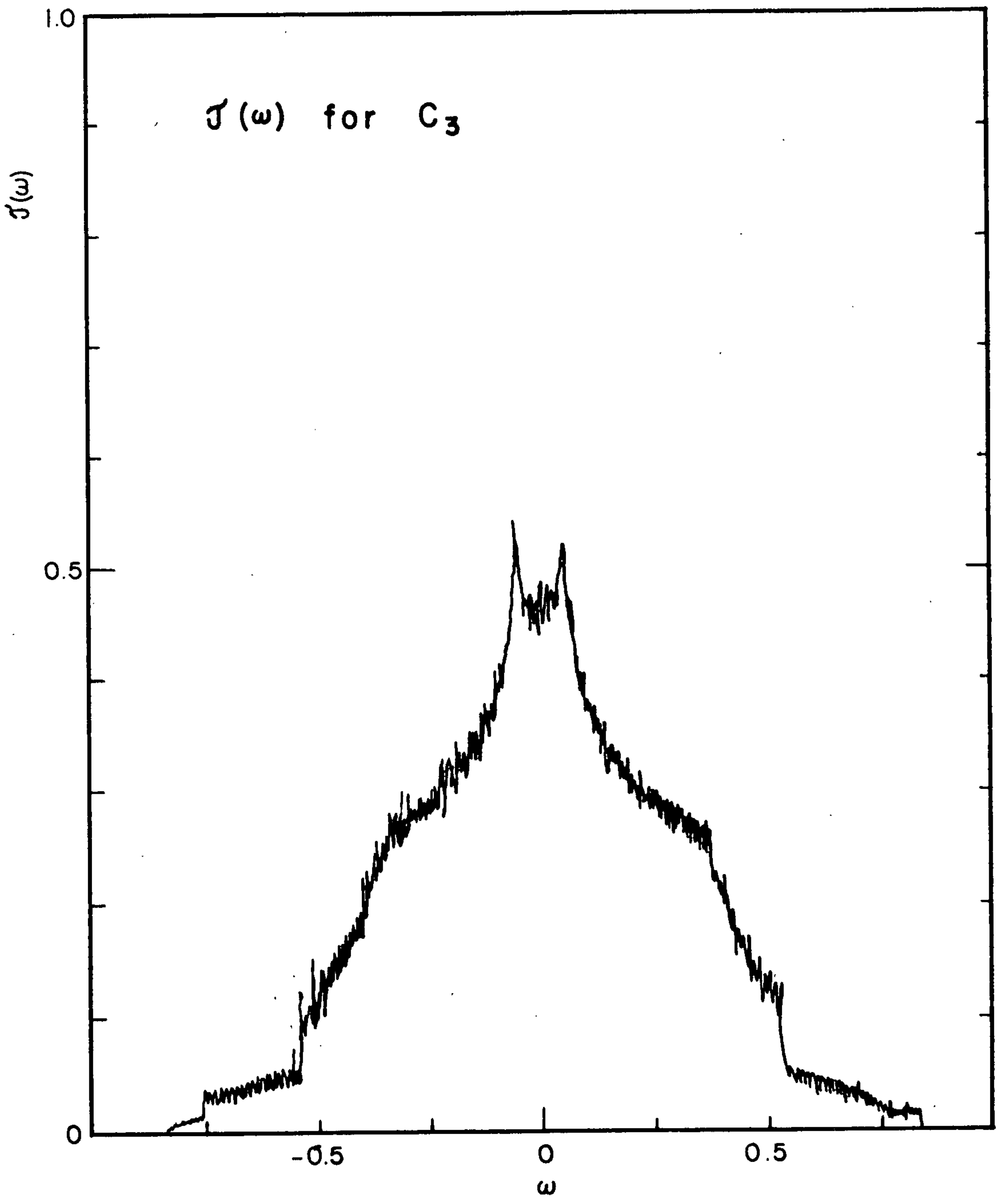

Figure 7 $\mathcal{J}(\omega)$ for the Transition C_3

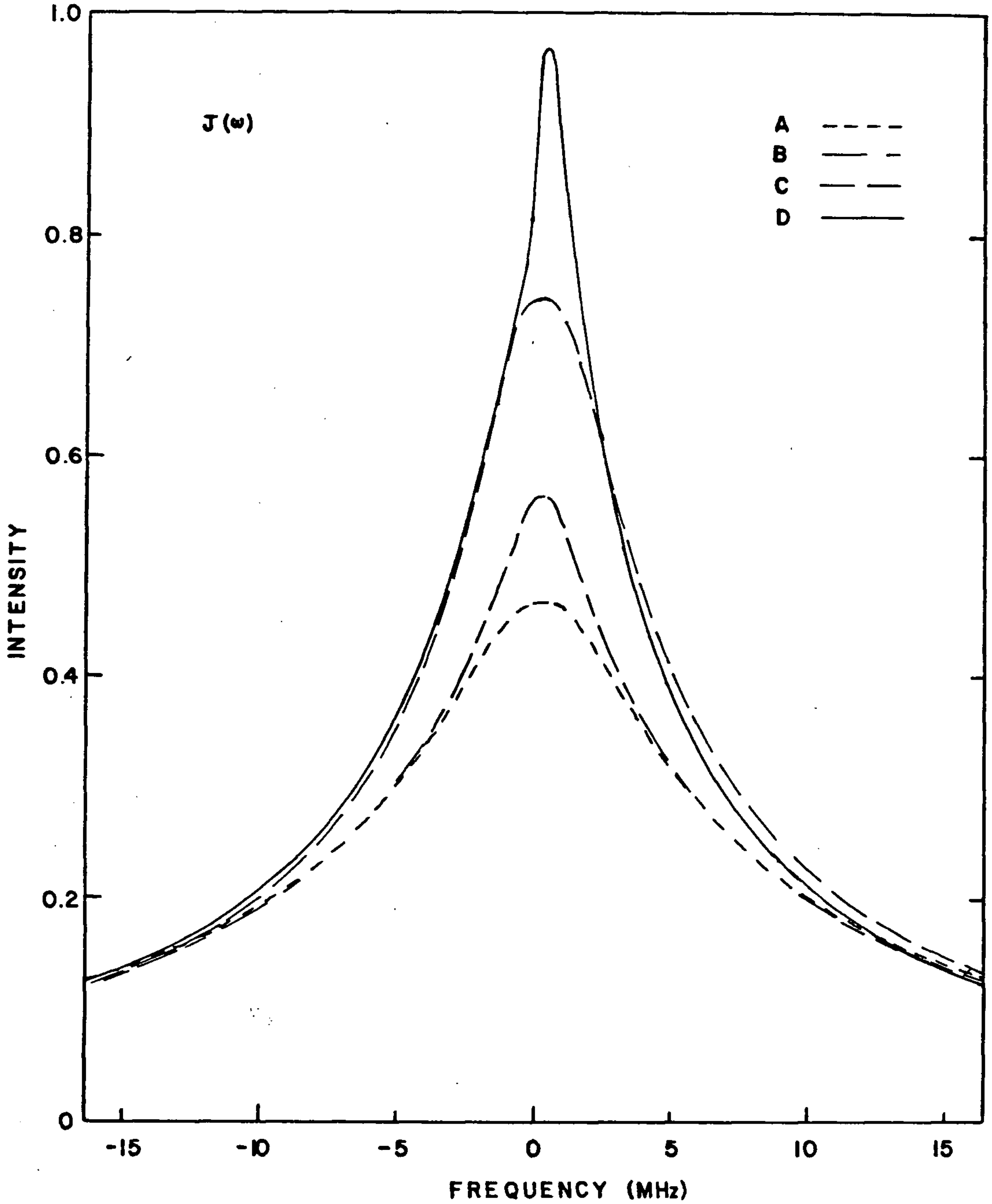

The lineshapes above correspond to A: C_1 ; B: C_3 ; C: G_6 ; and D: G_7 . See text for a complete list of identical lineshapes (pg. 43). Here we have taken X=0.2%.

Figure 8 Lineshapes $J(\omega)$

When considering two different transitions one expects identical $\mathcal{J}(\omega)$'s if they involve the same pair type and have the same coefficients ΔC and $\Delta C'$. However, if two transitions involving different pair types are considered it is not so clear why identical $\mathcal{J}(\omega)$'s can result even if the values of ΔC and $\Delta C'$ are identical for the two pair types.

The value of r_o is chosen to be about two lattice sites away from the pair. A comparison of the lineshape generated with this value of r_o and one with $r_o/2$ shows little change as would be expected. The numerical integration method used, which is poor for small ω, causes a dip in the center of $J(\omega)$. However, for small ω, $J(\omega)$ can be replaced with $\mathcal{J}(\omega)$ and this will give the peak height. Unfortunately the noise present in $\mathcal{J}(\omega)$ makes the value of $\mathcal{J}(0)$ difficult to determine and hence the linewidths will have an extra uncertainty associated with them. Also note that each line is essentially symmetric except near $\omega=0$.

As expected the transitions with similar $\mathcal{J}(\omega)$'s lead to similar $J(\omega)$ lineshapes. There are basically three values for the second moments of $\mathcal{J}(\omega)$ (see Table II) but there are four dissimilar linewidths (full width at half maximum). A narrow $\mathcal{J}(\omega)$ will produce a small linewidth and a broad $\mathcal{J}(\omega)$ will produce a large linewidth even though the second moments are identical. The second moment of $J(\omega)$ is defined by

$$[27] \qquad J_2 = \int \omega^2 J(\omega)\, d\omega = 4\pi a \left(\frac{r_o}{r_x}\right)^{10} \Gamma\left(-\tfrac{7}{3}, \frac{r_o^3}{r_x^3}\right) \int \omega^2 \mathcal{J}(\omega)\, d\omega$$

$$\simeq \frac{9}{7}\left(\frac{r_o}{r_x}\right)^3 \int \omega^2 \mathcal{J}(\omega)\, d\omega$$

At X=0.2% this gives for G_4 a value of 445 MHz for $(J_2)^{1/2}$ whereas the linewidth is only 6.7 MHz. This is due to the large contribution the wings make to the second moment. For large ω, $J(\omega) \sim \omega^{-8/5}$ which would lead to an infinite second moment if not for the finite extent of $J(\omega)$ set by r_0. This asymptotic behavior is in fact observed in the wings of the computer generated $J(\omega)$. Upon inspection of $J(\omega)$ the following transitions have the same lineshape:

a) B_1, G_2', G_3', K_1, K_3, A_1, A_5, G_9, B_2^+, C_1

b) B_1', G_8, K_2, K_4, B_2^-, C_3

c) G_4, H_3, B_3, H_2, G_7

d) H_1, G_6

The appearance of $\omega^{3/5} r_x^3$ in the expression for $J(\omega)$, [26] implies that the lineshape and line width scale in frequency by $X^{5/3}$ again in agreement with the results of Hama et.al. Since $\int J(\omega)d\omega$ has been normalized to unity then the amplitude of $J(\omega)$ as defined will scale as $X^{-5/3}$. Since the integrated intensity must be proportional to the number of ortho pairs, i.e. X^2, then the observed lineshape is proportional to $X^2 J(\omega)$ whose amplitude therefore scales as $X^{1/3}$.

In the model we have just treated the effect of the ortho molecules beyond the closest one to the pair are ignored. This tends to underestimate the linewidths. A more serious omission is the motional narrowing caused by correlation effects. In the work of Fujio et.al. it is found that the linewidth decreases by about 60% when these effects are included.

3.2 Phonon Broadening of the Ortho-H_2 Pair Spectrum

Phonon broadening of the ortho-H_2 pair levels becomes important at low ortho concentrations ($X \leqslant 0.05\%$) where the inhomogeneous broadening due to isolated ortho molecules is less than the homogeneous phonon broadening. Calculations done by Currie and Van Kranendonk have stimulated our interest in pursuing this matter further. The phonons couple to the pair levels through the EQQ and crystal field (CF) interactions which dominate the pair Hamiltonian. The four phonon processes considered here are the following:

a) Direct	D
b) First Order Raman	1R
c) Second Order Raman	2R
d) Anharmonic Raman	aR

The Feynman diagrams in fig.9 illustrate these processes. Other processes involving two or more incident or scattered phonons will be ignored. These phonon processes will in general be temperature dependent and hence can be distinguished from the temperature independent isolated ortho broadening effect. The line broadening is given by the transition rate (Heitler, 1949) calculated using the Golden Rule. For simplicity the transition rate is calculated for each process assuming it is the only one in effect.

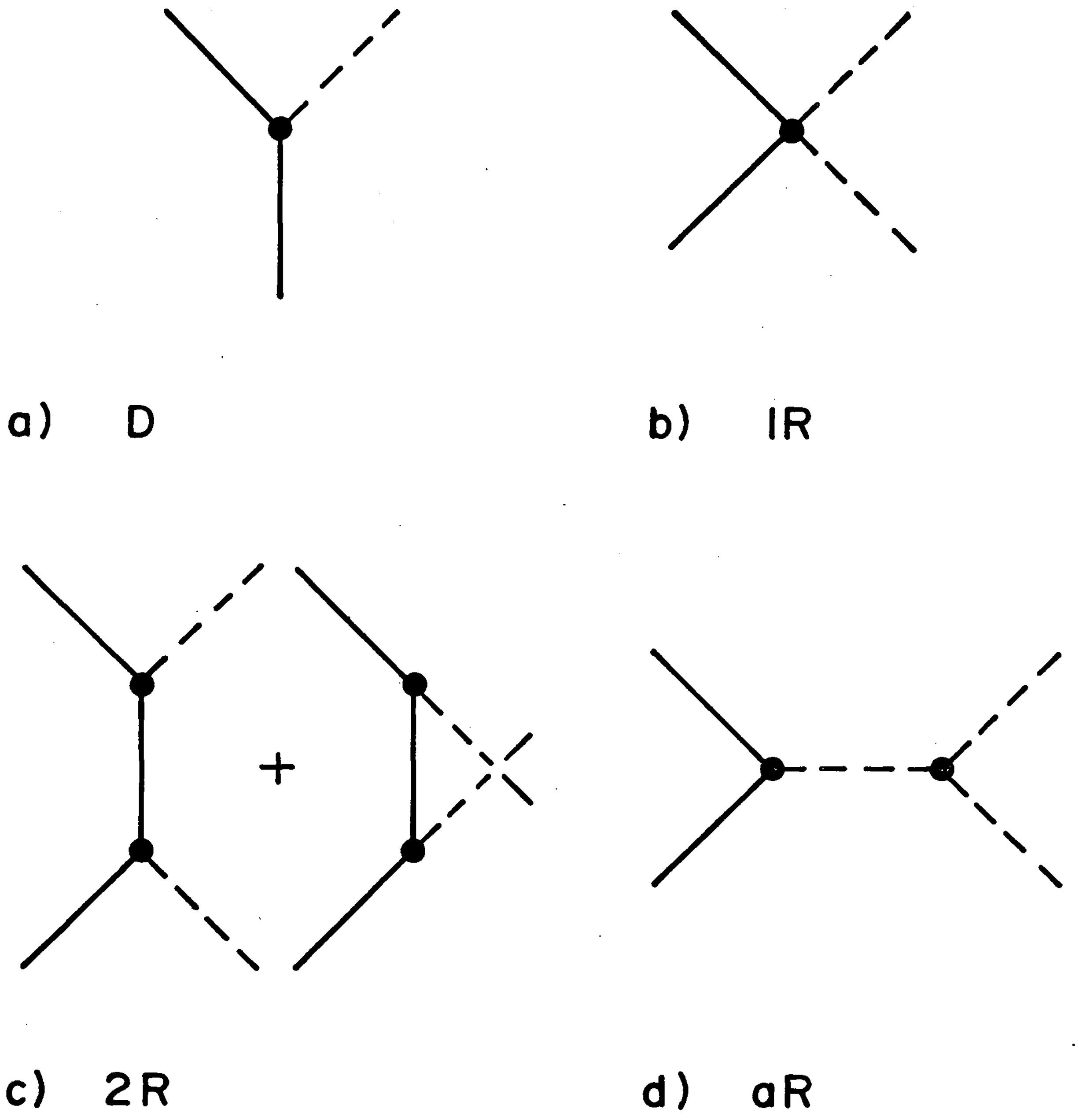

This figure illustrates the following phonon processes:
a) Direct b) First Order Raman c) Second Order Raman
d) Anharmonic Raman. The solid lines represent pair states and the dashed lines represent phonons.

Figure 9 Phonon Processes and Their Feynman Diagrams

The interaction Hamiltonian is selected from an expansion of either the EQQ or CF Hamiltonian in terms of the molecular displacements about the rigid lattice. The EQQ Hamiltonian is given by Harris (1970)

[28] $$\mathcal{H}_{EQQ} = \frac{20\pi\Gamma_0}{9}\sqrt{70\pi}\left|\frac{R_0}{r_{12}}\right|^5 \sum_{\mu,\nu} C(224;\mu\nu)\, Y_2^{\mu}(\omega_1)\, Y_2^{\nu}(\omega_2)\, Y_4^{*\mu+\nu}(\Omega_{12})$$

where ω_1 , ω_2 are the angles between the ortho molecular axes and the quantization axis , and r_{12} , Ω_{12} describe the position of one ortho molecule with respect to the other relative to the quantization axis. The crystal field interaction will be described by a local lattice distortion model where the surrounding para molecules deform about the ortho molecule. The CF Hamiltonian is given by Raich and Kanney (1977)

[29] $$\mathcal{H}_{CF}^{ij} = \sqrt{\frac{16\pi}{5}}\; B(R_{ij})\, Y_2^{0}(\Omega_{ij})$$

where $$B(R) = A e^{-\alpha R} - \frac{C}{R^6}$$

and R_{ij} is the distance between the ortho molecule i and a para molecule j and Ω_{ij} is the angle between the ortho molecular axis and $\vec{R}_{ij}$. The total CF Hamiltonian is obtained by summing over i=1,2 and j over the hcp lattice (excluding i).

The states used here are $|F,M\rangle|n\rangle$ where $|F,M\rangle$ is the pair state given in HBHII by

[30] $$|F,M\rangle = \sum_{m} C(11F;m,M-m)\, Y_1^{m}(\omega_1)\, Y_1^{M-m}(\omega_2)$$

and $|n\rangle = |\{n(\vec{k},\lambda)\}\rangle$ are the phonon states. In order to simplify the calculations the isotropic Debye model will be used.

Hence an

average velocity of sound will be used defined by $\frac{3}{v^3} = \frac{2}{v_t^3} + \frac{1}{v_\ell^3}$, as is done in the phonon density of states, where v_t and v_ℓ are the transverse and longitudinal velocities of sound.

Direct Process:

This process involves the emission of a phonon accompanied by a pair transition. The interaction Hamiltonian is given by $\vec{u}\cdot\vec{\nabla}H$ and hence the transition rate is

$$[31] \qquad W_D = \frac{2\pi}{\hbar} \sum_{n,\kappa,\lambda} P_{n_\kappa} \left| \langle F_f M_f | \langle n_k+1 | \vec{u}\cdot\vec{\nabla}H | n_k \rangle | F_i M_i \rangle \right|^2 \delta(\epsilon_i - \epsilon_f - \hbar\omega_\kappa)$$

The Boltzmann distribution, P_{n_κ}, describes the phonon populations and ϵ_i and ϵ_f are the energies of the initial and final pair states. The lattice displacement is quantized in terms of the phonon creation and annihilation operators $a^\dagger_{\vec{k},\lambda}$ and $a_{\vec{k},\lambda}$ where $\vec{k}$ is the wavevector and λ is the polarization of the phonon concerned. Now the lattice displacement at site i is given by

$$[32] \qquad \vec{u}_i = \frac{1}{\sqrt{N}} \sum_{\vec{q},\lambda} \sqrt{\frac{\hbar}{2m\omega_{\vec{q},\lambda}}} \left(a_{\vec{q},\lambda} + a^\dagger_{-\vec{q},\lambda} \right) \hat{\mathcal{E}}_{\vec{q},\lambda}\, e^{i\vec{q}\cdot\vec{R}_i}$$

where $\hat{\mathcal{E}}_{\vec{q},\lambda}$ is the polarization vector.

The following formula will be useful in evaluating the derivatives of H_{EQQ} and H_{CF} (Harris, 1970)

$$[33] \qquad R\,\nabla^{e} V(R)\, Y_n^m(\hat{R}) = \left(\frac{n+1}{2n+3}\right)^{1/2} C(1,n,n+1; e,m)\, Y_{n+1}^{m+e}(\hat{R}) \left[R\frac{d}{dR} - n \right] V(R)$$
$$- (-)^{e} \left(\frac{n}{2n+1}\right)^{1/2} C(1,n-1,n; e,-e-m)\, Y_{n+1}^{m+e}(\hat{R}) \left[R\frac{d}{dR} + n+1 \right] V(R)$$

Evaluating W_D for the EQQ process gives

[34] $$W_D^{EQQ} = \frac{17500}{33}\left(\frac{\Gamma_0}{\hbar}\right)^2\left(\frac{\Delta\epsilon}{\hbar}\right)^2 \frac{K_B T}{\rho v^5} \; S(F_i\, M_i\, F_f\, M_f) \sum_\lambda C^2(145;\lambda,\Delta M) \left| Y_5^{\Delta M+\lambda}(0,0)\right|^2$$

where $\Delta M = M_f - M_i$ and

[35] $$S(F_i M_i F_f M_f) = \sum_{m,m'} C(224;\, m-m',\, \Delta M+m'-m)\, C(11F_f;\, m, M_f-m)$$

$$\cdot\, C(11F_i;\, m', M_i-m')\, C(121;\, m', m-m')\, C(121;\, M_i-m', \Delta M+m'-m)$$

The high temperature expansion for n(k) has been used since $\frac{\Delta\epsilon}{K_B T}<1$ at T=4K where $\Delta\epsilon = \epsilon_i - \epsilon_f \lesssim 3K$. This gives rise to the linear temperature dependence of W_D. Upon calculation it is noted that $S(F_i, M_i, F_f, M_f)$ is non-zero only if $F_i = F_f = 2$. This is to be expected since the EQQ interaction only lifts the degeneracy of the F=2 states of the pair. Hence the EQQ processes only broaden the transitions involving $F_i = F_f = 2$. Also note the $\Delta\epsilon^2$ dependence of W_D. Next evaluating W_D for the CF process gives

[36] $$W_D^{CF} = \frac{32}{25} \; \frac{K_B T}{\rho \hbar^2 v^5} \; \left(\frac{\Delta\epsilon}{\hbar}\right)^2 (2F_i+1) W^2(21F_f1;1F_i) C^2(2F_iF_f;\Delta M, M_i) S(\Delta M)$$

where $S(\Delta M)$ involves a lattice sum which will be restricted to the nearest neighbours of the ortho molecule i of the pair. Because of the symmetry of the lattice with respect to the pair molecules one only needs to perform the lattice sum about one ortho molecule and then multiply the result by 2 (see HBHII).

[37] $$S(\Delta M) = \sum_\lambda \sum_{jj'} \left[2 - (\hat{R}_{jj'})^2\right] a_{j\lambda}\, a^*_{j'\lambda}$$

and

[38] $$a_{j\lambda} = \sqrt{\tfrac{3}{7}}\, C(123;\lambda,\Delta M)\, Y_3^{\Delta M+\lambda}(\omega_{ij}) \left[R_0 B' - 2B\right]$$

$$-(-)^\lambda \sqrt{\tfrac{2}{5}}\, C(112;\lambda,-\lambda-\Delta M)\, Y_1^{\Delta M+\lambda}(\omega_{ij}) \left[R_0 B' + 3B\right]$$

where $\omega_{1j} = (\beta, \gamma)$ is given by the Euler angles rotating the ortho(1)-para(j) frame into the pair frame and $\hat{R}_{jj'} = \frac{|\vec{R}_j - \vec{R}_{j'}|}{R_o}$.

For comparison the transition $C_{1,3}$; $|2,2\rangle \rightarrow |2,1\rangle$ will be considered at T=4K. The two processes discussed here yield

$$W_D^{EQQ} \sim 2 \times 10^6 \text{ rad/sec} \qquad W_D^{CF} \sim 1.4 \times 10^7 \text{ rad/sec}$$

It should be noted that other transitions with similar values for $\Delta\epsilon$ result in essentially the same transition rates.

First Order Raman Process:

This process involves the scattering of a phonon accompanied by a pair transition. It will be assumed that first the phonon is absorbed by the pair that then undergoes a transition and finally emits another phonon with random orientation and polarization with respect to the initial phonon. The interaction Hamiltonian is $\mathcal{H}' = \frac{1}{2!} \sum_{e,\eta} u_e u_\eta \frac{\partial^2 \mathcal{H}}{\partial u_e \partial u_\eta}$ where only the $a^\dagger a$ term is retained. The transition rate is now given by

$$[39] \quad W_{IR} = \frac{2\pi}{\hbar} \sum_{\substack{n,k,\lambda \\ i,f}} P_{n_k} \left| \langle n_f+1, n_i-1 | \langle F_f M_f | \mathcal{H}' | F_i M_i \rangle | n_f, n_i \rangle \right|^2 \delta(\Delta\epsilon + \hbar\omega_{k_i} - \hbar\omega_{k_f})$$

The sum over $\vec{k}$ is converted into an integral from k=0 to k_D, the Debye wave vector. After integrating over the delta function the other integral is carried out in the low temperature limit since $\Theta_D/T >> 1$ where $\Theta_D = \frac{\hbar v K_D}{K_B}$ is the Debye temperature. This approximation involves integrals of the form

$$\int_0^{\Theta_D/T} x^n e^x (e^x - 1)^{-2} dx \simeq \int_0^\infty x^n e^{-x} dx = n!$$

Upon calculation

$$[40] \qquad W_{IR}^{EQQ} = \frac{7.0\times10^{4}}{9\pi^2} S^2(F_iM_iF_fM_f)\frac{\Gamma_o^2}{e^2 v^3}\left(\frac{K_BT}{\hbar v}\right)^7 \sum_{\lambda_i,\lambda_f}\left|\frac{\partial^2 H}{\partial u_{\lambda_i}\partial u_{\lambda_f}}\right|^2$$

where

$$[41] \qquad \frac{\partial^2 H}{\partial u_{\lambda_i}\partial u_{\lambda_f}} = 95\sqrt{\frac{30}{143}}\, C(145;\lambda_f,\Delta M)\,C(156;\lambda_i,\Delta M+\lambda_f)\,Y_6^{*\Delta M+\lambda_i+\lambda_f}(0,0) + \Big[\frac{20}{11}(-)^{\lambda_i}C(145;\lambda_f,\Delta M)$$

$$\cdot C(145;\lambda_i,-\Delta M-\lambda_i-\lambda_f) - \frac{20}{9}(-)^{\lambda_f}C(134;\lambda_f,-\Delta M-\lambda_f)\,C(134;\lambda_i,\Delta M+\lambda_f)\Big]\,Y_4^{*\Delta M+\lambda_i+\lambda_f}(0,0)$$

$$+(-)^{\lambda_i+\lambda_f}\frac{10}{3}\sqrt{\frac{3}{7}}\,C(134;\lambda_f,-\Delta M-\lambda_f)\,C(123;\lambda_i,-\Delta M-\lambda_i-\lambda_f)\,Y_2^{*\Delta M+\lambda_i+\lambda_f}(0,0)$$

and

$$[42] \qquad W_{IR}^{CF} = 0.243\,(2F_i+1)\,W^2(21F_f1;1F_i)\,C^2(2F_iF_f;\Delta M,M_i)\frac{1}{e^2v^3}\left(\frac{K_BT}{\hbar v}\right)^7 S'(\Delta M)$$

where

$$[43] \qquad S'(\Delta M) = \sum_{\lambda_i,\lambda_f}\ \sum_{j,j'}\left[2-(\hat{R_{jj'}})^2\right] a_j^{\lambda_i\lambda_f}\, a_{j'}^{*\lambda_i\lambda_f}$$

and

$$a_j^{\lambda_i\lambda_f} = \frac{2}{3}\sqrt{\frac{3}{7}}\,C(123;\lambda_i,\Delta M)\,C(134;\lambda_f,\Delta M+\lambda_i)\,Y_4^{\Delta M+\lambda_i+\lambda_f}(\omega_{ij})\,(R_o^2B''-5R_oB'+6B)$$

$$-\Big[(-)^{\lambda_f}\frac{3}{7}\,C(123;\lambda_i,\Delta M)\,C(123;\lambda_f,-\Delta M-\lambda_i-\lambda_f)(R_o^2B''+2R_oB'-8B)$$

$$+(-)^{\lambda_i}\frac{2}{5}\,C(112;\lambda_i,-\Delta M-\lambda_i)\,C(112;\lambda_f,\Delta M+\lambda_i)(R_o^2B''+2R_oB'-3B)\Big]\,Y_2^{\Delta M+\lambda_i+\lambda_f}(\omega_{ij})$$

$$+(-)^{\lambda_i+\lambda_f}\sqrt{\frac{2}{15}}\,C(112;\lambda_i,-\Delta M-\lambda_i)\,C(101;\lambda_f,-\Delta M-\lambda_i-\lambda_f)(R_o^2B''+5R_oB'+6B)\,Y_0^{\Delta M+\lambda_i+\lambda_f}(\omega_{ij})$$

This process has a strong temperature dependence of T^7 and does not depend on $\Delta\epsilon$ as is to be expected of a Raman process. Again note that the EQQ process only broadens transitions with $F_i=F_f=2$.

Second Order Raman Process:

This process is the same as the first order Raman process except that now the pair changes to a virtual state before going to the final state. Energy is conserved only between the initial and final states. The virtual states used here will be the pair states and will not include higher rotational and rotational-vibrational states of the H_2 molecules. These latter states lie above the phonon band and will contribute to W_{2R} as $\Delta\epsilon^{-2}$ and hence can be ignored.

The interaction Hamiltonian is given by (Heitler 1949)

$$[44] \quad \mathcal{H}' = \sum_I \frac{\langle f|\vec{u}\cdot\vec{\nabla}\mathcal{H}|I\rangle\langle I|\vec{u}\cdot\vec{\nabla}\mathcal{H}|i\rangle}{\epsilon_i + \hbar\omega_{k_i} - \epsilon_I} + \frac{\langle f|\vec{u}\cdot\vec{\nabla}\mathcal{H}|I\rangle\langle I|\vec{u}\cdot\vec{\nabla}\mathcal{H}|i\rangle}{\epsilon_i - \hbar\omega_{k_f} - \epsilon_I}$$

where $|I\rangle$ is the virtual intermediate state. The two terms correspond to either a phonon first being absorbed and then one being emitted or a phonon being emitted first and then one being absorbed. Inserting the two interaction terms yields

$$[45] \quad W_{2R}^{EQQ} = \frac{12}{\pi}\left[\frac{17500}{33}\right]^2 \left(\frac{\Gamma_0}{\hbar}\right)^4 \frac{\hbar^2}{\rho^2 \quad v^5} \left(\frac{k_B T}{\hbar v}\right)^5 S$$

where

$$[46] \quad S = \sum_{\lambda_i,\lambda_f} \Bigg| \sum_I S(F_I M_I F_f M_f)\, S(F_i M_i F_I M_I) \Big[C(145;\lambda_f,\Delta M_f)\, C(145;\lambda_i,\Delta M_I) \cdot Y_{5\,(0,0)}^{*\Delta M_f+\lambda_f}\, Y_{5\,(0,0)}^{*\Delta M_I+\lambda_i} - C(145;\lambda_i,\Delta M_f)\, C(145;\lambda_f,\Delta M_I)\, Y_{5\,(0,0)}^{*\Delta M_f+\lambda_i}\, Y_{5\,(0,0)}^{*\Delta M_I+\lambda_f} \Big] \Bigg|^2$$

and $\Delta M_f = M_f - M_I$, $\Delta M_I = M_I - M_i$ Also

$$[47] \quad W_{2R}^{CF} = \frac{2\cdot 16^3}{1875\,\pi}(2F_i+1)\frac{1}{\rho^2 R_0^{\,2} v^3}\left(\frac{k_B T}{\hbar v}\right)^5 \sum_{I,I'} B_I B_{I'} \Big[S_{\lambda_i}^{\Delta M_1 \Delta M_1'} S_{\lambda_f}^{\Delta M_2 \Delta M_2'} - S_{\lambda_i}^{\Delta M_1 \Delta M_2'} S_{\lambda_f}^{\Delta M_2 \Delta M_1'} \Big]$$

where

[48] $$S_\lambda^{m,n} = \sum_\lambda \sum_{j,j'} \left[2-(\hat{R}_{jj'})^2\right] a_{j\lambda}^m a_{j'\lambda}^n$$

$a_{j\lambda}^m$ and $\hat{R}_{jj'}$ are as before and

$$B_I = \sqrt{3(2F_I+1)}\; W(2 1 F_I 1; 1 F_i)\, W(2 1 F_f 1; 1 F_I)\, C(2 F_i F_I; \Delta M_i, M_i)\, C(2 F_I F_f; \Delta M_f, M_I)$$

The sum over I is the sum over intermediate states. This process is also evaluated in the low temperature limit and yields a T^5 dependence, to be contrasted with T^7 for the first order Raman process.

Anharmonic Raman Process:

This process has been discussed by Van Kranendonk and Walker (1968) and is a second order process involving the direct process and the scattering of the resulting phonon with another one. This phonon scattering does not occur in a harmonic lattice. The intermediate phonon does not have to conserve energy and hence does not contribute to the temperature dependence of W_{aR}. Hence this process will have the temperature dependence of W_{1R}. Van Kranendonk and Walker (1968) estimate that $W_{aR} \simeq 100\, W_{1R}$.

Of the two interactions considered the crystal field interaction is dominant. The direct process and the anharmonic Raman crystal field process are of the same order of magnitude at 4K. However most of the experimental data is taken at T=1-2K where the direct CF process is dominant. This process is proportional to $\Delta\epsilon^2 T$ and results in a linewidth of about 1 MHz at T=2K for the $C_{1,3}$ transitions. In summary, tables III and IV list the effect these processes have on the linewidth of two lines at various temperatures.

TABLE III

Summary of Transition Rates

Process	Transition Rate	M_{if} (C_3)
W_D^{CF}	$\frac{k_B T}{\rho \hbar^2 v^5}\left(\frac{\Delta\epsilon}{\hbar}\right)^2 M_{if} = 4.51\times10^{37}\ \mathrm{erg}^{-2}\,\mathrm{sec}^{-1}\,M_{if}$	$3.16\times10^{-31}\ \mathrm{erg}^2$
W_D^{EQQ}	$\left(\frac{\Gamma_0}{\hbar}\right)^2\left(\frac{\Delta\epsilon}{\hbar}\right)^2 \frac{k_B T}{\rho v^5} M_{if} = 8.06\times10^{5}\ \mathrm{sec}\ M_{if}$	$2.65\ \mathrm{sec}^{-2}$
W_{1R}^{CF}	$\frac{1}{\rho^2 v^3}\left(\frac{k_B T}{\hbar v}\right)^7 M_{if} = 9.90\times10^{32}\ \mathrm{erg}^{-2}\,\mathrm{sec}^{-1}\,M_{if}$	$1.00\times10^{-28}\ \mathrm{erg}^2$
W_{1R}^{EQQ}	$\frac{\Gamma_0^2}{\rho^2 v^3}\left(\frac{k_B T}{\hbar v}\right)^7 M_{if} = 1.77\times10^{1}\ \mathrm{sec}^{-1}\,M_{if}$	1.26×10^{2}
W_{2R}^{CF}	$\frac{1}{\rho^2 R_0^2 v^3}\left(\frac{k_B T}{\hbar v}\right)^5 M_{if} = 4.27\times10^{34}\ \mathrm{erg}^{-2}\,\mathrm{sec}^{-1}\,M_{if}$	$1.35\times10^{-28}\ \mathrm{erg}^2$
W_{2R}^{EQQ}	$\left(\frac{\Gamma_0}{\hbar}\right)^4 \frac{\hbar^2}{\rho^2 v^5}\left(\frac{k_B T}{\hbar v}\right)^5 M_{if} = 1.03\ \mathrm{sec}^{-1}\ M_{if}$	2.35×10^{3}

Values of constants used are as follows:

$T = 4$ K $\quad \Delta\epsilon = 87$ GHz

$\Gamma_0 = 20.15$ GHz $\quad R_0 = 3.784$ Å (HBHI)

$\rho = 0.08868$ g/cc (V.V. Goldman)

$v_l = 2.19\times10^{5}$ cm/sec ; $v_t = 1.16\times10^{5}$ cm/sec (Bezuglyi and Minyfaev)

$A = 7.247\times10^{-11}$ erg $\quad \alpha = 3.425$ Å^{-1} $\quad C = 5.970\times10^{-13}$ erg Å^{6} (Raich and Kanney)

TABLE IV

Phonon Induced Linewidths for G_1 and C_3

Process	Temperature	G_1 FWHM (MHz)	C_3 FWHM (MHz)
W_0^{CF}	1.2 K	0.02	0.7
	2.1 K	0.04	1.2
	4.0 K	0.08	2.2
W_0^{EQQ}	1.2 K	0.002	0.10
	2.1 K	0.004	0.17
	4.0 K	0.008	0.33
W_{1R}^{CF}	1.2 K	-	-
	2.1 K	<0.001	<0.001
	4.0 K	0.016	0.016
W_{1R}^{EQQ}	1.2 K	-	-
	2.1 K	-	-
	4.0 K	<0.001	<0.001
W_{2R}^{CF}	1.2 K	0.002	0.002
	2.1 K	0.04	0.04
	4.0 K	0.92	0.92
W_{2R}^{EQQ}	1.2 K	-	-
	2.1 K	-	-
	4.0 K	<0.001	<0.001
W_{aR}^{CF}	1.2 K	<0.001	<0.001
	2.1 K	0.02	0.02
	4.0 K	1.60	1.60
W_{aR}^{EQQ}	1.2 K	-	-
	2.1 K	<0.001	<0.001
	4.0 K	0.035	0.035

Note that results quoted for G_1 are obtained by scaling those for C_3 appropiately.

3.3 Isotopic Impurity Broadening:

The presence of the isotopic impurities of HD and D_2 in solid H_2 can cause an inhomogeneous broadening of the pair lines via the strain field surrounding the impurity site. Since HD and D_2 have virtually the same intermolecular potential as H_2, the effect is due entirely to the different mass. In particular, the heavier molecules have less zero point motion and this tends to pull the lattice in towards the mass defect. For an isotropic solid the strain field at $\vec{r}$ is proportional to r^{-2} where $\vec{r}$ is the vector from the impurity site to a point in the lattice. Therefore the shift in the pair frequencies for a single defect is proportional to r^{-3}. At finite concentrations, one has to find the distribution of strains produced by the randomly situated impurities.

The calculation of the lineshape proceeds as follows. A random distribution of impurities with concentration c is arranged about a single ortho pair in an otherwise pure para H_2 lattice. One first calculates the strain at the pair site due to each impurity and then adds these strains to obtain a total frequency shift. This is repeated for all possible configurations and a spectral distribution function is formed from the results. A Lorentzian line shape is obtained which might be expected of a r^{-3} interaction (cf. the case of dipolar broadening in NMR (Abragam, 1961)).

This problem is solved on a computer using a Monte Carlo program. A random configuration of impurities in an hcp lattice is formed out to a predetermined radius from the pair. The frequency shift is then calculated assuming the transition frequencies scale as $|\vec{r}_1 - \vec{r}_2|^{-5}$ since the EQQ interaction makes by far the largest contribution to the separation of the pair levels. The shift is then recorded and a histogram of shifts is formed from N configurations. The lineshapes obtained are then fitted to a Lorentzian and a Gaussian and the results compared.

The ortho separation displacement $\Delta\vec{u}$ is assumed to be given by

[49] $$\Delta\vec{u} = A\left(\frac{\vec{r}_1}{r_1^3} - \frac{\vec{r}_2}{r_2^3}\right)$$

where $A = \frac{\delta r_0}{r_0}$ the fractional shift of the nearest neighbor distance. In a discrete lattice the actual motion close to the impurity may be far from isotropic. Here we are mainly concerned with the asymptotic behaviour away from the impurity which we assume to be isotropic. Fig.10 illustrates the relationships between impurity and pair molecules. Expanding $\vec{r}_1$ and $\vec{r}_2$ in terms of r and θ gives

[50] $$\left|\vec{u}_{12} + \Delta\vec{u}\right|^2 = u_{12}^2 + \frac{2Au_{12}^2}{r^3}\left(3\cos^2\theta - 1\right) + O(r^{-5})$$

so that

[51] $$\frac{\delta f}{f} = \frac{-5\,\delta u}{u_{12}} \simeq \frac{-5A}{r^3}\left(3\cos^2\theta - 1\right)$$

Since $\int d\Omega(3\cos^2\theta - 1) = 0$ then the spectral distribution of an

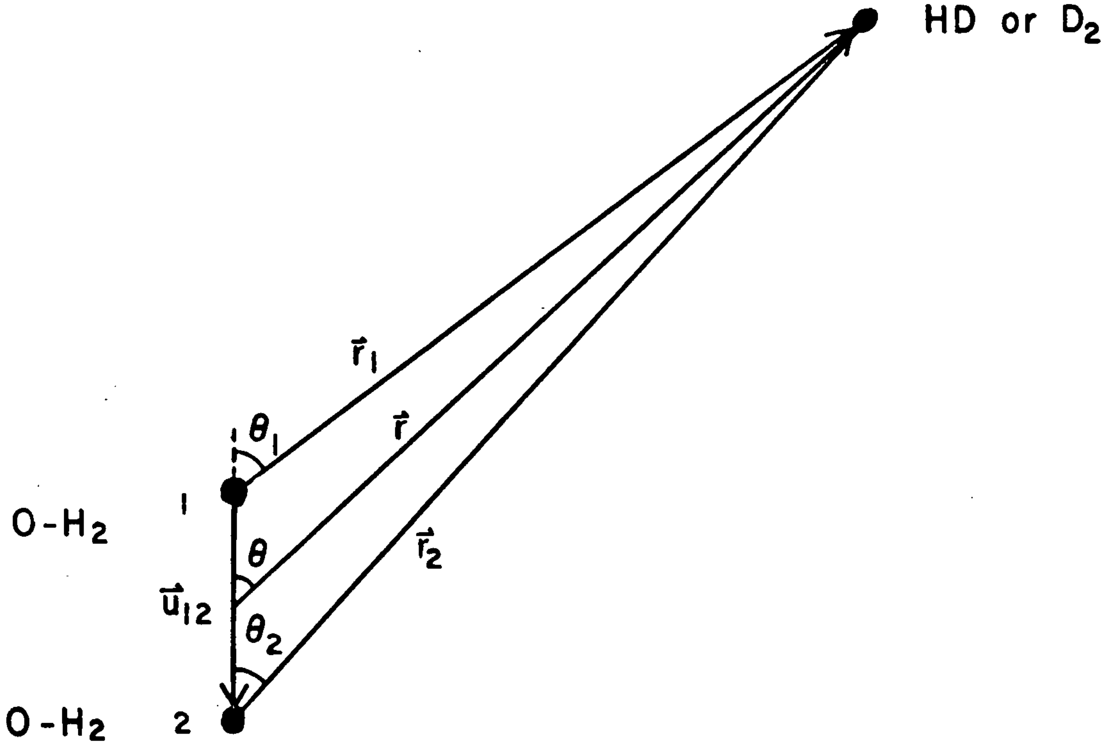

Figure 10 Ortho Pair-Impurity Configuration

impurity molecule situated on a shell of radius r has an average value of zero. This implies that for this model the average value of the pair frequencies will not change. One can see immediately from [51] that the full width at half maximum, is proportional to $f_0 A$. Furthermore one expects a linear dependence on the impurity concentration as for the dipolar broadening case (see Abragam, 1961 and Hama et.al., 1972).

A typical lineshape is shown in fig.11 where $c=3X10^{-4}$, the natural abundance of HD, along with the fitted Lorenztian. Attempts to fit a Gaussian to the lineshape give very poor agreement whereas the Lorenztian gives an excellent fit. A plot of fitted linewidths vs. c is shown in fig.12 confirming the linear dependence of $\Delta\nu$ on c. Note that the linearity breaks down at higher concentrations. Each of the points at c=0.03% were computed with a different set of random configurations of impurity sites as well as varying maximum radii. The value used for A is 0.01. From this graph one gets

[52] $$\Delta\nu = 85.7\ f_0 A c$$

The average frequency shifts from zero are negligible as expected.

In the calculation so far it has been assumed that the lattice constant remains fixed at infinity and hence the molar volume does not change. This is not the case for a real crystal where one finds for an elastically isotropic crystal (Krivoglas, 1969) that the strain at a point r from an impurity site is given by

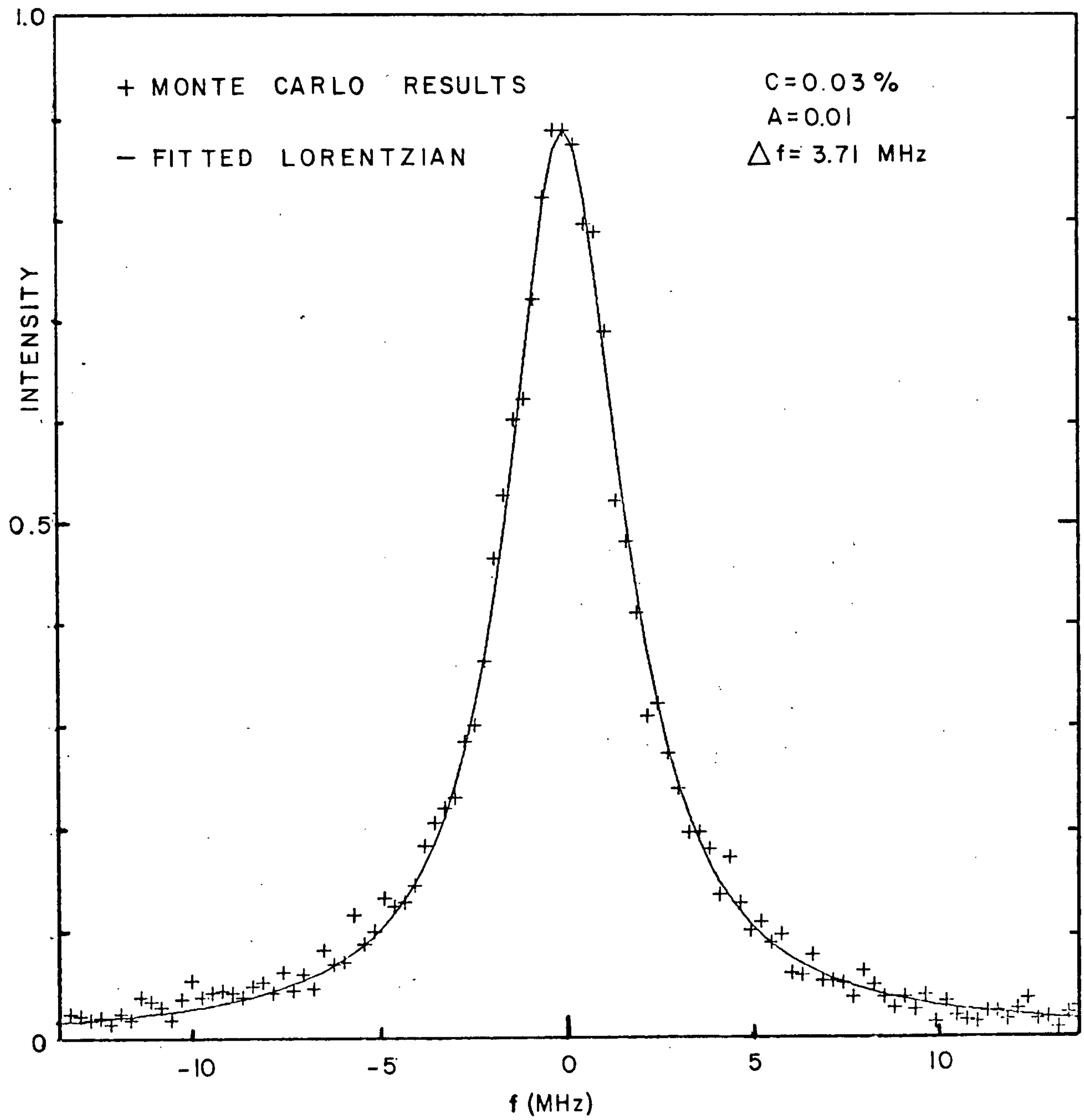

Figure 11 Lineshape Due To Isotropic Mass Defect Impurities

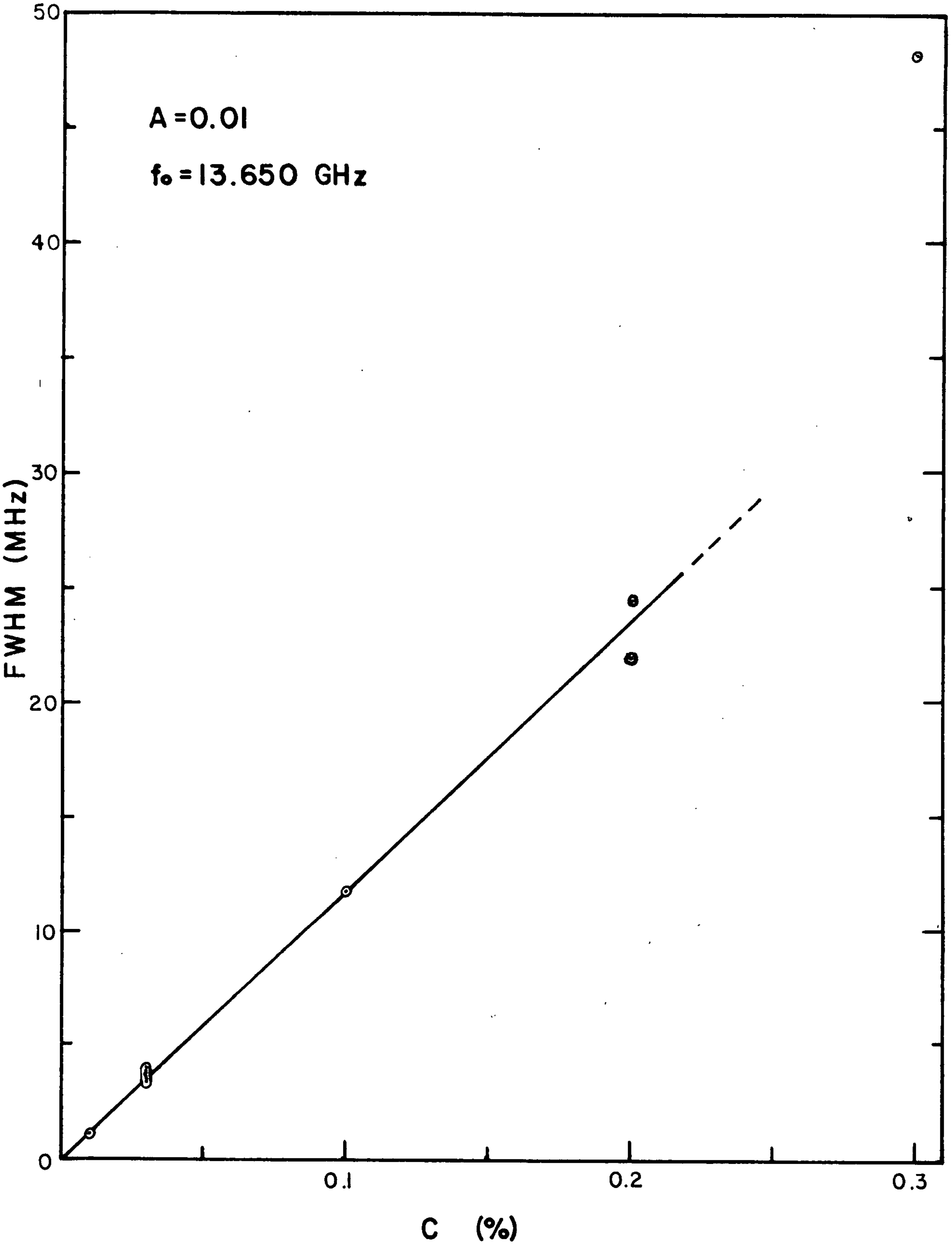

Figure 12 Impurity Concentration Dependence of Linewidths

[53] $$\delta\vec{r}(\vec{r}) = \frac{1}{12\pi}\left(\frac{1+\nu}{1-\nu}\right)\frac{d\upsilon}{dc}\frac{\vec{r}}{r^3}$$

where ν is Poisson's ratio of the host and $\frac{\partial\upsilon}{\partial c}$ is the change in unit volume due to a concentration c of impurities. In this way one can relate the change in molar volume to the asymptotic strain fields and hence determine the value of A.

One way to obtain $\frac{\partial\upsilon}{\partial c}$ is to consider the shift in the average frequency, Δf, of the pair lines due to the lattice contraction.

[54] $$\frac{\Delta f}{f_o} = -\frac{5\Delta r}{r} = -\frac{5}{3}\frac{c}{\upsilon}\frac{d\upsilon}{dc}$$

Now, with [52] and [53], the full width at half maximum (FWHM) of the lineshape is given by

[55] $$\Delta\nu = 1.61\ f_o c\left(\frac{1+\nu}{1-\nu}\right)\frac{1}{\upsilon}\frac{d\upsilon}{dc} = 0.966\left(\frac{1+\nu}{1-\nu}\right)\Delta f$$

There is another complication when considering HD as the impurity. The center of mass is not coincident with the geometric center of the molecule and hence it rotates off center. This would have the tendency to expand the lattice, opposing the zero point motion effect. Since the rms zero point motion is comparable to the H-D bond length then these two effects are of the same order and would lead to a smaller distortion effect. One could perhaps determine this experimentally by comparing the strain fields for HD to that of D_2 (correcting for the fact that the mass defect for D_2 is larger).

CHAPTER IV Experiment

4.1 Cryostat:

The ortho pair absorption intensities are expected to be quite weak (HBHI). Therefore transmission spectroscopy would involve detecting very small changes in the transmitted power. Instead the power absorbed is measured directly using a calorimetric technique. The solid H_2 sits in a niobium cell forming the bottom of a shorted waveguide (see fig.13). After the microwave energy is absorbed by the pairs it is released to the solid causing a temperature rise in the sample. The temperature change is detected with a 31 element thermopile whose output is measured with a nanovoltmeter.

The niobium cell (described in HBHI) contains the solid H_2 in its bottom half. The cell is filled with H_2 up to the step. This step is constructed with the dimensions of the waveguide reduced by $\sqrt{\epsilon}=1.14$ where ϵ is the dielectric constant of solid H_2. This is done to avoid mismatch in the characteristic impedance of the waveguide due to the hydrogen. When working with frequencies well above the fundamental band of the waveguide trapped modes can exist in the unstepped waveguide. These modes then resonate at certain frequencies causing a multitude of absorption peaks, the energy being dissipated by absorption in the Nb. The step eliminates most of these resonances, the rest of which can then be distinguished from the H_2 absorptions because of the lack of temperature dependence of

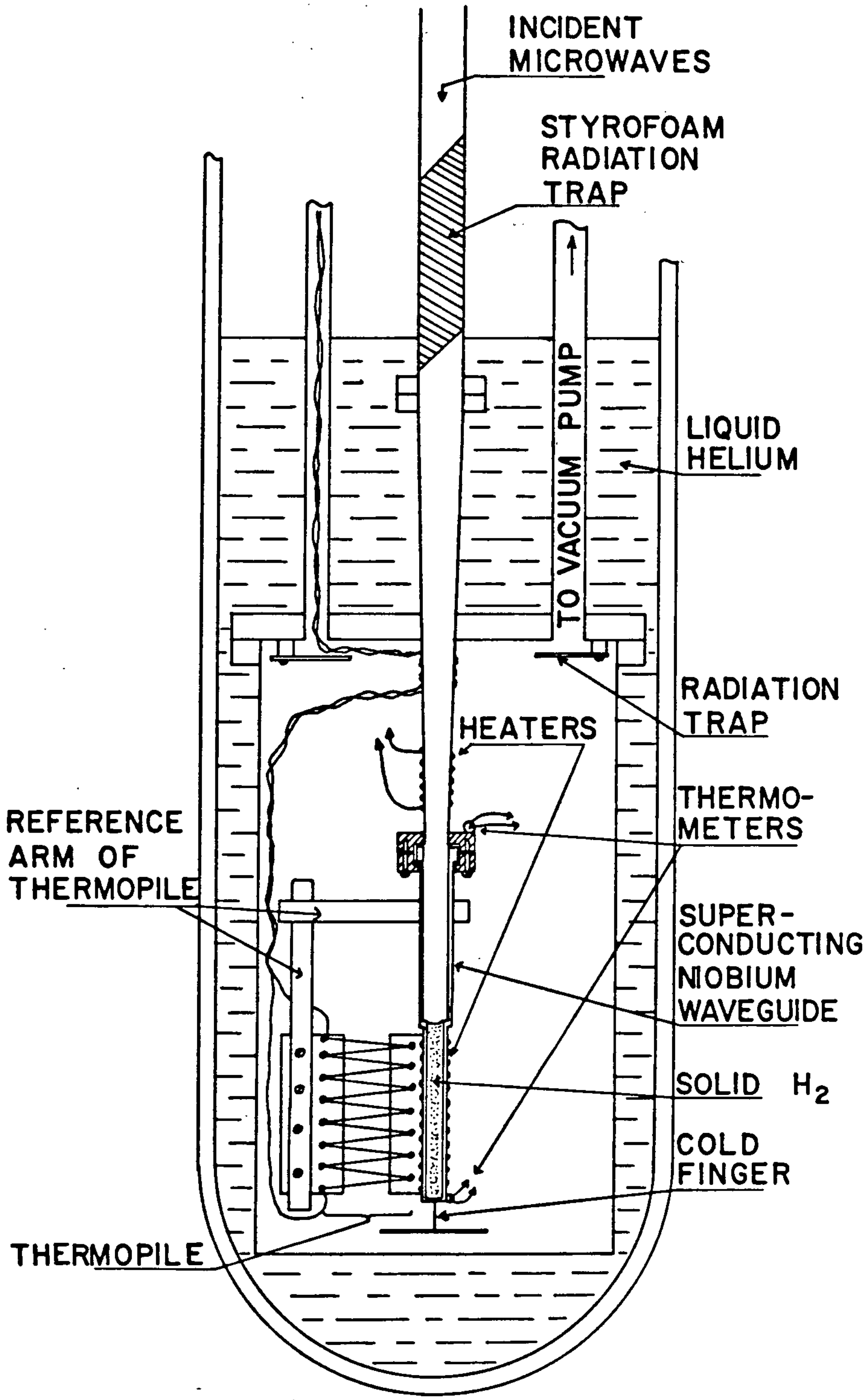

Figure 13 Cryostat

their intensities.

The niobium cell is superconductiong below 9 K and therefore has a low thermal conductivity which thermally isolates the H_2 sample from the thermal bath. The thermopile consists of 31 Au(0.07% Fe)-Nb elements with a sensitivity of 5 μK at T=1.2 K. One side of the thermopile is connected to a copper assembly clamped to the waveguide above the sample serving as the reference arm. The other side of the thermopile is connected to a copper sheet wrapped around and bonded to the cell to provide good thermal contact between the cell and the thermopile. The cell walls are thin enough (0.4mm) that the temperature drop between the H and the copper sheet is small. Mounted on this copper sheet is a heater resistor used to calibrate the sensitivity of the system thereby allowing quantitative measurments of the H_2 absorptions. The large thermal mass of copper and hydrogen leads to a cell response time of about 2 seconds. This puts an upper limit on the microwave scanning rate.

The source of microwaves is the computer controlled spectrometer. The spectral width of the source is much less than the smallest absorption linewidth. Therefore if the scanning rate is chosen slow enough the lineshape measured will represent the absorption lineshape. Standing waves between the source and the bottom of the cell cause the power incident on the cell to change with frequency and thus affects the background absorption. The background absorption also varies across the band since the delivered power is not uniform even when the microwave source is levelled. This necessitates the division of two spectra with different line intensities in order to eliminate the background. This process will be described later.

4.2 Sample Preparation:

At room temperature the equilibrium concentration of the ortho to para species is 3:1. In order to reduce the ortho concentration, the liquid H_2 sample is is placed in contact with a paramagnetic catalyst ($Fe(OH)_3$ powder). The equilibrium ortho concentration is given by $n_o \simeq 9e^{-2B/k_BT} = 9e^{-170.8/T}$. This allows one to obtain ortho concentrations down to 0.004% at T =13.8 K, the triple point. The liquid is circulated through the catalyst by convection heating to ensure an even concentration distribution. The gas above the liquid and in the connecting tubes is flushed out regularly with converted vapour in an attempt to reduce the regions of high ortho concentration. The conversion process can be monitered down to $n_o \simeq 1\%$ with a standard thermal conductivity bridge. One can then estimate the time needed to complete the conversion.

After the equilibrium ortho concentration has been reached the sample is transferred to a metering bulb and then immediately condensed into the cell to keep any back conversion at room temperature to a minimum. For the purposes of condensation and growth a small amount of liquid He is transferred into the dewar, up to the flange on the bottom vacuum can. Once in the cell the solid is melted with the waveguide heater and with He exchange gas in the stainless steel can surrounding the cell a positive temperature gradient is maintained with respect to the cell bottom. The cell temperature is then slowly lowered using a temperature controller and the solid starts growing from the bottom of the cell. The cold finger mounted on the bottom of the cell should induce nucleation to occur first at the center of the cell bottom. If the solid then grows from this nucleation center it should be possible to obtain a single crystal. The growing time is about one-half hour and is monitored by recording the temperature gradient in the cell with the thermopile. After the sample has solidified it is slowly cooled to about T=10 K. By the time this temperature is reached most of the thermal contraction in the solid has taken place. Since the H_2 sticks to the cell walls a large amount of strain exists which must then be removed. By pumping on the solid and applying heat pulses to the cell walls with one of the two heaters, one attempts to break the sample away from the walls. After this procedure the sample is annealed for about an hour in order to remove as many internal strains as possible. The total amount of time to grow and anneal the sample is limited by the length of time the liquid helium lasts. The final step is to gradually cool the sample to 4 K and then fill the dewar with liquid heluim, taking care not to heat up the cell with warm gas.

Originally only the waveguide heater was present and this was used to break the sample away from the walls. In an attempt to obtain a better success rate in breaking away samples, another heater was installed on the copper sheet at the bottom of the cell. This was done in order to supply a uniform heat pulse to all portions of the cell walls. The effect differs from that of the waveguide heater, where a heat pulse would travel down the waveguide and reach the top portion of the sample first.

After preparing many samples it became apparent that the new heater caused more problems than it solved. Less power was needed than for the waveguide heater and before the correct amount was discovered, several samples had been popped out of the cell. Apparently the combination of a large heat pulse to the cell walls and the pumping forced the H_2 solid out of the cell and up the waveguide where it then attatched itself. This fact was deduced from the absence of H_2 vapour pressure upon low level heating using the new heater but the presence of H_2 vapour when the waveguide heater was used. Confirming this was the thermopile response to a pulse given the cell heater which indicated the absense of any thermal mass associated with the H_2 sample.

In an attempt to reduce the amount of hydrogen melting at the walls during each heat pulse, the pulse width was reduced from 5 seconds to 0.5 seconds. While this was enough to relieve some of the stress caused by sticking to the walls it also caused shifts in the line centers. One sample showed three lines near G_5, a narrow one in the usual position and two broader components shifted downwards in frequency, suggesting the presence of at least three fairly uniformly strained crystallites. Upon regrowing this sample and applying long heat pulses to the new heater these duplicate lines did not appear. Subsequent regrowths with heat pulses to the waveguide heater also failed to cause the unusual shapes to materialize. This appears to eliminate one of our concerns, namely the possibility of impurities affecting the pair frequencies.

These experiences show that the improvements to the cell and growing procedures have probably resulted in larger and fewer crystallites being produced. Unfortunately this was accompanied by line replicas which severely complicated the data analysis. Subsequently the waveguide heater was used exclusively to apply heat pulses to the sample.

CHAPTER V Experimental Results

5.1 Data Analysis:

In order to obtain the absorption lineshape $\delta(\omega)$, one must correct the raw data for variations in the incident power $P_o(\omega)$. This can be done only if the hydrogen absorption changes relative to the absorption in the niobium walls. This can happen in two different ways. One is due to the change in Boltzmann factors when the temperature is changed and the other is due to ortho molecule clustering which causes the number of pairs to change in time. The latter occurs through the ortho-para exchange mechanism (Amstutz et.al. 1968; Oyarzun and Van Kranendonk 1971,1972). Following HBHI the initial spectrum is described by

[56] $S_o(\omega)=P_o(\omega)[1+\delta(\omega)]$

where $\delta(\omega)$ is the hydrogen absorption relative to that of the niobium. The enhanced spectrum is given by

[57] $S_t(\omega)=\alpha P_o(\omega)[1+(1+\beta)\delta(\omega)]$

where β reflects the change in the enhancement factor. From this one can obtain the incident power spectrum as follows:

[58] $P_o(\omega)=S_o(\omega)+\frac{1}{\beta}[S_o(\omega)-\frac{1}{\alpha}S_t(\omega)]$

The constant α can be determined precisely since it is either due to changes in the nanovoltmeter scale or changes in the thermopile sensitivity with temperature. However β is not so well determined. It can be calculated in principal if temperature changes and clustering are taken into account but the latter is especially difficult to determine precisely when it occurs simultaneously with a gradual temperature change. Fortunately there is another way to estimate β. The lineshapes are in general much narrower than the standing wave pattern. Therefore one can vary β in such a way as to subtract the sharp hydrogen absorption signal from the raw data leaving only the broad standing wave pattern. Once $P_o(\omega)$ is determined then

[59] $$\delta(\omega) = \frac{S_o(\omega)}{P_o(\omega)} - 1$$

If there is a large noise component to $\delta(\omega)$ then the spectrum can be passed through, for example, a low pass gaussian filter to remove the noise. This broadens the lines but is useful in bringing out the weak ones.

5.2 New Lines:

The spectroscopy reported in HBHI covers most of the transitions one is able to observe with this technique. A few more lines have been observed with the addition of the higher frequency millimeter wave source, and six low intensity lines have been observed with the help of computer ratioing. In addition, the lines G_6 and G_7 have been reassigned. Energy level diagrams for the three pair types are shown in fig.14 along with the observed transitions. Table V contains a list of all observed transitions with some of their properties.

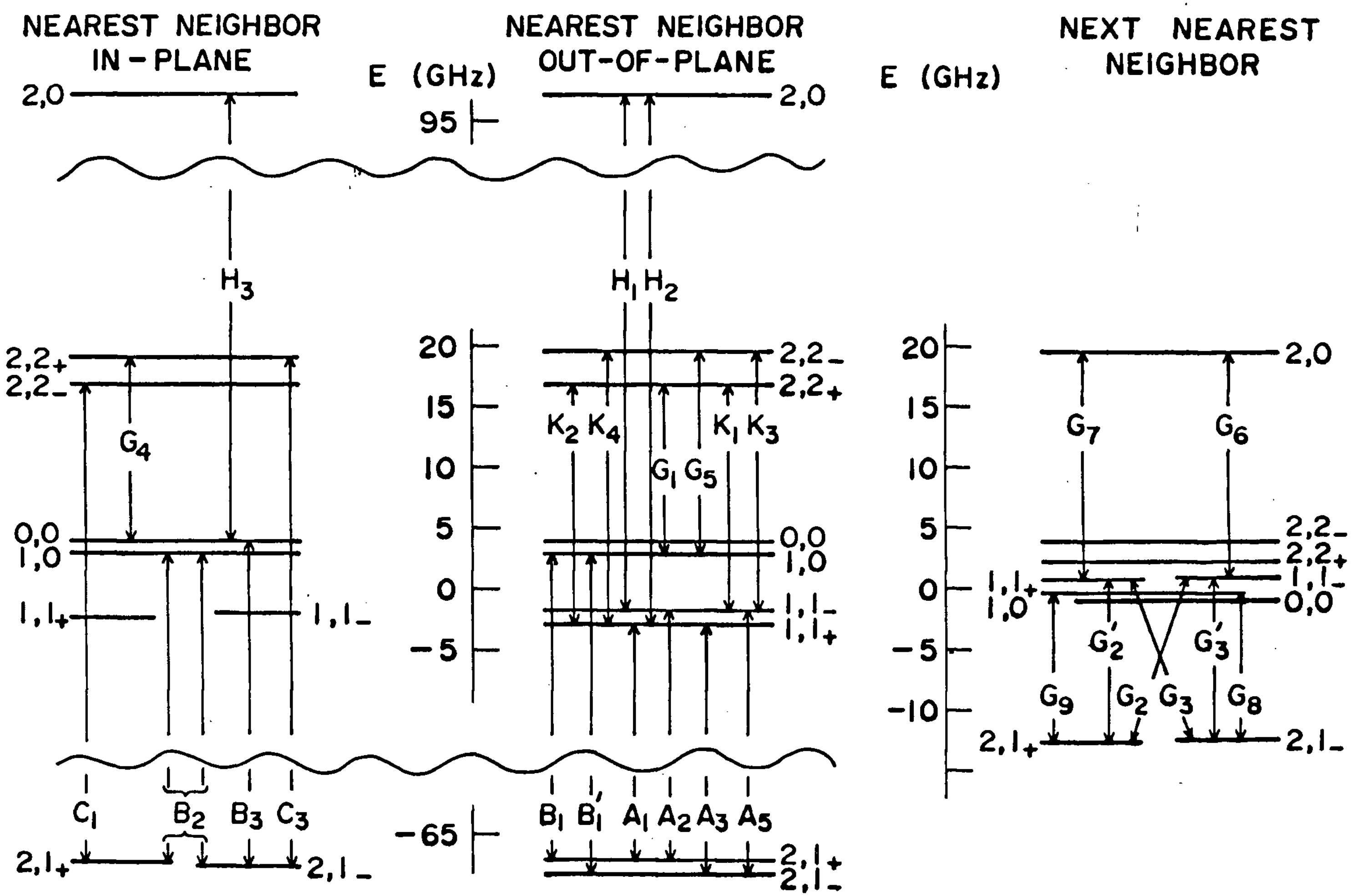

Figure 14 Ortho Pair Energy Levels

Table V Observed Ortho Pair Transitions

Line	Assignment	Frequency (GHz)
Nearest neighbour out-of-plane		
A_1	$(2,1)_+ \rightarrow (1,1)_+$	64.110
A_2	$(2,1)_+ \rightarrow (1,1)_-$	64.947
A_3	$(2,1)_- \rightarrow (1,1)_+$	65.430
A_5	$(2,1)_- \rightarrow (1,1)_-$	66.280
B_1	$(2,1)_+ \rightarrow (1,0)$	69.834
B_1'	$(2,1)_- \rightarrow (1,0)$	-
G_1	$(1,0) \rightarrow (2,2)_+$	13.650
G_5	$(1,0) \rightarrow (2,2)_-$	16.617
K_1	$(1,1)_- \rightarrow (2,2)_+$	18.534
K_2	$(1,1)_+ \rightarrow (2,2)_+$	19.375
K_3	$(1,1)_- \rightarrow (2,2)_-$	21.489
K_4	$(1,1)_+ \rightarrow (2,2)_-$	22.353
H_1	$(1,1)_- \rightarrow (2,0)$	98.875
H_2	$(1,1)_+ \rightarrow (2,0)$	99.716
Nearest neighbour in-plane		
B_2	$(2,1)_\pm \rightarrow (1,0)$	70.228
B_3	$(2,1)_- \rightarrow (0,0)$	71.280
C_1	$(2,1)_+ \rightarrow (2,2)_-$	84.113
C_3	$(2,1)_- \rightarrow (2,2)_+$	86.595
G_4	$(0,0) \rightarrow (2,2)_+$	15.327
H_3	$(0,0) \rightarrow (2,0)$	93.26
Next nearest neighbour		
G_2	$(2,1)_+ \rightarrow (1,1)_-$	14.018
G_3	$(2,1)_- \rightarrow (1,1)_+$	14.051
G_6	$(1,1)_- \rightarrow (2,0)$	17.000
G_7	$(1,1)_+ \rightarrow (2,0)$	17.074
G_8	$(2,1)_- \rightarrow (1,0)$	12.058
G_9	$(2,1)_+ \rightarrow (1,0)$	11.956
G_3'	$(2,1)_- \rightarrow (1,1)_-$	14.125

Those frequencies not observed in this experiment are taken from HBHI.

Perhaps the most useful set of lines discovered are those connecting to the |2,0> level for in- and out- of-plane pairs. The theory of HBHII and of Luryi and Van Kranendonk (1979) both predict the position of the |2,0> level. Table VI lists these predictions along with the experimentally determined value. Fig.15 shows the experimentally observed line shapes. The relative intensities of H_1 to H_2 observed is 2.4 in reasonable agreement with theory (3.4) considering the difficulty in measuring these lines with poor signal to noise ratios. Intensity comparisons are made at T=2.1 K, relative to the unclustered value. By comparing the absorption in the niobium between H_1 and G_1 and the integrated intensities the ratio of the intensities of H_1 to G_1 is 15 in good agreement with the theoretical result of 14.6 . Excellent agreement is obtained for the out-of-plane lines and HBHII, however there is a slight discrepancy between experiment and theory with the in-plane line. The two sets of values given by Luryi and Van Kranendonk do not agree very well with experiment. A fit of the parameter $\Delta\xi$ to the out-of-plane lines would be very interesting especially if it then predicted the correct position for the in-plane line. The parameter $\Delta\xi$ is associated with the difference between the oblateness of the zero point motion of pair molecules in the in-plane and out-of-plane configurations.

It is also interesting to note that the frequency for the ground state to 10Γ level transition of in-plane pairs, inferred from the experimental values of H_3 and B_3, is consistent with the result obtained by Raman scattering (Silvera et.al. 1971).

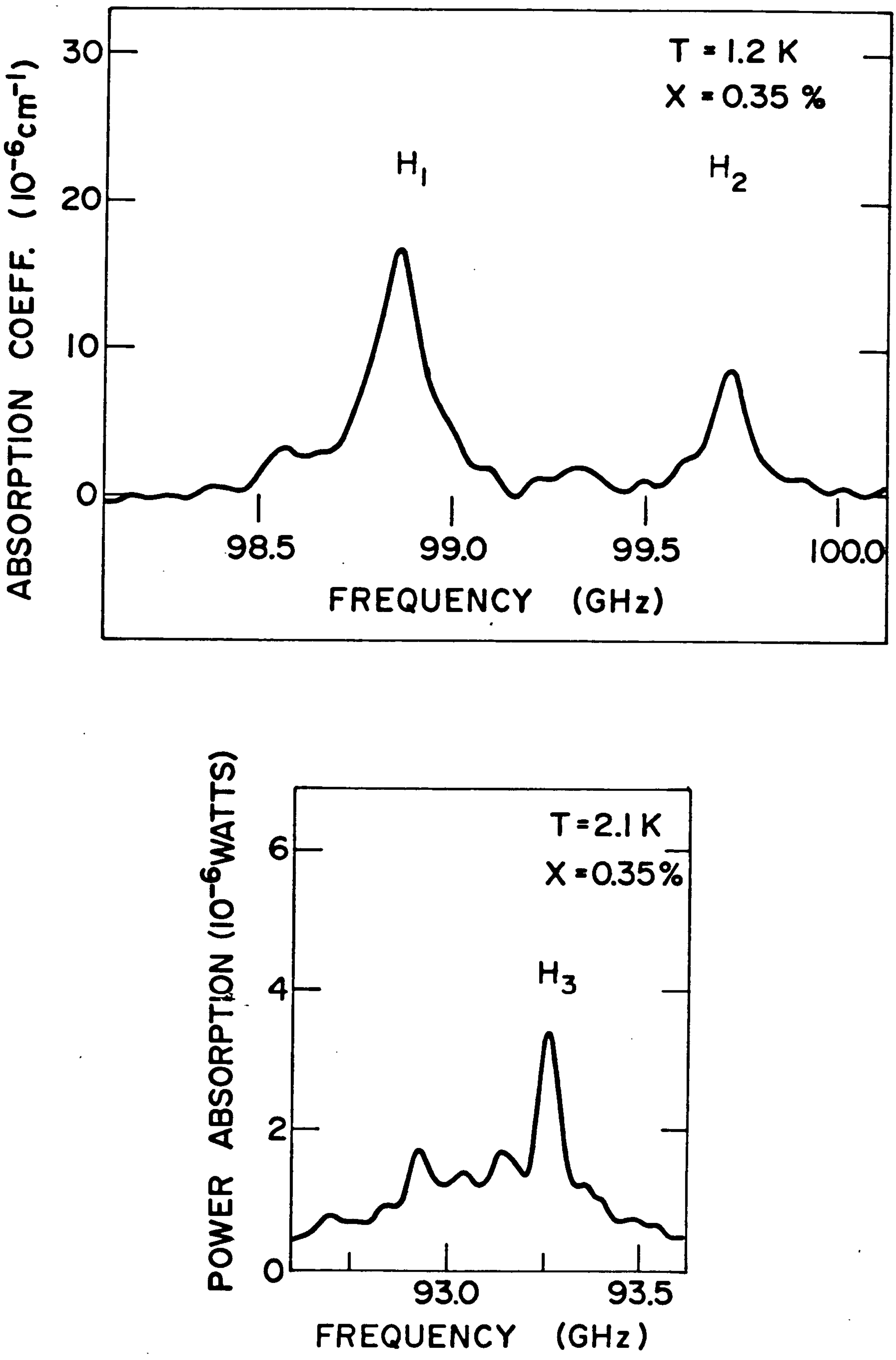

Figure 15 High Frequency Spectra

Table VI High Frequency Lines

Line	HBHII	LVK ($\Delta\xi=0$)	LVK ($\Delta\xi=0.001$)	Experiment
H_1	98.898	97.54	96.6	98.875 ± 0.009
H_2	99.742	98.38	97.5	99.716 ± 0.014
H_3	93.509	91.99	93.4	93.26 ± 0.02
$(2,0) \rightarrow (2,1)$	164.79	163.27	164.7	164.54*
				165 ± 3 **

All frequencies in GHz.

*as obtained from H_3 and B_3 (see text)

LVK refers to Luyri and Van Kranendonk (1979)

**Raman scattering; Silvera et.al. (1971).

One problem with the assignment of H_3 is the lack of a temperature dependence of its intensity. This will be discussed later.

Confirming the previous out-of-plane assignments is the discovery of the lines K_1 through K_4. The locations of these lines were determined by the already observed transitions. Unlike most of the other lines these are quite weak and are not visible in the raw data. Only after computer processing did these lines appear, showing the value of precisely reproduceable frequency scanning (see fig.16 and 17). When one compares the results obtained with a temperature ratio and a time ratio the reproduceable features are assigned to the appropriate transitions. The other features occuring in one spectrum and not the other are considered to be noise. The noise level is relatively high because of the weak absorption intensities. There is good agreement between the frequencies of these lines and those determined previously. The relative intensities observed are about the same for K_2, K_3, and K_4 whereas K_1 has about four times the intensity of the others. The relative intensity of K_2, K_3, and K_4 compared to G_1 is about 0.17 at 2.1 K whereas theory predicts 0.25. This discrepency may be due partly to the ortho broadening of the K lines smearing part of the line well into the noise (which does not occur with G_1), as well as the fact that an uncalibrated power meter was used for the K-band measurement. A companion to K_1 is a feature at 18.66 GHz which does not seem to fit any possible transition in the pair spectra. This will be discussed later.

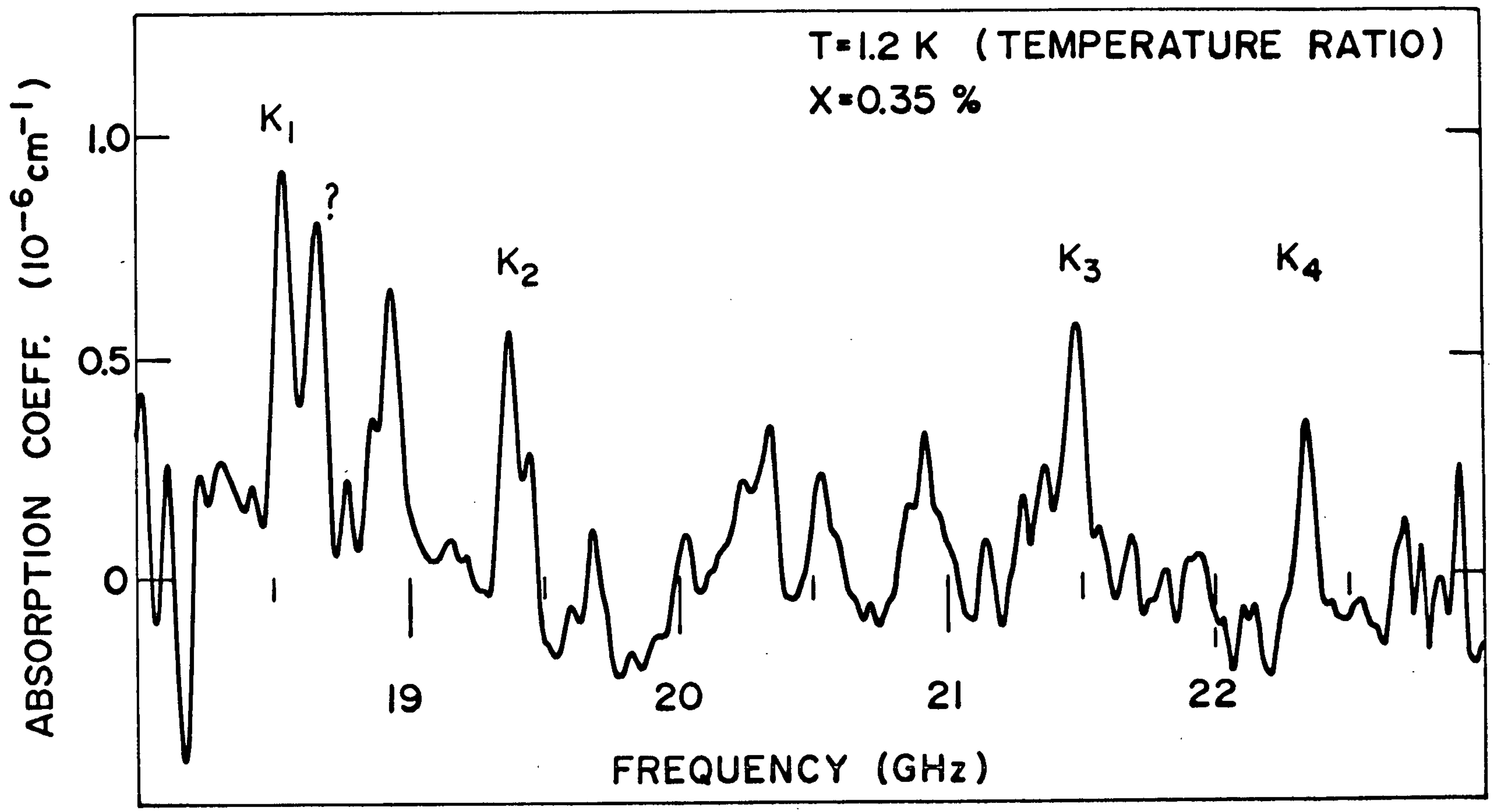

Figure 16 K-Band Spectra

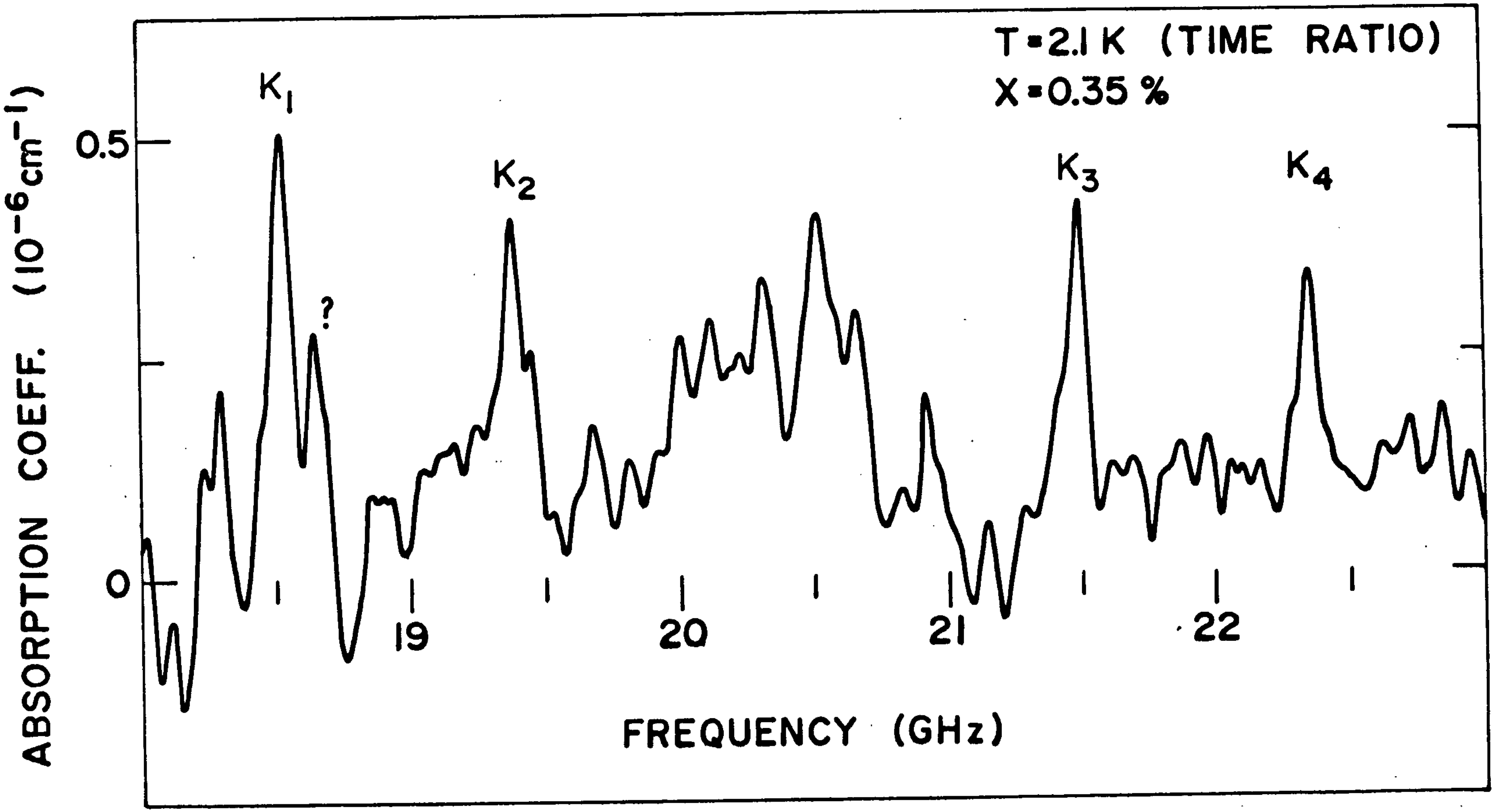

Figure 17 K-Band Spectra

A close look at the next nearest neighbour spectrum reveals the need to reassign G_6 and G_7. If G_6 and G_7 are now taken to be the transitions from $|1,1\rangle_-$ and $|1,1\rangle_+$ to $|2,0\rangle$ respectively, then the theoretical intensity ratio of G_6 to G_7 of 2.50 agrees with the experimentally observed ratio of 2.5. Now by using the theoretical splitting between the $|1,0\rangle$ and $|1,1\rangle_\pm$ states of 2.35 GHz and the other known splittings one gets a value of 11.59 and 11.70 GHz for the $|2,1\rangle_+$ and $|2,1\rangle_-$ to $|1,0\rangle$ transitions respectively. This is consistent with two features observed in the X-band search of the 0.1% o-H_2 sample at 11.96 and 12.06 GHz. Signal averaging the results in the 0.35% o-H_2 sample shows two lines at 11.956 and 12.058 GHz with approximately the right relative intensity ratio to confirm this assignment (see fig.18). The origin of the feature at 11.979 GHz is presently unknown. The relative intensity of G_8 to G_2 observed is about 0.25, which is in good agreement with the theoretical intensity ratio of 0.21 considering the poor signal-to-noise ratio. Also, the observed thermal enhancement between T=1.2 K and 2.1 K is 1.7 compared to the predicted value of 1.9 .

The thermal factor of G_6 and G_7 between T=1.2 K and 2.1 K is found to be 1.2 whereas theory predicts 1.43. This gives additional support for the new assignment since the thermal factor for the previously assigned transitions $|2,1\rangle_\pm \rightarrow |1.0\rangle$ would be 1.90. We now compare these results to the analogous results for G_2. The thermal factor of G_2 between T=1.2 K and 2.1 K is found to be 1.4, compared with 1.88 predicted with

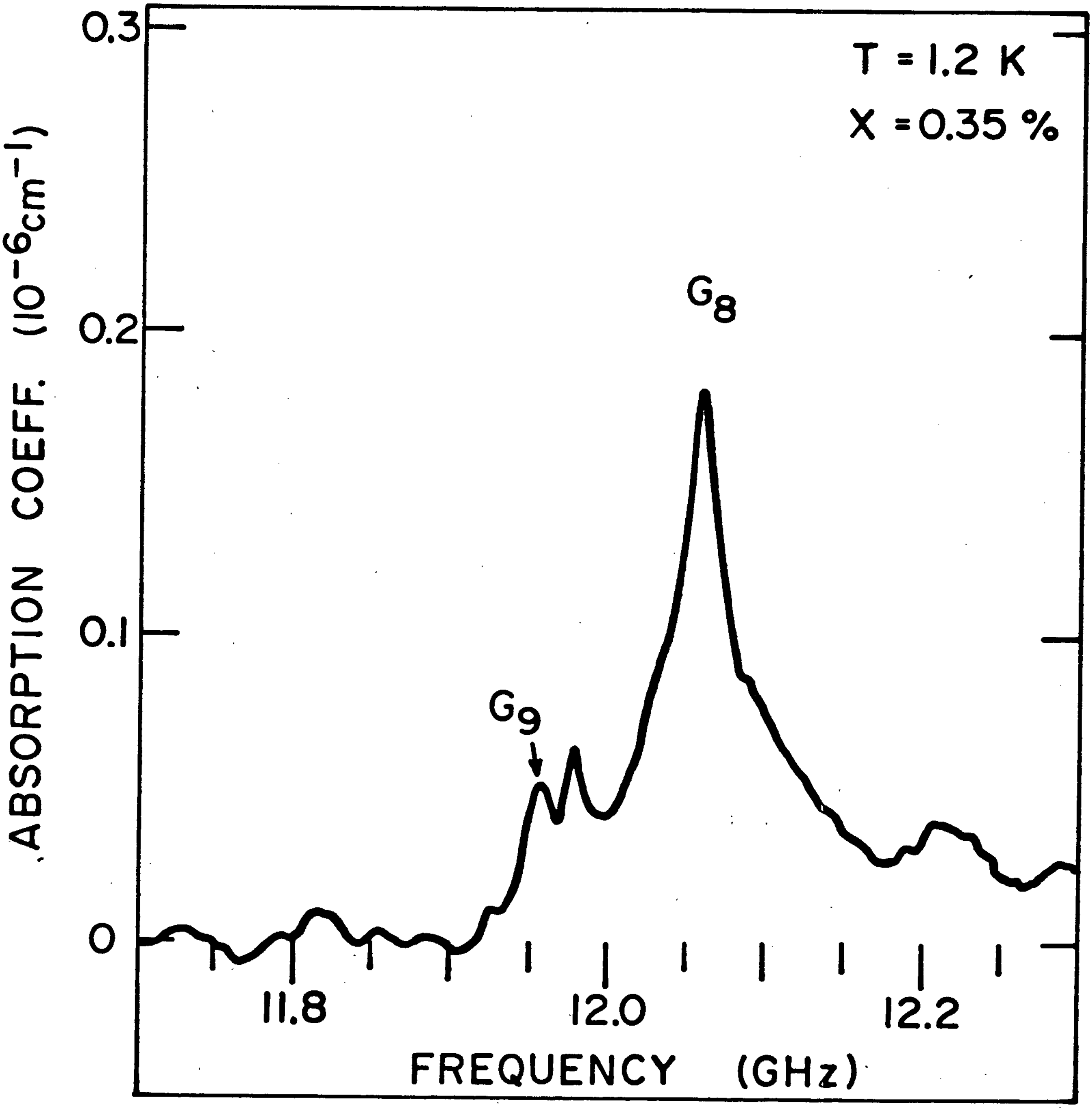

Figure 18 X-Band Spectra

Boltzmann factors. The clustering enhancement factors for G_6 and G_7 are 1.3 and 1.2 at T=2.1 K and T=1.2 K respectively which is to be compared with 1.4 and 1.3 with G_2, indicating good agreement. However the relative intensity of G_6 and G_7 to G_2 at T=2.1 K is 0.98 which is not in good agreement with the theoretical value of 0.73. Note that the discrepancy would be substantially larger if the previous assignments of G_6 and G_7 where taken.

The two lines, G_2' and G_3', associated with G_2 and G_3 are the $|2,1\rangle_+ \rightarrow |1,1\rangle_+$ and $|2,1\rangle_- \rightarrow |1,1\rangle_-$ transitions. Their frequencies, 13.944 and 14.125 GHz respectively, are determined once G_2, G_3, G_6 and G_7 are specified. The $|1,1\rangle_\pm$ splitting is set by the assignments of G_6 and G_7. Therfore when G_2 and G_3 are chosen, the $|2,1\rangle_\pm$ splitting is determined, fixing the frequencies of G_2' and G_3'. In the 0.1% o-H_2 sample a small feature was seen at 14.122 GHz and in the 0.35% o-H_2 sample two small features are seen in the appropriate places but could also be a noise fluctuation . Therefore one can say that G_3' has been observed experimentally whereas the presence of G_2' is uncertain. These lines are much harder to see since they are ortho-broadened, in contrast to G_2 and G_3 which are not. This will be discussed later in detail.

As mentioned before it is suspected that some of the intensity of these lines is strain broadened out far into the wings. The absolute integrated intensity for G_1 of this last sample is 0.24×10^{-6} GHz cm^{-1} in comparison with 1.35×10^{-6} GHz cm^{-1} predicted theoretically. This discrepancy is apparent in many of the samples except for the first 0.35% sample (on its last regrowth) which showed an integrated intensity for G_1 of 0.89×10^{-6} GHz cm^{-1}, much closer to the predicted value. The variability of integrated intensity with regrowth of the same sample supports the claim that the intensity is being partially smeared out into the wings of the lines.

5.3 Temperature Dependence of Lineshapes:

The most accurate lineshapes are obtained in the low frequency bands where the microwave power level is high, and where the linewidths are much less than the period of the standing wave pattern. For these reasons and because of their large intensities, G_1 and G_5 are the best candidates. Plots of G_1 and G_5 were made for runs at T=1.2, 2.1, 3.0, 4.2 K on the 0.1% o-H_2 sample (see fig.19). These runs were not under synthesizer control and hence are not as accurate as other runs. However, to within experimental error the lineshape and linewidth is temperature independent. These results put an upper limit on the change in linewidth of 0.18 MHz. Results from the 0.35% o-H_2 sample put an even lower limit on the phonon broadening. Plotted in fig.20 is G_1 at T=2.1 K and 1.2 K. There is virtually no difference between the two plots at the different temperature. It is also noted that G_5 has a lineshape very similar to G_1. An upper limit of 100 KHz will then be put on this effect between T=1.2 and 2.1 K (due to the finite frequency steps at which the data is collected). This is consistent with the theory developed earlier which suggests a difference of about 100 KHz between the linewidths at the two temperatures due to the crystal field processes.

In some recent experiments we have looked very closely at the lineshapes of G_1, G_5 and G_2 at T=4.2 K for the X=0.35% crystal. In contrast to earlier results for the X=0.1% sample where the position of the lines did not change with temperature, G_1 and G_5 were found to decrease in frequency from the low temperature values by 2.7 MHz, and G_2 by 2.0 MHz. At present there is no plausible explanation for these surprisingly large shifts. Because of the shift one cannot obtain the lineshape in the usual manner. Instead, we used the background obtained previously at T=2.1 K from time ratioed spectra. This leads to the result shown in fig.20. The linewidth is 2.9 MHz, slightly <u>less</u> than the value 3.1 MHz obtained at T=1.2 K or T=2.1 K. However, the background in the vicinity of the line appears to have changed which causes some distortion of the lineshape. This dip also occurs at the other two lines, G_5 and G_2. Since it is unlikely that the standing wave pattern has changed drastically in temperature there must be some broad temperature dependent absorption associated with the hydrogen. The slight difference in the linewidth at the two temperatures could probably be accounted for by this change in background. We therefore conclude that to within 0.2 MHz the line width is temperature independent. This is substantially less than the calculated width at 4.2 K of about 2 MHz (see Table IV). However the crystal field coupling coefficient is somewhat uncertain and in addition a small change in the effective value of the sound velocity (which occurs to high powers in the formulae) could make a significant change in the predicted width.

5.4 Strain and Ortho Broadening:

As mentioned earlier mechanical strains contribute a large portion to the linewidth of the pair transitions. This component, because of its nature, cannot be predicted in advance and with the present apparatus has not been eliminated. If one recalls the three other contributions to the linewidth of G_1 discussed earlier, one notes they are negligible compared to the typically observed linewidth of a few MHz. A glance at table VII, which contains the smallest linewidths observed at a particular o-H_2 concentration, shows that the strain broadening has no particular correlation with concentration. However by using G_1 as a standard, one can extract the inhomogeneous ortho broadening contribution to the linewidths.

In general the strain broadening will have a different effect on each transition due to the complicated dependence of the level splittings on pair separation. Therefore one cannot take the line width of G_1 as the strain broadening effect but must scale it by some factor. These factors will be determined by data collected from samples of 0.03% o-H_2 concentration where the ortho broadening should be negligible. These factors are listed in table VIII. Now using these factors and assuming all the lineshapes concerned are Lorenztian (in order that one can add and subtract linewidths) the ortho broadening contribution

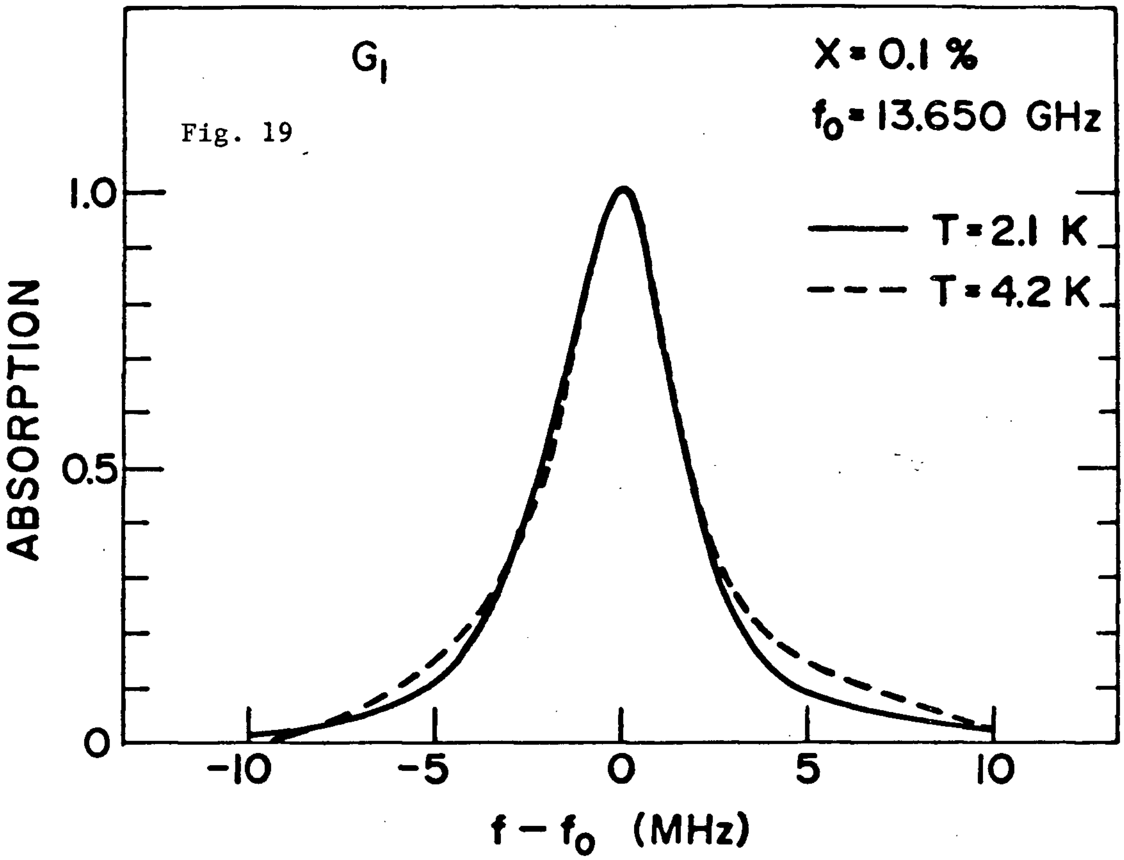

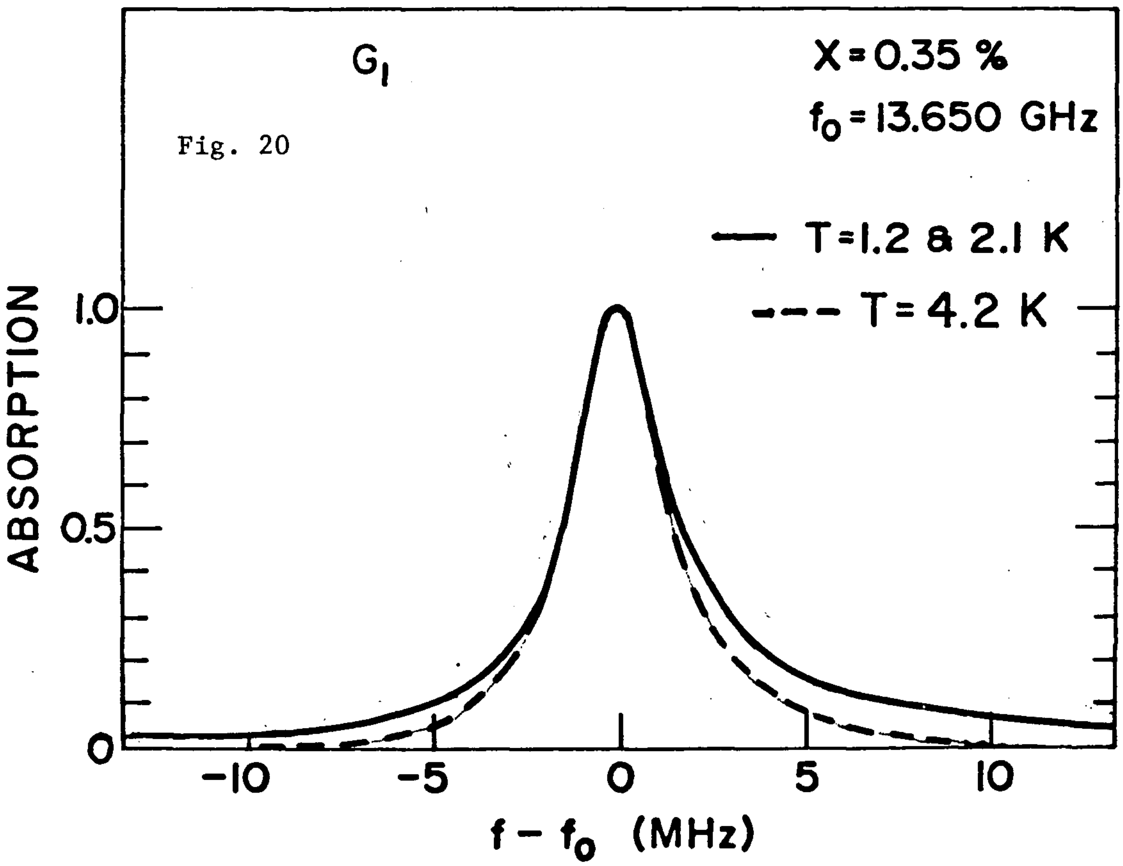

Figure 19 G_1 for 0.1% o-H_2 Sample

Figure 20 G_1 for 0.35% o-H_2 Sample

Table VII Observed Linewidths

Narrowest linewidths (MHz) vs. O-H_2 concentration

Line	0.03%		0.1%	0.2%		0.35%
	(a)	(b)		(a)	(b)	
G_1	2.1	2.67	3.83	5.0	4.9	3.09
G_2	3.8	3.9	9.77*	8.26	-	5.20
G_4	2.0	3.3	8.46	-	-	18
G_5	2.1	2.55	4.40	-	4.6	3.09
G_6	-	8.4	20.6	-	-	25.2
G_7	-	8.0	15.9	-	-	25.5

*Appeared as an partially unresolved doublet in this sample only.

In each case (a) and (b) refer to two different samples of the same concentration.

to the linewidths at 0.1% and 0.35% o-H_2 are found and listed in table IX. As one can see there is general agreement with the results predicted earlier. The lines G_1, G_5 and G_2 (and G_3 by looking at the spectra directly in fig.21) are not broadened whereas G_4, G_6 and G_7 are. Recalling the limitations of the theory presented earlier the agreement of the predicted widths with experiment is good at 0.35% o-H_2. There is however a problem with the 0.1% o-H_2 widths in that they should be $(0.1/0.35)^{5/3}=0.12$ times smaller than those for a 0.35% sample. The measured ratio is about 0.29. This discrepency could be due to an error in the concentration (which cannot be conveniently measured), or due to the fact that the lineshapes are not Lorentzian and one should not simply add the linewidths together but should do a proper convolution.

5.5 Isotopic Substitution Effects:

In order to investigate the effect on the linewidths of substitutional isotopic mass defects in the lattice, several 0.2% o-H_2 samples where doped with about 0.2% o-D_2 (J=0 species). Deuterium was used rather than HD because it should have the largest effect of the two and in addition does not have the added complication of off center rotation (see section 3.3). The changes in frequency and linewidth are now discussed. In order to establish the mechanical strain broadening component of the linewidth the sample is grown undoped and the linewidths observed. Then the sample is evapourated into a bulb containing a small amount of o-D_2 and quickly condensed back into the cell

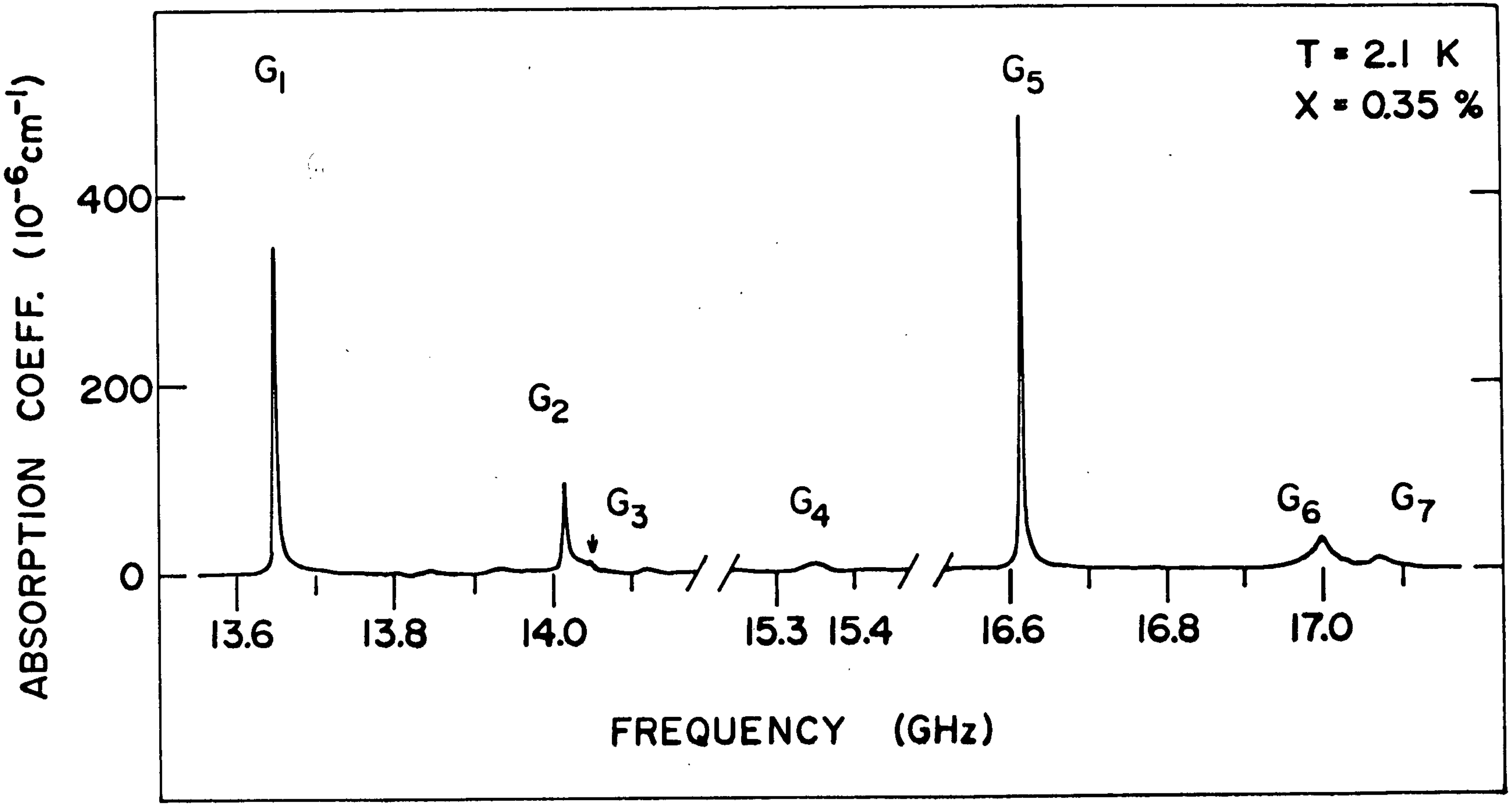

Figure 21 P-Band Spectra

Table VIII Relative Strain Broadening Factors

Linewidths at 0.03% relative to G_1

G_5	1.06±0.08
G_2	1.57±0.25
G_4	1.08±0.22
G_6	3.15
G_7	3.00

(Average values taken over many samples)

Table IX Observed Ortho Broadening

Linewidths (MHz) with strain component removed

Line	0.1%	0.35%	Theory (0.35%)
G_1	0.00	0.00	0.00
G_2	3.76	0.35	0.00
G_4	4.32	14.7	17.0
G_5	0.34	0.00	0.00
G_6	8.54	15.5	26.2
G_7	4.41	16.2	17.0

and regrown.

Considering G_1 and G_5 , the undoped linewidth is 5 MHz and with 0.2 % o-D_2 is 13 MHz. The average line position of G_1 and G_5 has increased by Δf=6 MHz, the sign of which is consistent with the lattice contraction expected due to the reduced zero point motion of the impurities relative to the host. Again assuming one can add linewidths the mass defect strain broadending linewidth $\Delta\nu$ is 8 MHz. Relating Δf to $\Delta\nu$ gives $\frac{\Delta f}{\Delta\nu}$ = 0.75 which is consistent with the result predicted earlier of $\frac{\Delta f}{\Delta\nu}=1.04\left(\frac{1-\nu}{1+\nu}\right)=0.6$.

If one takes the measured value of Δf and uses [54], one finds the change in molar volume with o-D_2 concentration to be $\frac{1}{v}\frac{\partial v}{\partial c}=-0.12$. This is consistent with the linear approximation applied to results for the pure species $v=v_0+\frac{\partial v}{\partial c}c$ which gives[1] $\frac{1}{v}\frac{\partial v}{\partial c}=-0.125$. The value of $\Delta\nu$=8 MHz yields, from [52], a nearest neighbor distortion of A=-0.0034 for o-D_2 impurities (cf. A=-0.03 for ^{4}He in ^{3}He, P.G. Klemens et.al. (1964)). From this we can predict the linewidth for a D_2 concentration of 0.03%, the natural abundance of HD in hydrogen, to be 1.2 MHz. Therefore since the broadening effect of HD is expected to be less than that for D_2, we can conclude that the lineshape of the pair transitions in "natural" hydrogen contains a Lorentzian component with a width less than 1.2 MHz.

[1]using V(o-D_2)= 19.88 cc/mole and V(p-H_2)= 22.73 cc/mole and ν=0.269. Bostanjoglo and Kleinschmidt (1967) and Goldman (1977)

5.6 New Features:

While studying the many samples grown in this experiment several unexpected phenomena were observed. The first of these is the apparent temperature independence of the intensities of in-plane transitions while out-of-plane and next nearest neighbour transitions display the expected temperature dependence. In addition to this a new spectral feature has been observed at 17.5 GHz which does not display the same characteristics of the ortho pair lines. Also there are some very broad background lines observed in the 11.0 to 24.0 GHz region.

A temperature independence of the intensities of C_1, C_3 and H_3 was found between T=1.2 K and T=2.1 K in two samples containing 0.35% o-H_2. This effect was not observed by Hardy et.al. where the ortho concentrations were 0.2% or less. Time ratios also show nothing, indicating either a very fast or very slow clustering rate, whereas temperature ratios show only a broad background feature about 500 MHz wide and no sign of the lines which are obviously there in the raw data. In order to gain more information a set of scans was taken at T=4.2 K . These spectra are much noisier than those taken below the lambda point of liquid He but are still useful. When ratios are taken between the T=4.2 K and 1.2 K data a sharp line of low intensity about 20 MHz wide sits on top of the broad background peak at the expected positions of the three lines. This indicates the possibility of two temperature dependent and competing processes which happen to cancel out when comparing T=1.2 K to

T=2.1 K. Recalling from HBHI that in-plane lines do not show the same effects of clustering as do out-of-plane lines, one might suggest that there is a temperature dependent effect on the clustering which is counteracting the Boltzmann population factors. Also the fact that this effect has not been observed in samples of 0.2% o-H_2 or less suggests that the process may be concentration dependent.

The temperature independence could also be due to microwave power saturation, i.e. thermal equilibrium is not being maintained in the system. This possibility has been checked many times for G_1 and now with C_1 and C_3 by either comparing the lineshapes at two different incident power levels or by observing the time dependence of the absorbed power at the absorption peak. These tests were always negative and the rough calculation done in HBHI indicates that a much higher power level would be needed to saturate these levels. Now that the possibility of saturation has been eliminated there is an inconsistency between experiment and the compensating clustering effect suggested in the last paragraph. The Boltzmann factors for the ground state transitions C_1 and C_3 <u>decrease</u> as the temperature is raised whereas those for excited state transitions such as H_3 <u>increase</u> . This means that any effect cancelling out the Boltzmann factor between T=1.2 K and 2.1 K would have to be level dependent.

There is a distinct feature occuring near 17.5 GHz in many of the samples. This feature shows an increase in intensity when the temperature is lowered from 2.1 K to 1.2 K and shows no change with time. It was not observed in the 0.1% $o\text{-}H_2$ sample nor the 0.03% $o\text{-}H_2$ samples but appears at 17.24 GHz in the 0.2% samples with or without $o\text{-}D_2$ and at 17.4 GHz in one 0.35% sample and at 17.49 GHz in the other 0.35% sample. This line displays the unusual behaviour of losing intensity upon repeated annealing whereas the pair lines generally increase in intensity. This indicates that this absorption is not due to the usual pair transitions. There are two other weaker transitions observed at 18.66 GHz and 11.90 GHz that one would be tempted to associate with this feature. The line at 11.90 GHz displays the same characteristics as the 17.5 GHz line, except that the effect of annealing was not monitored. Therefore these two lines could be related. However the line at 18.66 GHz changes in time because of clustering, and also grows in intensity as the temperature is increased from 1.2 K to 2.1 K and hence it does not seem likely that this line is related to the other two.

The source of these lines is unknown as is the reason they appear in some samples and not others. One possibility to consider is that the 11.90 GHz and 17.49 GHz lines are the ground state to $|2,0\rangle$ level transitions for the two further neighbour pairs, ie. $r/r_o = \sqrt{8/3}$ and $\sqrt{3}$. The EQQ splittings for these transitions are 17.35 GHz and 12.93 GHz respectively and if one were to include 3-body polarization and crystal field effects these could easily shift a few hundred MHz into place. The temperature dependence is consistent with this hypothesis as is the fact that both of these pair types have the same symmetry as the in-plane pairs, and are therefore allowed transitions.

Scanning from 12.5 to 18.0 GHz has revealed two large peaks in the background which are about 0.6 to 1.0 GHz wide. These peaks are observed in all the samples which where scanned across this band. In all cases these peaks are temperature independent and show no clustering. Their centers are located at about 13.7 GHz and 16.1 GHz. Since the integrated intensities of the pair lines in this region are usually about an order of magnitude smaller than theory predicts it is assumed that a large portion of the sample is strain broadened and that a large portion of the intensity resides in the wings. One might then suggest that these large background peaks are the strain broadened parts of the pair lines. In order to check this hypothesis the integrated intensity of the lower frequency peak was measured in a 0.03% o-H_2 sample and was found to be about 7 x 10^{-6} GHz cm^{-1} whereas the theoretical integrated intensity for G_1 plus G_2 is 0.013 x 10^{-6} GHz cm^{-1}. In addition, these peaks do not change in temperature or time. We conclude that these peaks are not due to ortho pair transitions.

However the fact that these peaks are not seen when there is no sample in the cell implies that they are somehow connected with the presence of hydrogen. Channel spectra due to the H_2 fit all the above criteria and in order to confirm this possibility, data from 11 to 24 GHz is examined in (fig.22) and the center positions of the broad lines are tabulated in table X. One calculates the expected frequencies from the waveguide wavelength λ_g as follows.

[60] $$f = \frac{c}{\sqrt{\varepsilon}\,\lambda} \qquad\qquad \frac{\lambda_g}{2} = \frac{\ell}{n}$$

[61] $$\left(\frac{2\pi}{\lambda}\right)^2 = \left(\frac{2\pi}{\lambda_g}\right)^2 + \left(\frac{\pi}{a}\right)^2$$

for the TE_{10} mode. Here a is the larger transverse dimension of the waveguide and ℓ is the length of the hydrogen sample. These results are tabulated in table X and show good agreement for n=2-6. Although channel spectra usually take on a sinusoidal shape the geometry of the cell may change this situation. The cell flange connection to the waveguide taper is 2.55 times the sample length away from the bottom of the cell and reflections from this boundary may superimpose another sinusoid of a different wavelength on top of the first one. Also there will be some reflections from the cell-taper flange which will change the standing wave pattern.

In principle the step in the waveguide should eliminate any reflections. However if the sample volume is not precisely correct there will be an impedance mismatch near the step and hydrogen surface causing some reflection.

The peak to trough ratio of the simple sinusoid is given by

[62] $$\frac{P_{max}}{P_{min}} \simeq \left(\frac{1+r}{1-r}\right)^2 \simeq 1.30$$

where the reflectance of the hydrogen-vacuum surface has been taken to be

[63] $$r = \frac{1-\sqrt{\varepsilon}}{1+\sqrt{\varepsilon}} = 0.065$$

The observed value tends to decrease with frequency and has an

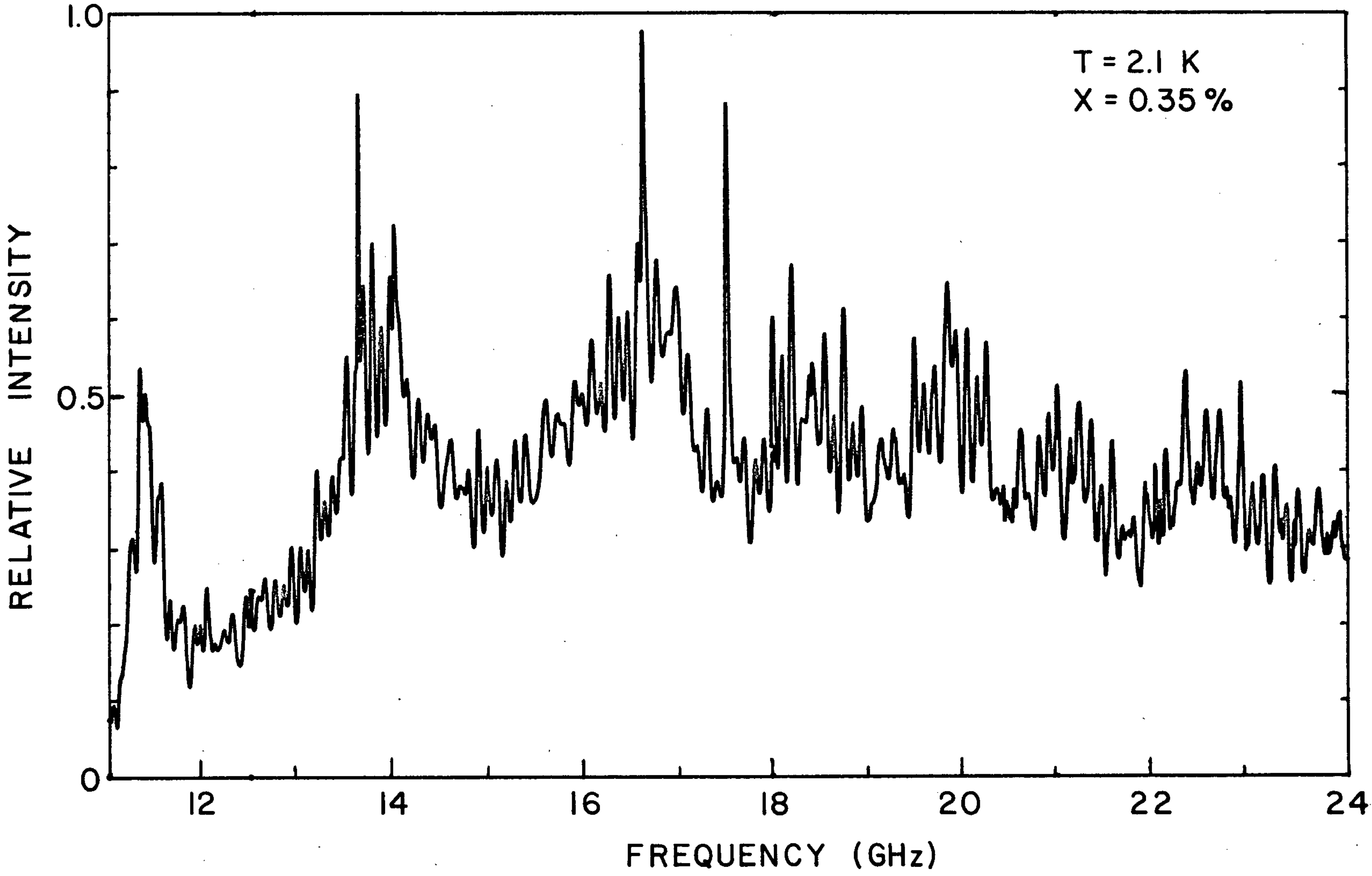

Figure 22 Channel Spectrum From 11-24 GHz

Table X Channel Spectra Peaks

$2l/\lambda_g$	Expected Frequency (GHz)	Observed Frequency (GHz)
2	11.8	11.4
3	14.0	13.7
4	16.5	16.1
5	19.4	19.9
6	22.3	22.6

l=hydrogen sample length=3.92 cm.

λ_g=waveguide wavelength

average value of about 1.5 which is in reasonable agreement.

CHAPTER VI Conclusions

To conclude we list the main results obtained in this work as well as some suggestions for further developement.

(1) Out-of-plane pairs:

The $|2,0\rangle$ level has now been established with the discovery of the two transitions H_1 and H_2. In addition, the four recently observed lines K_1 through K_4 have confirmed the assignments of transitions connecting to the $|1,1\rangle_\pm$ and $|2,2\rangle_\pm$ states. All the levels have now been determined except that of the $|0,0\rangle$ state. Most processes do not couple to this state, making an experimental determination of it very difficult.

(2) In-plane pairs:

The $|2,0\rangle$ level has also been established for the in-plane pairs with the measurement of H_3. This leaves only the $|1,1\rangle_\pm$ level to be determined. The lack of temperature dependence of the in-plane pair transitions is cause for concern and further effort will be necessary to provide an explanation for this effect.

(3) Next-nearest neighbor pairs:

Considerable progress has been made in the determination of the next nearest neighbor pair levels. The recent discovery of the two lines G_8 and G_9, as well as the reassignment of G_6 and G_7, have established the position of most of the levels.

(4) Inhomogeneous broadening:

A first order theory for the broadening of the pair lines due to the finite concentration of ortho molecules has been developed. Experimental verification has been obtained for this theory with the low frequency lines. A more quantitative comparison of experimental lineshapes with theory awaits improvement in the strain broadening.

(5) Homogeneous broadening:

The effect of phonon induced lifetime broadening on the pair lines has been calculated. Although an upper limit has been placed on this effect, experimental verification of the temperature dependence of the linewidths is needed. Again, it is important that strain effects be reduced.

(6) Further ortho pairs:

The observation of the two lines at 11.90 and 17.49 GHz and the possibility that these are transitions of the third and fourth nearest neighbor pairs will hopefully stimulate interest in the calculation of their expected frequencies and intensities. The results of these calculations will be awaited with a great deal of interest.

APPENDIX A: Device Codes and Instructions

The following provides a description of the custom peripherals available in the system. Each item contains the octal device code (DC) and operating instructions.

1) 16 bit D/A Converter: DC 75

DOA	AC,75	sets a voltage proportional to the contents of accumulator AC.
DOB	AC,75	bits 14,15 of accumulator AC turn on or off the two digital outputs on the converter.

2) Synthesizer Control: DC 2

This device requires the input to be in BCD.

DOA	AC,2	bits 8-11	set the 100 MHz digit
		bits 12-15	set the 10 MHz digit
DOB	AC,2	bits 0-3	set the 1 MHz digit
		bits 4-7	set the 100 KHz digit
		bits 8-11	set the 10 KHz digit
		bits 12-15	set the 1 KHz digit
DOC	AC,2	bits 4-7	set the 100 Hz digit
		bits 8-11	set the 10 Hz digit
		bits 12-15	set the 1 Hz digit

3) 12 bit D/A converters: DC 4

The 12 bit twos complement contents of accumulator AC (bits 4-15) sets the output voltage of the converter, in the range 0 to 10 volts.

```
DOA   AC,4        D/A #1
DOB   AC,4        D/A #2
```

4) 14 bit A/D converter: DC 25

The input channel (0 through 7) is selected and conversion initialized with

DOAS AC,25 — where AC contains the channel number.

After conversion, signified by the interupt or busy and done logic, the 14 bit twos complement representation of the analog input is read in with the instruction

```
DIC   AC,25
```

5) Programmable interval timer: DC 5

The timer increment size of 10 microseconds ($0<a<6$) is selected with the instruction

DOA AC,5 — AC contains the number a.

The number of increments counted by the timer is loaded in and the timer started with the instruction:

DOBS AC,5 — AC contains the number of increments

The output pulse generated by this device is available through a set of complementary (TTL compatible) outputs or through the interrupt or busy and done logic.

6) Digital inputs, outputs and relay controls: DC 31

DOA	AC,31	bits 10-15 of accumulator AC set the relays #6 to #1.
DOB	AC,31	bits 10-15 of accumulator AC set the latched output ports #6 to #1
DIA	AC,31	bits 12-15 indicate the state of the input ports #4 to #1
DIB	AC,31	bits 12-15 indicate the latched state of these input ports.

These inputs are TTL compatible and are normaly high.

7) Timer clock: DC 55

The following instructions:

NIOC	AC,55	will reset the timer.
DIA	AC,55	reads in the most significant digits
DIB	AC,55	reads in the least significantdigits

The 32 bit binary number read in contains the number of millisecond intervals since the last reset instruction.

8) LED display: DC 45

DOB	AC,45	sets the lower four digits where AC contains the four BCD numbers to be displayed.
DOA	AC,45	sets the upper four digits in the same manner.
DOC	AC,45	sets the lone decade with bits 12-15 of accumulator AC and the decimal point is set with bits 4-7.

APPENDIX B: Assembler Subroutine Descriptions

Some of the assembler language subroutines used to control the microwave spectrometer are described in this appendix. Each heading will contain the name of the program as well as the Basic instruction used to call the subroutine.

SYNSW: CALL 16,FSTART,ΔF,START,N,ΔT,SYNTH,DUMMY,A/DCHAN

This is the routine which sweeps the BWO sweeper and synthesizer. The synthesizer frequency is set with SYNTH but the 16 bit D/A presetting voltage is set from a frequency-voltage conversion table located in DATA at location FSTART. This table is constructed before the program is called and requires that the D/A be calibrated. This is done with the routine CALIB which is to be described later. Every ΔF point in this table is read. SYNTH is a three element array containing the startng frequency of the synthesizer AAA,ABB,BB0 Hz and its increment frequency in Hz. AAA,A is stored in SYNTH(1), BB,BB in SYNTH(2) and SYNTH(3) contains the increment frequency. The sweeper is stepped N times with a time interval of ΔT (in 1 millisecond units). The data is collected at the end of each time interval before the frequency is stepped. Data from A/D channel A/DCHAN is stored in DATA starting at location START and data collected from A/D channel #1 is stored in DATA starting at location 6006. DUMMY is a "dummy" variable not used at present.

CALSW: CALL 12,FSTART, F,START,N, T,POPT,PARR,A/DCHAN

FSTSW: CALL 13,FSTART, F,START,N, T,POPT,PARR,A/DCHAN

These two programs sweep the BWO sweeper with the 16 bit D/A but not the synthesizer. CALSW is for slow single sweeps, T in millisecond units and FSTSW for fast repetitive sweeps, T in 1 microsecond units. The variables FSTART, F,START,N,A/DCHAN are defined as before. POPT is the CRT plot option.

POPT=0	no plot
POPT=1	store data (T) in specified block
POPT=2	calculate T/T0 and store
POPT=3	calculate 1-T/T0 and store

The Basic program will request the starting addresses of blocks T, T0 and TPLOT. The data is stored in T and can be divided by a background spectrum in T0. If this is done the result is stored in TPLOT. In FSTSW, the contents of T will be plotted for POPT=1 and the contents of TPLOT for POPT=2 or 3. For CALSW the block plotted will be that given in response to a request from the Basic program. The array PARR specifies the starting position of T0 and of TPLOT in its first two elements and in FSTSW the plot gain can be changed by typing in the desired gain change on the teletype as follows:

TTY key	Gain change
1	1
2	2
3	3
8	8
H	1/2

This gain factor is used to scale the data plotted. CALSW performs only one sweep whereas FSTSW sweeps repetitively and typing a carriage return (CR) on the teletype will return control to Basic. FSTSW is useful for adjusting experimental parameters and observing the effect this has on the spectrum in real time.

CALIB: CALL 11,START,N,VSTART, T

This routine allows one to calibrate the 16 bit D/A converter. When this routine is called it starts sweeping at VSTART (volts) and increments the voltage setting register by 1 bit every T milliseconds. A "black box" attatched to digital inputs 1 and 2 is used to control this program. Normally the three push buttons are open (both inputs low) and the sweeping continues. At the desired frequency, which is detected with a microwave frequency counter or wavemeter, the red button is pushed (both inputs high) and that voltage is recorded in DATA starting at START. This continues until the microwave band has been calibrated. Pressing either of the black buttons (one input high, one low) will either reverse the direction of the sweep or alternate the rate of sweep by a factor of 8. Typing a carriage return will terminate the sweep and the number of calibration points taken is returned in N. These calibration points can then be used to construct a frequency-voltage table by interpolation.

CRT: CALL 8,START,N,DUMMY,MARK

CRT: CALL 9,START,N,DUMMY,MARK,DUMMY

CRT1: CALL 10

These routines are used to display the contents of DATA on the monitor scope (CRT). Calling routine 8 will plot N points in DATA starting at START. The voltage applied to A/D channel 7 is read in and the point with the X-value corresponding to this voltage is intensified. If an M is typed it is echoed on the teletype and this point is stored in the array MARK. This feature can be useful when selecting portions of a spectrum for analysis. To exit this routine type a carriage return and control will be transfered back to Basic.

Routine 9 only sets up the parameters for the plot. This is necessary before calling the sweeper programs. A call to routine 10 will plot the data once and must be called repetitively in order to obtain a visual display.

DISKW CALL 14,FILENAME,START,N,ERR

DISKR CALL 15,FILENAME,START,N,ERR

These two routines transfer data between core and the disk. DISKR will read N words from the file FILENAME and place them in

DATA starting at START. The other routine DISKW will write data from DATA to the disk with the calling parameters defined above. The RDOS error code for the disk operation is returned in ERR.

XYPLT: CALL 18,YSTART,XSTART,N,ΔT

STRIP: CALL 19,YSTART,XSTART,N,ΔT

POINT: CALL 20,YSTART,XSTART,N

These three entries to XYPLOT will plot a portion of DATA on either an X-Y recorder, strip chart recorder or point plotter. The X and Y values plotted come from DATA starting at locations XSTART and YSTART respectively. N points are plotted at ΔT millisecond intervals. If XYPLT or POINT are called then the X and Y voltages are applied to the X and Y inputs of the plotter. In this case the X input is usually a linear ramp from 0 to 10 volts. However if STRIP is called the Y value is applied to the chart recorder input and the X value is applied to the marker input. When one of these programs is called the following keyboard commands can be executed:

CR - start plotting

1 - plot 0V,0V

2 - plot 10V,10V

3 - plot first point

These commands are especially useful in setting up the X-Y recorder. During the plot typing a CR will terminate the plot. After plotting, control is returned to Basic automatically by the STRIP routine whereas a CR is necessary with the other two routines. If one then lifts the pen from the plotter, this will then eliminate the flyback to (0,0) from being plotted.

FUNC: CALL 22,F,I,J,K,N,C(5)

This program contains a number of routines which can be used to manipulate the arrays in DATA. F specifies the function to be executed as follows:

F=1 Add two arrays

F=2 Baseline adjust

F=3 Divide two arrays

F=4 Multiply two arrays

F=5 Integrate over an array

F=6 Find the minimum and maximum points in an array

The details on how to specify the other parameters are available in the listing of the program ANALYSIS, in appendix C.

APPENDIX C: Basic Program

```
0010 PRINT "    --SWEEPER CONTROL PROGRAM--"
0015 LET E=0
0016 LET E=0
0020 DIM C$[2],B$[6],M[2],N[3],F$[25],D$[12],G$[12],L[10],C[105],G[3],F[50]
0021 LET B$="NNNNNN"
0025 INPUT "INPUT DEFAULT DIRECTORY FOR DISK OPERATIONS    ",D$
0030 INPUT "ENTER CALIBRATION POINTS FROM DISK (INPUT FILENAME) OR TTI (INPUT T)
   ",F$;
0040 LET F$=F$," "
0050 INPUT "   ENTER FSTART,DELTA F,NO.PTS    ",F1,F9,N
0060 IF F$="T " THEN GOTO 0110
0070 CALL 15,F$,7500,N,E
0080 IF E=0 THEN GOTO 0105
0081 PRINT N;"  POINTS TAKEN",
0090 PRINT "READ ERROR    ",E
0100 STOP
0105 CALL 5,F[1],7500,N
0106 GOTO 0150
0110 PRINT "ENTER POINTS"
0120 FOR I=1 TO N
0130   INPUT F[I];
0140 NEXT I
0150 FOR I=1 TO N
0151   IF F[I]<0 THEN LET F[I]=F[I]+65536
0152 NEXT I
0155 PRINT
0160 ON ESC THEN STOP
0165 INPUT ">",C$;
0170 LET P=0
0175 LET M=0
0180 IF C$[2,2]="P" THEN LET P=1
0185 IF C$[2,2]="M" THEN LET M=1
0187 ON ESC THEN GOTO 0155
0190 IF C$[1,1]="R" THEN GOTO 1000
0210 IF C$[1,1]="P" THEN GOTO 6000
0220 IF C$[1,1]="D" THEN GOTO 3000
0225 IF C$[1,1]="A" THEN GOTO 9000
0230 PRINT "    ILLEGAL COMMAND"
0240 GOTO 0160
0630 INPUT "ENTER FILENAME ",F$
0640 LET F$=F$," "
0660 CALL 14,F$,7500,N,E
0750 IF E=0 THEN STOP
0760 PRINT "WRITE ERROR  ";E
0770 STOP
1000 REM   ** RUN **
1010 IF M=0 THEN GOTO 1031
1020 LET P=1
1025 LET B$[1,1]="P"
1030 INPUT "     INPUT SLOW(12), FAST(13), SYNTH.(16) SCAN    ",Z1
1031 IF B$[1,1]="N" THEN GOTO 1020
1032 IF P=0 THEN GOTO 1060
1040 GOSUB 2000
1045 CALL 9,2002,N1,0,0,0
1060 IF Z1<>16 THEN LET G[1]=1
1070 LET N[1]=2002
1075 CALL Z1,1,1,2002,1,T1,G[1],N[1],C1
1076 INPUT "   RUN    ",Z8;
1080 CALL Z1,1,1,2002,N1,T1,G[1],N[1],C1
1090 CALL 8,2002,N1,0,0
1095 PRINT
1100 GOTO 0160
2000 REM   ** SWEEP PARAMETERS **
```

```
2010 INPUT "    FSTART,DELTA F,NO.PT,DELTA T (1 MSEC/1 MMSEC),A/D CHANNEL    ",F4
,F7,N1,T1,C1
2015 LET G4=F4
2020 LET F2=F4+F7*(N1-1)
2030 LET V9=INT((F2-F1)/F9)+1
2040 LET V2=(F[V9+1]-F[V9])*(F2-F1-(V9-1)*F9)/F9+F[V9]
2050 LET V9=INT((F4-F1)/F9)+1
2060 LET V1=(F[V9+1]-F[V9])*(F4-F1-(V9-1)*F9)/F9+F[V9]
2070 LET V3=V2
2080 LET F3=F2
2100 IF F[V9+1]>V2 THEN GOTO 2205
2110 LET V3=F[V9+1]
2120 LET F3=V9*F9+F1
2205 LET J9=1
2206 INPUT "     S=",S
2207 LET V8=V1
2210 FOR I=1 TO 30
2215   LET N2=INT((F3-F4)/F7)
2217   IF N2=0 THEN GOTO 2450
2220   IF V3<0 THEN LET V3=V3+65536
2240   LET V7=(V3-V1)/N2
2241   LET V4=V3+V7
2245   LET N2=N2+1
2250   FOR J=1 TO 101
2260     LET C[J]=V8+S
2270     LET V8=V8+V7
2280   NEXT J
2290   CALL 1,C[1],1,J,J9
2300   LET J9=J9+J
2310   LET N2=N2-101
2340   IF N2>0 THEN GOTO 2250
2345   LET J9=INT((F3-G4)/F7)+1
2347   LET V8=V3
2350   LET V1=V3
2360   LET V9=V9+1
2370   LET V3=F[V9+1]
2380   LET F4=F3
2390   LET F3=V9*F9+F1
2400   IF F3<=F2 THEN GOTO 2440
2410   LET F3=F2
2420   LET V3=V2
2424   LET Y9=V8+V7+S
2425   IF J9=N1 THEN CALL 1,Y9,1,1,J9
2430   IF J9>=N1 THEN GOTO 2450
2440 NEXT I
2450 IF Z1<>16 THEN RETURN
2460 LET N=4
2470 IF F4>15 THEN LET N=5
2480 LET G1=(G4+.2)/(N*8)*1000
2490 LET G2=F7/(N*8)*1E+06
2500 LET G[1]=INT(G1*10)
2510 LET G9=G1-G[1]/10
2511 IF ABS(G9)<.001 THEN LET G9=0
2512 LET G[2]=INT(G9*100000+.5)
2520 LET G[3]=INT(G2*100+.5)
2530 PRINT "SYNTH. FREQ.= ";G1;" MHZ    DELTA F=";G2;" KHZ     2ND HARMONIC= ";G1*
2;" MHZ";
2550 RETURN
3000 REM     ** DISK READ OR WRITE**
3010 INPUT "    WRITE(0) OR READ(1) ?    ",X3;
3020 INPUT "    ENTER FILENAME & NO.PT    ",G$,N3
3030 LET F$=D$,G$," "
3035 LET M3=N3
```

```
3040 INPUT "TO BE WRITTEN OR READ FROM CAL. PTS.(0),CAL. TBL.(1),T0(2),T1(3),TPL
OT(4)    ",Y3
3050 LET X3=X3+14
3060 LET E3=0
3070 ON Y3+1 THEN GOTO 3080, 3100, 3120, 3140, 3160
3080 CALL X3,F$,7500,N3,E3
3090 GOTO 3170
3100 CALL X3,F$,1,N3,E3
3110 GOTO 3170
3120 CALL X3,F$,2002,N3,E3
3130 GOTO 3170
3140 CALL X3,F$,4004,N3,E3
3150 GOTO 3170
3160 CALL X3,F$,6006,N3,E3
3170 IF X3=14 THEN GOTO 3190
3180 IF M3<>N3 THEN PRINT N3;" POINTS READ INSTEAD OF ";M3
3190 IF E3=0 THEN GOTO 0160
3200 PRINT "ERROR CODE ";E3
3210 GOTO 0160
6000 REM     ** SCOPE PLOT **
6010 IF P=0 THEN GOTO 6035
6020 LET B$[6,6]="P"
6030 GOSUB 6500
6035 IF B$[6,6]="N" THEN GOTO 6020
6036 PRINT
6040 CALL 8,S6,N6,0,L[1]
6050 IF L[1]=0 THEN GOTO 0160
6060 FOR I=1 TO 10
6070   IF L[I]=0 THEN GOTO 0160
6080   PRINT "M(";I;")=";L[I],"FREQ.=";F1+(L[I]-1)*F8
6090 NEXT I
6100 GOTO 0160
6500 INPUT "     PLOT CAL.OTS.(0),CAL.TBL.(1),T0(2),T1(3),TPLOT(4)     ",X6;
6501 LET L[1]=0
6510 INPUT "    NO.PT TO BE PLOTTED=    ",N6;
6515 LET S6=(X6-1)*2002
6520 IF X6=0 THEN LET S6=7500
6530 IF X6=1 THEN LET S6=1
6540 RETURN
9000 REM    **  TRANSFER CONTROL TI ANALYSIS PROGRAM  **
9010 SAVE "SWCNTRL"
9020 CHAIN "ANALYSIS"

*
```

```
0010 REM   ** ANALYSIS ROUTINES FOR "SWCONTROL"  **
0015 DIM C$[2],C[27],B$[6],F$[25],D$[12],G$[12],P[10]
0016 LET B$="NNNNNN"
0020 PRINT
0022 INPUT "DEFAULT DIR.   ",D$
0025 PRINT
0030 ON ESC THEN STOP
0032 INPUT "  #",C$;
0033 LET S=1
0034 LET M=0
0035 LET P=0
0037 ON ESC THEN GOTO 0025
0038 IF C$[2,2]="M" THEN LET M=1
0039 IF C$[2,2]="P" THEN LET P=1
0040 IF C$[2,2]="S" THEN LET S=0
0045 IF C$[1,1]="A" THEN GOTO 2000
0050 IF C$[1,1]="V" THEN GOTO 7000
0052 IF C$[1,1]="I" THEN GOTO 7500
0055 IF C$[1,1]="P" THEN GOTO 2500
0058 IF C$[1,1]="X" THEN GOTO 5500
0060 IF C$[1,1]="B" THEN GOTO 3000
0065 IF C$[1,1]="D" THEN GOTO 3500
0070 IF C$[1,1]="M" THEN GOTO 5000
0075 IF C$[1,1]="S" THEN GOTO 4500
0080 IF C$[1,1]="T" THEN GOTO 6000
0085 IF C$[1,1]="R" THEN GOTO 1000
0087 IF C$[1,1]="F" THEN GOTO 8000
0090 PRINT "   ILLEGAL COMMAND"
0160 GOTO 0030
0500 ON N THEN GOTO 0030, 0510, 0530, 0550, 0570, 0590, 0610
0510 INPUT P[1],P[2]
0520 RETURN
0530 INPUT P[1],P[2],P[3]
0540 RETURN
0550 INPUT P[1],P[2],P[3],P[4]
0560 RETURN
0570 INPUT P[1],P[2],P[3],P[4],P[5]
0580 RETURN
0590 INPUT P[1],P[2],P[3],P[4],P[5],P[6]
0600 RETURN
0610 INPUT P[1],P[2],P[3],P[4],P[5],P[6],P[7]
0620 RETURN
1000 SAVE "ANALYSIS"
1010 PRINT
1020 PRINT
1030 CHAIN "SWCNTRL" THEN GOTO 0160
2000 REM
2010 IF S=1 THEN GOTO 2040
2020 INPUT "   D(I)=C1*D(J)+C2*D(K)   ENTER I,J,K,N,C1,C2   ",P[1],P[2],P[3],P[4
],P[5],P[6]
2030 GOTO 2060
2040 LET N=6
2050 GOSUB 0500
2060 CALL 22,1,P[1],P[2],P[3],P[4],P[5]
2070 GOTO 0030
2500 REM
2505 IF S=1 THEN GOTO 2800
2510 IF P=0 THEN GOTO 2540
2520 LET B$[6,6]="P"
2530 GOSUB 2630
2540 IF B$[6,6]="N" THEN GOTO 2520
2560 CALL 8,S6,N6,0,L[1]
```

*

```
2565 IF P=0 THEN PRINT
2570 IF L[1]=0 THEN GOTO 0030
2580 FOR I=1 TO 10
2590   IF L[I]=0 THEN GOTO 0030
2600   PRINT "M(";I;")=";L[I],"FREQ.=";F1+(L[I]-1)*F8
2610 NEXT I
2620 GOTO 0030
2630 INPUT "     PLOT CAL.OTS.(0),CAL.TBL.(1),T0(2),T1(3),TPLOT(4)    ",X6;
2650 INPUT "    NO.PT TO BE PLOTTED=    ",N6
2660 LET S6=(X6-1)*2002
2670 IF X6=0 THEN LET S6=7500
2680 IF X6=1 THEN LET S6=1
2685 LET L[1]=0
2690 RETURN
2800 LET N=2
2805 IF P=0 THEN GOTO 2560
2810 GOSUB 0500
2820 LET X6=P[1]
2830 LET N6=P[2]
2840 GOSUB 2660
2850 GOTO 2560
3000 REM
3010 IF S=1 THEN GOTO 3040
3020 INPUT "    D(I)=C1*D(J)+C2+C3*IP+C4*IP*IP    ENTER I,J,N,C1,C2,C3,C4    ",P[1]
,P[2],P[3],P[4],P[5],P[6],P[7]
3030 GOTO 3060
3040 LET N=7
3050 GOSUB 0500
3060 CALL 22,2,P[1],P[2],1,P[3],P[4]
3070 GOTO 0030
3500 REM
3510 INPUT "    WRITE(0) OR READ(1) ?    ",X3;
3520 INPUT "    ENTER FILENAME & N    ",G$,N3
3530 LET F$=D$,G$," "
3540 LET M3=N3
3550 INPUT "TO BE WR OR READ FROM 0,1,2,3,4    ",Y3
3560 LET X3=X3+14
3570 LET E3=0
3580 ON Y3+1 THEN GOTO 3590, 3610, 3630, 3650, 3670
3590 CALL X3,F$,7500,N3,E3
3600 GOTO 3680
3610 CALL X3,F$,1,N3,E3
3620 GOTO 3680
3630 CALL X3,F$,2002,N3,E3
3640 GOTO 3680
3650 CALL X3,F$,4004,N3,E3
3660 GOTO 3680
3670 CALL X3,F$,6006,N3,E3
3680 IF X3=14 THEN GOTO 3700
3690 IF M3<>N3 THEN PRINT N3;" POINTS READ INSTEAD OF ";M3
3700 IF E3=0 THEN GOTO 0030
3710 PRINT "ERROR CODE ";E3
3720 GOTO 0030
4500 REM
4510 IF M=0 THEN GOTO 4550
4520 LET P=1
4530 LET B$[5,5]="P"
4540 INPUT "    STRIP CHART(19) OR X-Y(18) OR POINT(21)    ",Z2
4550 IF B$[5,5]="N" THEN GOTO 4520
4555 IF S=1 THEN GOTO 4800
4560 IF P=0 THEN GOTO 4680
4570 GOSUB 2630
4573 LET T5=1
```

```
4575 IF Z2=21 THEN GOTO 4590
4580 INPUT "   TIME IN MSEC. PER POINT   ",T5
4590 INPUT "   START OF RAMP IN DATA   ",S7;
4600 LET P[1]=0
4610 LET P[2]=0
4620 LET P[3]=32767/(N6-1)-.0001
4630 LET P[4]=0
4640 CALL 22,2,S7,S7,S7,N6,P[1]
4680 CALL Z2,S6,S7,N6,T5
4690 PRINT
4700 LET P=0
4710 LET M=0
4720 GOTO 0030
4800 LET N=4
4820 GOSUB 0500
4822 LET S6=P[1]
4824 LET N6=P[2]
4826 LET T5=P[3]
4828 LET S7=P[4]
4830 GOTO 4600
5000 REM
5010 IF S=1 THEN GOTO 5040
5020 INPUT "   D(I)=C1*D(J)*D(K)   ENTER I,J,K,N,C1   ",P[1],P[2],P[3],P[4],P[5]
5030 GOTO 5060
5040 LET N=5
5050 GOSUB 0500
5060 CALL 22,4,P[1],P[2],P[3],P[4],P[5]
5070 GOTO 0030
5500 REM
5510 IF S=1 THEN GOTO 5540
5520 INPUT "   FIND MIN,MAX FROM I TO I+N   ENTER I,N   ",P[1],P[2]
5530 GOTO 5560
5540 LET N=2
5550 GOSUB 0500
5560 CALL 22,6,P[1],1,1,P[2],P[3]
5570 PRINT "      MAX=";P[3],"MIN=";P[4]
5580 PRINT "LOCATION=";P[5];"    ";P[6]
5590 GOTO 0030
6000 REM
6010 INPUT "   ENTER I,NO.PT   ",I,N2
6020 LET I1=INT(N2/25+.5)
6030 LET I2=N2-I1*25
6040 PRINT
6050 FOR J1=1 TO I1
6060   CALL 5,C[1],I+(J1-1)*25,25
6070   FOR K=1 TO 25
6080     PRINT C[K],
6090   NEXT K
6100 NEXT J1
6110 IF I2=0 THEN GOTO 6200
6120 CALL 5,C[1],I+I1*25,I2
6130 FOR K=1 TO I2
6140   PRINT C[K],
6150 NEXT K
6200 PRINT
6210 GOTO 0030
7000 REM
7010 IF S=1 THEN GOTO 7040
7020 INPUT "   D(I)=C1*D(J)/(D(K)+C2)   ENTER I,J,K,N,C1,C2   ",P[1],P[2],P[3],P
[4],P[5],P[6]
7030 GOTO 7060
```

*

```
7040 LET N=6
7050 GOSUB 0500
7060 CALL 22,3,P[1],P[2],P[3],P[4],P[5]
7070 GOTO 0030
7500 REM
7510 IF S=1 THEN GOTO 7540
7520 INPUT "   INTEGRATE FROM I FOR N POINTS   ENTER I,N   ",P[1],P[2]
7530 GOTO 7560
7540 LET N=2
7550 GOSUB 0500
7560 CALL 22,5,P[1],P[1],P[1],P[2],P[3]
7570 PRINT "INTEGRAL FROM ";P[1];" TO ";P[1]+P[2];" = ";P[3]
7580 GOTO 0030
8000 REM
8010 INPUT "   DATA(I)->DATA(J) , SMOOTHED M TIMES   ENTER I,J,NO.PT,M   ",I,J,N
8,M8
8020 CALL 20,I,J,N8
8030 LET M8=M8-1
8040 IF M8=0 THEN GOTO 0030
8041 CALL 9,J,N8,0,0,0
8043 FOR I2=1 TO 25
8044   CALL 10
8045 NEXT I2
8050 FOR I1=1 TO M8
8060   CALL 20,J,J,N8
8062   FOR I2=1 TO 25
8063     CALL 10
8064   NEXT I2
8070 NEXT I1
8080 GOTO 0030

*
```

```
0010 PRINT "--CALIBRATION ROUTINE--"
0015 DIM F$[20]
0016 LET E=0
0020 PRINT
0030 INPUT "VSTART & DELTA T IN MSEC.  ..",V,T
0040 LET N=-1
0050 CALL 11,7500,N,V,T
0060 IF N>1 THEN GOTO 0081
0070 PRINT "N<=1 , ERROR"
0080 GOTO 0020
0081 PRINT N;"  POINTS TAKEN",
0630 INPUT "ENTER FILENAME ",F$
0640 LET F$=F$," "
0660 CALL 14,F$,7500,N,E
0750 IF E=0 THEN STOP
0760 PRINT "WRITE ERROR  ";E
0770 STOP

*
```

BIBLIOGRAPHY

Abragam, A., The Principles of Nuclear Magnetism , Oxford University Press, London (1961)

Amstutz, L.I., Thompson, J.R., and Meyer, H., Phys. Rev. Lett. 21 ,1175(1968)

Bezuglyi and Minyfaev, Sov. Phys.-Solid State 9 ,480(1967)

Bostanjoglo, O. and Kleinschmidt, R., J. Chem. Phys. 46 ,2004(1967)

Currie, J. and Van Kranendonk, J., private communication (1974)

Fujio, M., Hama, J. and Nakamura, T., Prog. Theor. Phys. 54 ,293(1975)

Goldman, V.V., J. Low Temp. Phys. 26 ,203(1977)

Hama, J., Inuzuka, T. and Nakamura, T., Prog. Theor. Phys. 48 ,1769(1972)

Hardy, W.N., Berlinsky, A.J. and Harris, A.B., Can. J. Phys. 55 ,1150(1977)

Harris, A.B., Phys. Rev. B1 ,1881(1970)

Harris, A.B., Berlinsky, A.J and Hardy, W.N., Can. J. Phys. 55 ,1180(1977)

Heitler, W., The Quantum Theory of Radiation ,2nd. edition, Oxford University Press, London (1949)

Klemens, P.G., De Bruyn Ouboter, R. and Le Pair, C., Physica, 30 ,1863(1964)

Krivoglas, M.A., Theory of X-ray and Thermal Neutron Scattering by Real Crystals ,Plenum Press, New York (1969)

Kroupa, V.F., Frequency Synthesis; Theory, Design and Application , Halsted Press, John Wiley and Sons, Inc., New York, Toronto (1973)

Luryi, S. and Van Kranendonk, J., Can. J. Phys. 57 ,(1979), in press

Oyarzun, R. and Van Kranendonk, J., Phys. Rev. Lett. 26 ,646(1971)

Oyarzun, R. and Van Kranendonk, J., Can. J. Phys. 50 ,1494(1972)

Raich, J.C. and Kanney, L.B., J. Low Temp. Phys. 28 ,95(1977)

Rose, M.E., Elementary Theory of Angular Momentum ,John Wiley and Sons, Inc., New York, Toronto (1957)

Silvera, I.F., Hardy, W.N. and McTague, J.P., Phys. Rev. B4 ,2724(1971)

Van Kranendonk, J. and Walker, M.B., Can. J. Phys. 46 ,2441(1968)